INFLUENCES OF SEEPAGE INTO WALLS, CURVATURE AND BIFURCATION ON PRESSURE DROP CALCULATION IN IDEALIZED ARTERIES – A COMPUTATIONAL FLUID DYNAMICS APPROACH

GOVINDARAJU KALIMUTHU

THESIS SUBMITTED IN FULFILMENT OF THE REQUIREMENTS FOR THE DEGREE OF DOCTOR OF PHILOSOPHY

FACULTY OF ENGINEERING
UNIVERSITY OF MALAYA
KUALALUMPUR
2015

UNIVERSITI MALAYA

ORIGINAL LITERARY WORK DECLARATION

Name of Candidate: **Govindaraju Kalimuthu** (I.C/Passport No:

Registration/Matric No: **KHA080061**

Name of Degree: **PhD**

Title of Project paper/Research Report/Dissertation/Thesis ("This Work"):

Influences of seepage into walls, curvature and bifurcation on pressure drop calculation in idealized arteries – a computational fluid dynamics approach

Field of Study: **Bio Fluid Dynamics**

I do solemnly and sincerely declare that:

(1) I am the sole author/writer of this work;
(2) This work is original;
(3) Any use of any work in which copyright exists was done by way of fair dealing and for permitted purposes and any excerpt or extract from, or reproduction of any copyright work has been disclosed expressly and sufficiently and the title of the work and its authorship have been acknowledged in this work;
(4) I do not have any actual knowledge nor do I ought reasonably to know that the making of this work constitutes an infringement of any copyright work;
(5) I hereby assign all and every rights in the copyright to this work to the University of Malaya ('UM"), who henceforth shall be owner of the copyright in this work and that any reproduction or use in any form or by any means whatsoever is prohibited without the written consent of UM having been first had and obtained;
(6) I am fully aware that if in the course of making this work I have infringed any copyright whether intentionally or otherwise, I may be subject to legal action or any other action as may be determined by UM.

Candidate's Signature Date

Subscribed and solemnly declared before,

Witness's Signature

Name:
Designation

ABSTRACT

Evaluation of physiological significance of coronary stenosis severity is of great importance than the anatomical significance to identify potentially ischemic stenosis for revascularization whereas non-culprit stenosis has been deferred from stenting. In a clinical settings, the functional severity of the stenosis is evaluated by fractional flow reserve (FFR) which is derived from mean pressure drop ($\Delta\tilde{p}$) across the stenosis. The other parameters such as Pressure Drop Coefficient (CDP) and Lesion Flow Coefficient (LFC) which are derived from fluid dynamic principles also useful to evaluate the functional severity of the stenosis. The diagnostic accuracy of measuring severity of stenosis is enhanced by using small diameter guide-wire sensor under hyperemic flow condition. In the presence of stenosis, a cutoff value of FFR < 0.75 could almost induce myocardial ischemia, whereas FFR > 0.8 never associated with exercise-induced ischemia in a single vessel coronary artery disease (CAD) from numerous clinical trials. This means that the gray zone for FFR is between 0.75 and 0.80.

In this thesis, a possible region of misinterpretation of stenosis severity was evaluated when it was assessed in vitro by considering the variations of FFR, CDP and LFC for a given percent area stenosis (AS) under the following three different cases. (i) The arterial wall and plaque region were considered as highly permeable to blood in the event of plaque rupture (ii) variations in the angle of curvature of the artery wall and (iii) variations in the bifurcation angle of coronary artery. In all the above cases without guide wire condition was considered.

To understand the effect of porous media on the diagnostic parameters, A computational fluid dynamic simulations were carried out in rigid artery (RA) and Fluid

porous Interface (FPI) stenotic artery wall models. The $\Delta\tilde{p}$ across the stenosis was compared for the given percent AS. The $\Delta\tilde{p}$ was lower in the FPI model than in the RA model. As a result, a changes in the diagnostic parameters exist for a given percent AS which leads to misinterpretation in the intermediate stenosis severity. The misinterpretation region was found to be 81.83 to 83.2% AS

The influence of artery wall curvature i.e. 0°, 30°, 60°, 90° and 120° on the coronary diagnostic parameters have been studied. It was found that with increase in the curvature of the arterial wall for a given percent AS, the $\Delta\tilde{p}$ increases hence affects the FFR, CDP and LFC. These variations leads to misinterpretation in the evaluation of stenosis severity in vitro. The misinterpretation region was found to be 76.10 to 79.07% AS.

The influence of bifurcation angulation i.e. 30°, 60° and 90° on the coronary diagnostic parameters have been studied. It was found that with increase in the angulation, the $\Delta\tilde{p}$ decreases hence affects the FFR, CDP and LFC. These variations leads to misinterpretation in the evaluation of stenosis severity in vitro. The misinterpretation region was found to be 81.8 % to 84.12% AS.

ABSTRAK

Penilaian kepentingan fisiologi tahap stenosis koronari adalah amat penting daripada kepentingan anatomi untuk mengenal pasti stenosis berpotensi iskemia untuk revascularization manakala bukan punca-stenosis telah ditunda dari stenting. Dalam tetapan klinikal, tahap fungsi stenosis yang dinilai oleh rizab aliran pecahan (FFR) yang berasal dari kejatuhan tekanan min ($\Delta\tilde{p}$) di seluruh stenosis itu. Parameter lain seperti Tekanan Drop Pekali (CDP) dan luka Aliran Pekali (LFC) yang berasal daripada prinsip dinamik cecair juga berguna untuk menilai tahap fungsi stenosis itu. Ketepatan diagnostik untuk mengukur tahap stenosis dipertingkatkan dengan menggunakan diameter kecil sensor panduan-wayar di bawah keadaan aliran hyperemic. Di hadapan stenosis, nilai potong FFR <0.75 hampir boleh mendorong iskemia miokardium, manakala FFR> 0.8 tidak pernah dikaitkan dengan senaman yang disebabkan oleh iskemia di sebuah kapal tunggal penyakit arteri koronari (CAD) daripada banyak ujian klinikal. Ini bermakna bahawa zon kelabu untuk FFR adalah antara 0.75 dan 0.80.

Dalam tesis ini , sebuah kawasan kemungkinan salah tafsir tahap stenosis dinilai apabila ia dinilai dalam vitro dengan mempertimbangkan variasi FFR, CDP dan LFC untuk stenosis kawasan peratus diberikan (AS) di bawah tiga kes yang berbeza yang berikut. (i) Dinding arteri dan rantau plak dianggap sebagai sangat telap kepada darah sekiranya berlaku plak pecah (ii) perubahan dalam sudut kelengkungan dinding arteri dan (iii) perubahan dalam sudut pencabangan dua di arteri koronari. Dalam semua kes-kes di atas tanpa syarat panduan wayar dianggap.

Untuk memahami kesan media berliang kepada parameter diagnostik , A pengiraan simulasi dinamik cecair telah dijalankan dalam arteri tegar (RA) dan Fluid Interface berliang (FPI) stenotic model arteri dinding. Di $\Delta\tilde{p}$ seluruh stenosis itu berbanding untuk peratus yang diberikan AS. $\Delta\tilde{p}$ Adalah lebih rendah dalam model FPI daripada dalam model RA. Hasilnya, satu perubahan dalam parameter diagnostik wujud untuk peratus diberikan AS yang membawa kepada salah tafsir di tahap stenosis pertengahan. Rantau salah tafsir didapati 81.83-83.2 % AS.

Pengaruh arteri dinding kelengkungan iaitu 0°, 30°, 60°, 90° dan 120° kepada parameter diagnostik koronari telah dikaji. Ia telah mendapati bahawa dengan peningkatan dalam kelengkungan dinding arteri untuk peratus yang diberikan AS, $\Delta\tilde{p}$ kenaikan itu memberi kesan FFR itu, CDP dan LFC. Perbezaan-perbezaan ini membawa kepada salah tafsir dalam penilaian tahap stenosis in vitro. Rantau salah tafsir didapati 76.10-79.07 % AS.

Pengaruh pencabangan dua angulation iaitu 30°, 60° dan 90° kepada parameter diagnostik koronari telah dikaji. Ia telah mendapati bahawa dengan peningkatan angulation itu, $\Delta\tilde{p}$ penurunan itu memberi kesan kepada FFR, CDP dan LFC. Perbezaan-perbezaan ini membawa kepada salah tafsir dalam penilaian tahap stenosis in vitro. Rantau salah tafsir didapati 81.8 % - 84.12 % AS.

ACKNOWLEDGEMENT

Firstly, I would like to extend my sincerest gratitude to my two supervisors Dr. Irfan Anjum Badruddin and Dr. Ahmad Badaruddin Badry. It has been my greatest pleasure to work under both of them and I have learned tremendously within these long years. Especially, Dr. Irfan Anjum Badruddin's excellent guidance, support and encouragement that make this thesis possible.

There is not a word that can describe how to thank my wife for all the support and understanding, as well as for all the pushing and nonchalant but meaningful advice throughout the years.

I am extremely thankful to Dr. Girish N Viswanathan, Fellow in interventional cardiology, Royal Bournemouth hospital, Bournemouth, United Kingdom provided many useful discussion throughout my research. I sincerely thank the management of HELP College of arts and technology (A member of HELP Group) for giving a support during my PhD. I would like to thank everyone and my good friends who helped me during my PhD

Last but not least, I would like to thank to my father and this thesis is dedicated to my beloved late mother.

TABLE OF CONTENTS

LIST OF FIGURES

LIST OF TABLES

LIST OF ABBREVIATION

AS	Area Stenosis
CABG	Coronary artery bypass graft
CAD	Coronary Artery Disease
CCTA	Coronary computed tomographic angiogram
CDP	Pressure drop coefficient
CFD	Computational fluid dynamic
CFR	Coronary flow reserve
CFVR	Coronary blood flow velocity reserve
CY	Contractility
FFR	Fractional Flow Reserve
FFR_{myo}	Myocardial fractional flow reserve
FPI	Porous stenosed artery
HR	Heart rate
IEL	Internal elastic lamina
IVUS	Intravascular ultrasound
LAD	Left anterior descending
LCA	Left coronary artery
LCX	Left circumflex
LFC	Lesion flow coefficient
LMS	Left Main Stem
MDCT	Multi-detector row computed tomography
NURD	Non-uniform rotational distortion
PCI	Percutaneous coronary intervention
PET	Positron emission tomography

QCA	Quantitative coronary angiography
RA	Rigid stenosed artery
RCA	Right coronary artery
RV	Right ventricle
SST	Shear stress transport
WSS	Wall Shear Stress

NOMENCLATURES

D	Diameter
P_v	Central Venous Pressure
E	Porosity
K	Permeability
μ	Dynamic viscosity
$\dot{\gamma}$	Shear rate
c_F	dimensionless parameter related to inertial effects
R_e	Reynolds number
u_p	Pore velocity
ν	Kinematic viscosity
t_a	Artery wall thickness
R	Radius
A	Radius of curved artery
L	Length
P	Density
T	Time
$\overline{u}/\overline{u}_{p-t}$	Normalized velocity
$\Delta\tilde{p}$	Time averaged pressure drop
$\tilde{Q}$	Mean hyperemic flow rate
$\tilde{p}_e$	Proximal pressure measured at the entrance (Z=0)
$\tilde{p}_a$	Proximal pressure measured at 3 mm
$\tilde{p}_d = \tilde{p}_r$	Distal recovery pressure

$\tilde{\eta}(\tilde{z})$	Radius if curved stenosis
L	Lesion length of curved stenosis
$\tilde{z}$	Length measured along the axis of the artery
H	Maximum projection of stenosis in curved artery

1. INTRODUCTION

1.1. Background

Biomechanics is the study of mechanics applied to biology and aim to explain mechanics of life and living organisms (Fung, 1993). Recent research in biomechanics is focused on physiological and medical applications due to its importance associated with human life. Coronary Artery Disease (CAD) is responsible for most of the deaths in patients with cardiovascular diseases. Most of the acute myocardial infarctions (heart attacks) are caused by non-obstructive vulnerable coronary atherosclerotic plaques by rupture of a thin fibrous cap covering fatty debris and subsequent thrombus formation and embolization (Tobis, Azarbal, & Slavin, 2007). Diagnosis of potentially ischemic coronary artery stenosis severity has been a challenging task for the cardiologist. In current clinical settings many diagnostic methods have been adapted effectively to treat the coronary artery stenosis. Among them, many diagnostic protocols have been developed from fluid dynamic principles to evaluate the functional significance of the coronary artery stenosis. Applications of Computer technologies have an influence on medical health care. Computational fluid dynamic (CFD) is an emerging area which is useful in the diagnostic management of the cardiovascular system. In this work, the anatomical factors such as porous media, curvature of an artery and bifurcation angulation of an artery influences on the physiological significance of the coronary stenosis severity measurements during vivo measurement are analyzed using CFD technique.

1.2. Coronary circulation: an overview

The main function of coronary arteries are supplying oxygenated blood to the heart muscles. Two coronary arteries, known as left coronary artery (LCA) and right coronary artery (RCA) originates from aorta near top of the heart as shown in Figure 1.1. Right side of the heart, which is smaller than left side of the heart receives blood mainly from RCA. The initial segment of the left coronary artery, which is less than an inch long and branches into two smaller arteries namely left anterior descending artery (LAD) and left circumflex artery (LCX). The LCA is embedded in the front side of the heart whereas LCX embedded in the surface of the back side of the heart. The coronary arteries further branches into smaller arteries called capillaries and penetrate into heart muscle. The smallest branches called capillaries through which red blood cells travel as single file. Red blood cells provides oxygen and nutrients to the cardiac muscle tissue (Vicini & Bassingthwaighte, 2014) . Blood flow pattern is normal in coronary artery and becomes disturbed when it flows through a narrowed or stenosed artery.

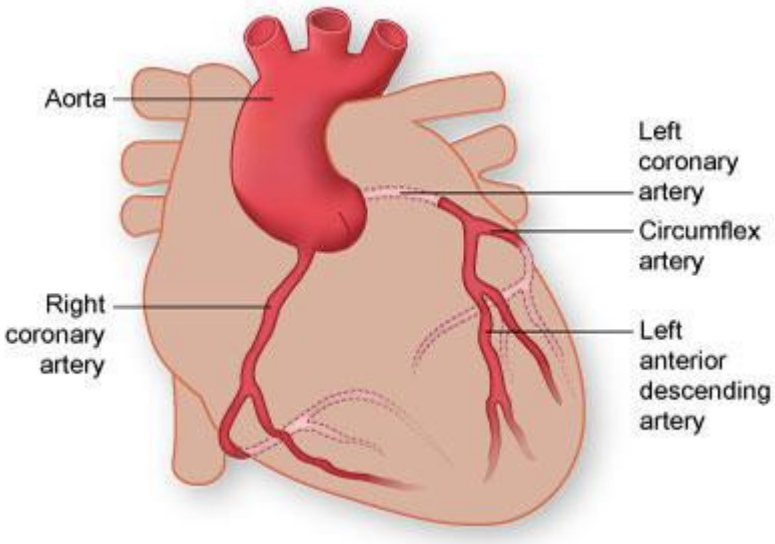

Figure 1.1: Coronary circulation in heart
Courtesy: Texas heart Institute.
http://www.texasheart.org/HIC/Anatomy/coroanat.cfm

1.3. Objectives

Researchers have acknowledged the usefulness of fluid mechanics principles applied to the coronary artery circulation. Cardiologist uses several methods to identify and treat the coronary artery stenosis effectively. The coronary diagnostic methods such as coronary angiography (Tobis, et al., 2007), intra-vascular ultrasound (IVUS) (Nissen & Gurley, 1991; Nissen & Yock, 2001), Coronary computed tomographic angiogram (CCTA) (W. Bob Meijboom et al., 2008) are useful to acquire anatomical knowledge of the coronary artery stenosis. But the functional significance of the stenosis severity is more valuable than anatomical significance to identify the potentially ischemic stenosis for revascularization or stenting whereas the non-ischemic stenosis could be deferred from revascularization or stenting and minimum medical therapy may be sufficient for better outcome (N. H. J. Pijls & Sels, 2012). The functional significance of stenosis in a single vessel CAD or multi vessel CAD has been evaluated by using trans-stenotic pressure drop, coronary flow myocardial resistance and percentage area of stenosis.

Coronary Flow Reserve (CFR) is the first diagnostic parameter assessing severity of coronary artery stenosis. CFR is defined as ratio of hyperemic flow to the basal flow. Hyperemic is a condition in which a maximum flow can occur in a stenosed artery by the infusion of adenosine or papaverine. The CFR is affected by several parameters such as epicardial and the micro-vascular resistance. It is also affected by myocardial chamber hypertrophy, diabetes, and age (Tobis, et al., 2007). The CFR was replaced by Fractional Flow Reserve (FFR) by virtue of its limitations. The FFR is defined as the ratio of the maximum myocardial flow in the stenotic artery to the maximum myocardial flow had the same artery been normal. This flow ratio is also expressed as the ratio of the distal coronary pressure to the aortic pressure (N. H. Pijls et al., 1995; N.

H. J. Pijls & Sels, 2012). The FFR has a unique value of 1 for normal person without stenosis. It is not influenced by the changes in the hemodynamic conditions, such as heart rate, variations in blood pressure, and contractility. The FFR accounts for the interaction between the severity of the epicardial stenosis and the extension of the perfusion territory. For FFR, there is a sharp threshold value discriminating between the ischemic and non-ischemic stenosis. FFR measurement is also applicable to decision making in patients with stent re-stenosis and bifurcation lesion severity.

Recently, the proposed functional parameters such as pressure drop coefficient (CDP; the ratio of mean trans-stenotic pressure drop to the proximal dynamic pressure) and lesion flow coefficient (LFC) derived from basic fluid dynamic principles (R. Banerjee et al., 2008; Banerjee et al., 2009) have been reported to be useful in diagnosing the functional significance of stenosis severity.

Among them, FFR is a clinically well-proven diagnostic parameter (N. H. J. Pijls & Sels, 2012) for the measurement of stenosis severity during clinical evaluation. In the stenosed artery, a intracoronary pressure wire of diameter 0.014" is used to record the distal pressure under hyperemic condition. Insertion of guide wire causes an obstructive effect, creating "artifactual stenosis" that will affect the FFR value (Sinha Roy, Back, & Banerjee, 2006). Similar to guide wire insertion, downstream collateral flows (Peelukhana, Back, & Banerjee, 2009), arterial wall compliance and plaque characteristics (Konala, Das, & Banerjee, 2011) and aortic and coronary outflow pressure (Maria Siebes, Chamuleau, Meuwissen, Piek, & Spaan, 2002) have been found to significantly affect the coronary diagnostic parameters which results in misdiagnosis of true stenosis severity.

For clinical decision making and for better clinical outcome from the heart disease assessment of stenosis severity is inevitable. As previously explained, coronary angiography, CCTA and IVUS techniques are being widely used to identify the anatomical significance of stenosis but fails to identify the functional significance of the stenosis. So, the physiological diagnostic parameters derived from fluid dynamics are widely accepted and useful as clinical decision making.

Depending on the measured diagnostic parameters which are calculated from pressure and flow measurements at the site of stenosis using guide wire, the functional severity of the stenosis is determined. The pressure and flow measurements are depend on the transducer placement and these measured parameters include the effects of anatomical variations such as plaque rupture, artery wall curvature and bifurcation angulation for a given stenosis severity whereas these anatomical variations are not included in the visual assessment.

By considering the pressure drop across the stenosis as a standard parameter, the present study provides the insight into the variations of the bio-physiological properties of the coronary artery and stenosis, and how these variations will influence the visual assessment of stenosis severity.

The specific objectives of this thesis are as follows:

To investigate factors influencing the visual assessment of stenosis severity and to find the region of possible misdiagnosis severity by calculating the pressure drop across the stenosis, the following factors have been considered.

(i) The effect of porous media of the arterial wall and stenosis in the event of plaque rupture

(ii) Influence of arterial wall curvature

(iii) Variations in bifurcation angulation of the coronary artery.

1.4. Outline of thesis

To understand the factors influencing on anatomic assessment of stenosis severity, Computational Fluid Dynamic (CFD) simulations were adopted in stenosed coronary artery models under hyperemic blood flow conditions and investigate the pressure drop across the stenosis and FFR. The following factors have been discussed in detailed manner in subsequent chapters (i) the effect of porous media on the arterial wall and plaque in the event of plaque rupture (ii) artery wall curvature and (iii) artery bifurcation. Brief outline of the thesis are as follows:

(i) In the second chapter, a comprehensive background and literature review of most pertinent fundamentals and issues of coronary stenosis diagnostics are provided. In this chapter, presently used clinical diagnostic methods are also discussed in detail.

(ii) In the third chapter, the governing equations for incompressible flow, two-equation turbulence models, namely k-ω standard transitional and SST transitional models are presented for investigating transition to turbulence of blood flow in three-dimensional models of axisymmetric arterial stenosis by using commercial Computational Fluid Dynamics (CFD) software, ANSYS CFX 14.0. Also, a Bench mark case for validation of software was presented.

(iii) In the fourth chapter, Effect of porous media on the coronary diagnostic parameters are discussed by comparing rigid artery wall having rigid plaque and porous artery wall having porous plaque and misdiagnosis region was identified for the clinical usefulness when the severity of stenosis assessed by CCTA.

(iv) In the fifth chapter, influences of stenosed artery wall curvature on the diagnostic parameters are discussed by introducing various angle of curvature of the artery wall. The changes in the coronary diagnostic parameters have been analyzed and misinterpretation region was identified in the visual assessment of stenosis severity for the clinical usefulness.

(v) In the sixth chapter, influence of stenosed bifurcated artery wall with various angulation on the diagnostic parameters are discussed. The changes in the coronary diagnostic parameters have been analyzed and misinterpretation region was identified as the stenosis severity assessed by in-vitro image assessment for the clinical usefulness.

(vi) In the seventh chapter, the findings of the above investigations are summarized and suggestions made for future research have been given.

2. LITERATURE REVIEW

2.1. Heart anatomy

Human or animal body requires blood circulation to maintain the metabolisms going. Heart is the pumping unit that drives the circulation. The heart itself needs blood to function. When the blood supply to the heart stops, it fails to function, leading to heart failure. Myocardial infarction (or heart failure) caused due to blockages in the coronary arteries, is one of the main health problems afflicting people.

Heart is the most important organ in any living animals. The human heart has four chambers: Right atrium, left atrium, right ventricle and left ventricle. Mechanically, these are the pumping elements that circulate blood to the organs, tissues and cells throughout our body. The anatomy of the heart is shown in Figure 2.1. The basic functions of heart are:

(i) To receive oxygen rich blood from lungs and send to the whole body and

(ii) To receive deoxygenated blood from body and pump to the lungs to pick up oxygen.

This whole action is performed in two phases called diastole and systole. Blood flow to the heart occurs mainly during diastole phase. In diastole phase, the arterial contracts which causes blood being pumped from left and right atrium to the left and right ventricles whereas in the systole phase, ventricles contract and blood pumped right ventricle to lungs through pulmonary artery and left ventricle to aorta. The whole action is performed periodically with heart beating about 60- 80 times per minute.

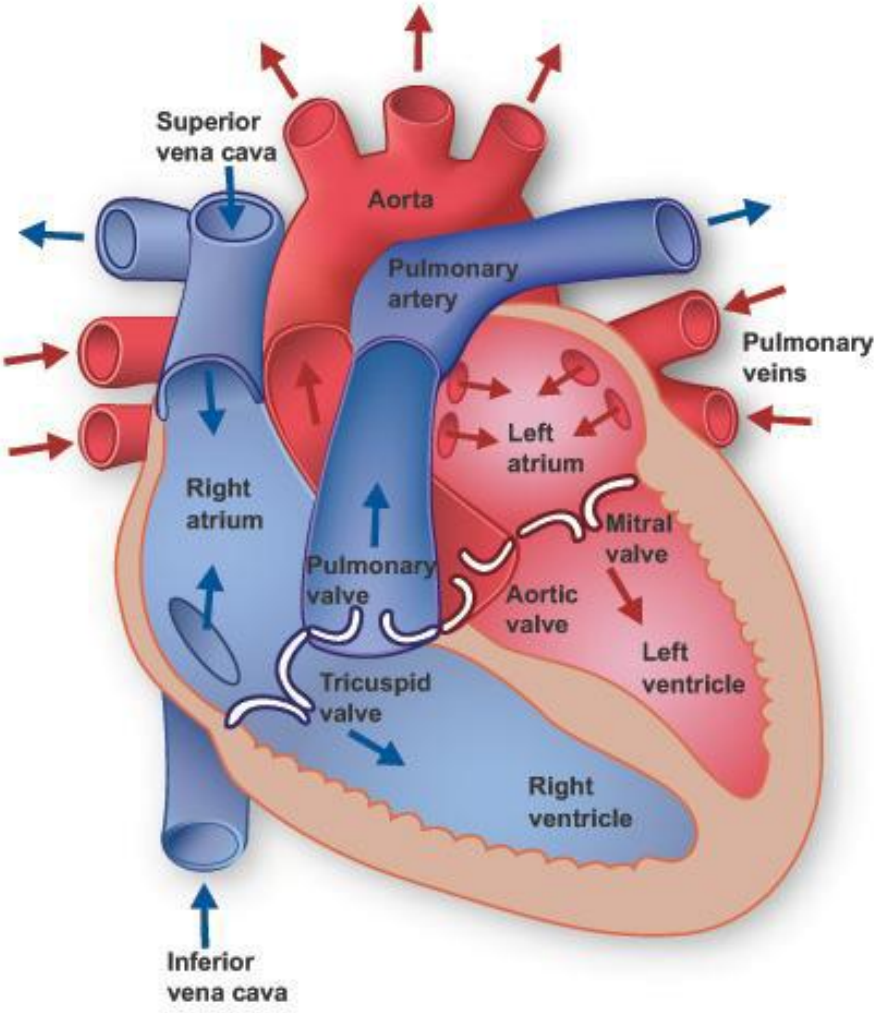

Figure 2.1: Anatomy of Heart
Courtesy: Texas heart Institute.
http://www.texasheart.org/HIC/Anatomy/anatomy2.cfm

2.2. Coronary artery wall

The main arteries originate from the root of aorta and then branches into two arteries namely left and right coronary arteries. Left coronary artery (Figure 2.2) branches into left anterior descending artery (LAD) and left circumflex coronary artery (LCX) (Waite & Fine, 2007). The non-dominant right coronary artery and their branches are shown in figure 2.3.

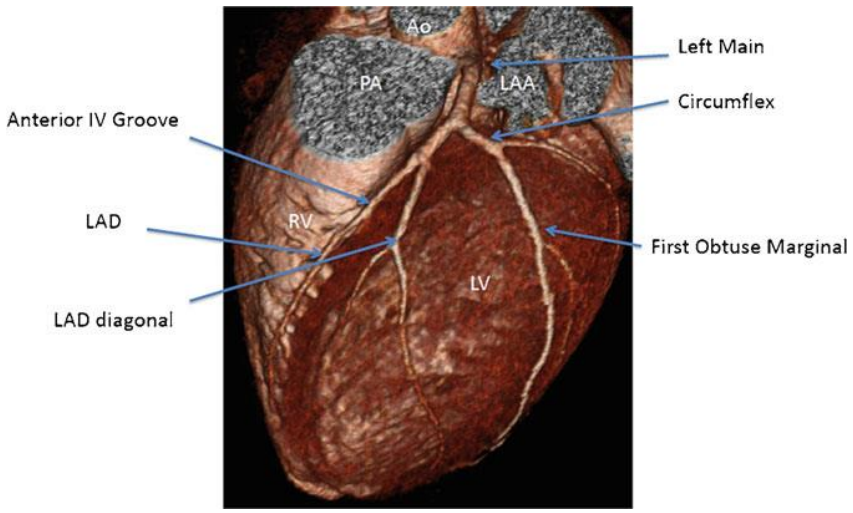

Figure 2.2: Volume-rendered image of the left coronary artery (LCA)
Reprinted from (Vlodaver & Lesser, 2012), Copyright (2015), with kind permission from Springer Science and Business Media

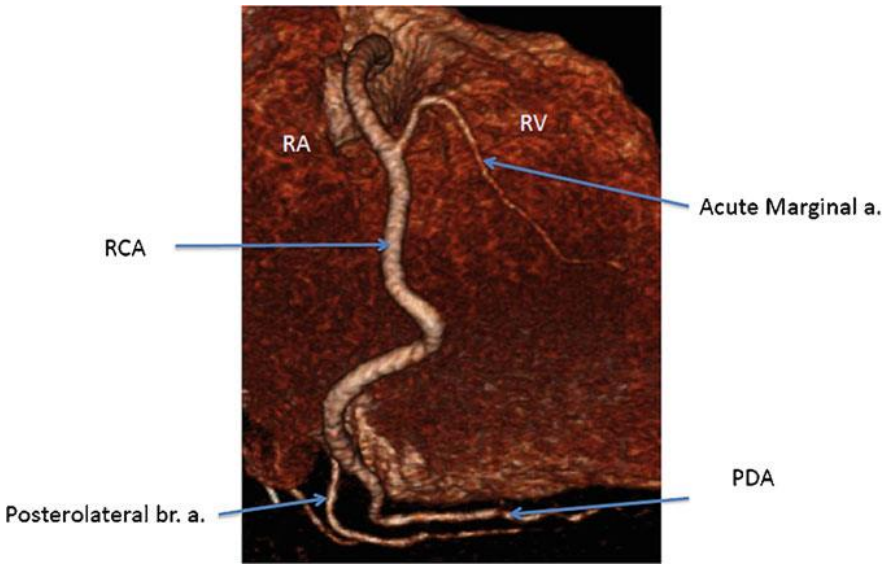

Figure 2.3: Volume-rendered image of the right coronary artery (RCA)
Reprinted from (Vlodaver & Lesser, 2012), Copyright (2015), with kind permission from Springer Science and Business Media

Arteries are normally straight through which the blood efficiently transport to distal organs. However, arteries may become tortuosity owing to vascular disease. Tortuous or twisted arteries and veins are commonly seen in humans and animals from common angiographic findings (Han, 2012). Coronary angiography showed tortuosity of the left

anterior descending artery and the circumflex artery without a fixed coronary stenosis (Figure 2.4).

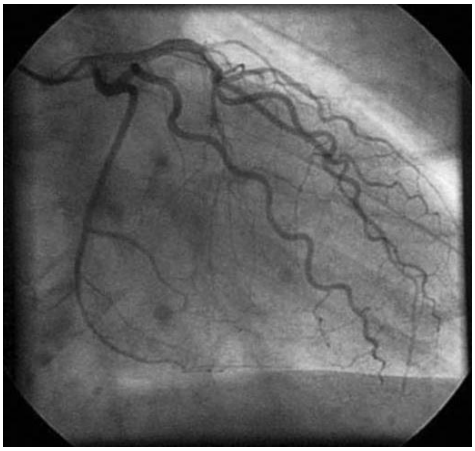

Figure 2.4: Coronary tortuosity (Zegers, Meursing, Zegers, & Oude Ophuis, 2007)

The normal arterial wall consists of endothelium, intima, internal elastic lamina (IEL), media and adventitia. The physiological properties for various layers are tabulated in Table 2.1 (Ai & Vafai, 2006). It is believed that the permeability of endothelium wall increases with deposition of cholesterol due to the damaged or inflamed arterial wall.

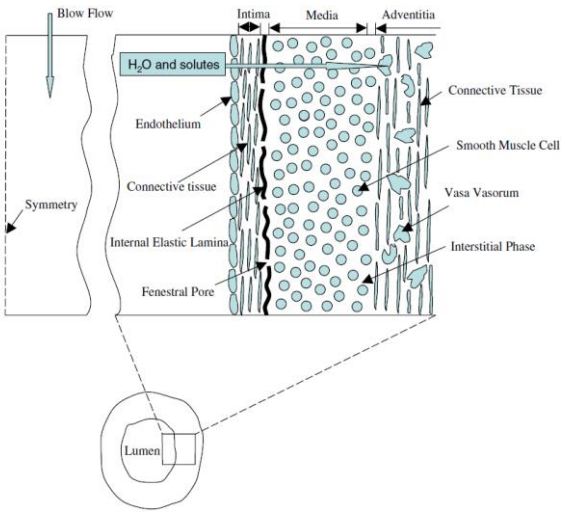

Figure 2.5: Cross section of blood vessel wall
Reprinted from (Ai & Vafai, 2006), Copyright (2015) with permission from Elsevier

Table 2.1: Values of the physical properties of the arterial wall region

	Layers			
	Endothelium	Intima	IEL	Media
Porosity	0.0005	0.96	0.004	0.15
Permeability (cm^2)	3.21715×10^{-17}	2.2×10^{-12}	3.2188×10^{-15}	2.0×10^{-14}

2.3. Coronary circulation

The blood supply to the heart muscle is termed as coronary circulation. Coronary circulation is primarily decided by local oxygen demand. 75% of blood flow to the heart muscle through left coronary artery and reaming through right coronary arteries. The RCA supplies blood to the right ventricle (RV). As seen from figure 2.1, left ventricle is responsible for coronary flow. The left lateral portion of the left ventricle and the anterior (front) portion of the ventricular septum receives blood from the LCA. The right coronary artery supplies the right ventricle, the posterior wall of the left ventricle and posterior third of the septum (Ramanathan & Skinner, 2005).

Coronary circulation is basically composed of: (a) large vessels known as the epicardial vessels, which are on the sub-epicardium of the heart; (b) the micro vessels that constitute the microcirculation. Under normal conditions, the flow resistance of the epicardial vessels is very small compared to that of the micro vessels. Thus, they are also known as conduit vessels. Epicardial coronary arteries and the microcirculation differ vastly in anatomy, vasoactive control systems, responses to vascular stimuli, and pathologic manifestations of disease. There are several factors responsible for the regulation of

coronary circulation. A few important factors are discussed here. Coronary flow in human under resting condition is around 250 ml/min and during exercise the coronary flow increases to fivefold (Ramanathan & Skinner, 2005). Since the perfusion pressure does not change significantly from resting to hyperemic flow (maximum flow), this implies that the coronary resistance at resting conditions is higher than resistance at elevated work load conditions. Thus at resting condition, the coronary network is a high resistance system with high intrinsic vasomotor tone (the ability to the coronary vessels to dilate or constrict), which can be regulated by selective use of different vasoconstrictors and vasodilators.

2.4. Dynamic mechanism in coronary stenosis

Deposits of lipids, smooth muscle proliferation and endothelial dysfunction reduce the luminal diameter. A progressive narrowing in the arterial system of human or animal heart is known as stenosis (Figure 2.6.), which impairs blood flow to the heart muscle and eventually results in atherosclerotic plaque rupture and life threatening myocardial infarction (Naghavi et al., 2003).

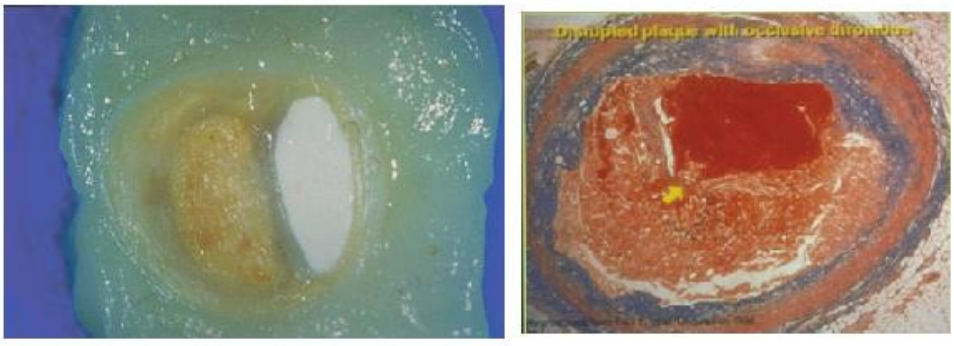

Figure 2.6: Left: Cross-section of coronary artery showing an eccentric atherosclerotic plaque. Right: A ruptured and thrombosed atherosclerotic coronary lesion

When the luminal diameter reduced by 50%, the coronary blood flow is unable to respond to an increase in metabolic demand also the normal resting flow becomes affected if the luminal diameter is reduced by 80%. Coronary stenoses are morphologically classified as concentric or eccentric stenoses. Concentric stenoses are symmetric narrowing of a coronary artery whereas eccentric stenoses are asymmetric narrowing of coronary artery. Both concentric and eccentric stenoses have the potential for dynamic behavior changes of blood flow. The magnitude of dynamic changes of caliber is also larger in eccentric than in concentric stenoses (Kaski et al., 1991). The stenoses are not always rigid but majority of the human stenosis are compliant. Coronary stenoses behave in a dynamic fashion. Energy loss (Pressure drop) takes place in blood flow when it passes through stenosis. The pressure drop across the stenosis is a key element of ischemia (Brown, Bolson, & Dodge, 1984). The potential ischemic starts when the distal pressure to the stenosis falls below that needed to perfuse the sub-endocardium. A good approximation of dynamic mechanism of a stenosis which is derived from fluid mechanics principle is given by

$$\Delta p = \frac{1.8\, Q_s}{d_{\min}^4} + \frac{6.1\, Q_s^2}{d_{\min}^4} \tag{2.1}$$

where Δp is the Pressure drop across the stenosis in terms of coronary flow Q_s and minimum luminal diameter $(d_{\min})$. The first term accounts for frictional losses whereas the second term accounts for energy transfer (Brown, et al., 1984).

2.5. Collateral vessels

When stenosis develops in coronary artery over a months or years collateral circulation can be developed. Coronary collateral flows or “natural bypass flows” play an active role when the myocardium doesn’t receive sufficient blood supply owing to stenosis (Figure

2.7 & 2.8). Coronary collateral vessels are an alternative source of blood supply to myocardium jeopardized by ischemia (Christian Seiler, 2003). Development of coronary collateral is stimulated in response to myocardial ischemia (Takeshita, Koiwaya, Nakamura, Yamamoto, & Torii, 1982) or in other words a pressure gradient occurs across the stenosis is mostly responsible for the development of coronary collaterals. Because of the low pressure at the distal to the stenosis the blood flow redistribute through the pre-existent arterioles (small capillary vessel) that connect high pressure to low pressure region.

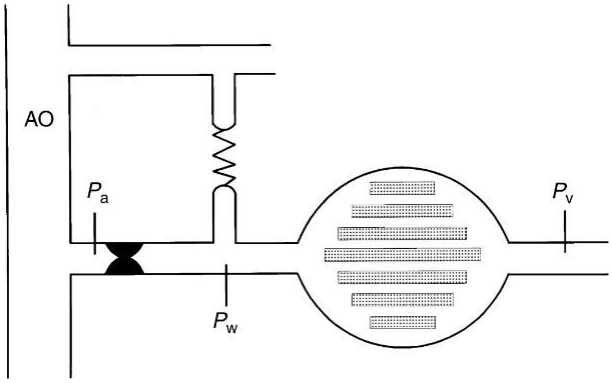

Figure 2.7: Model of the coronary circulation at total occlusion of the coronary artery
Reprinted from(Nico HJ Pijls, 2006), Copyright (2015) with permission from Oxford University Press

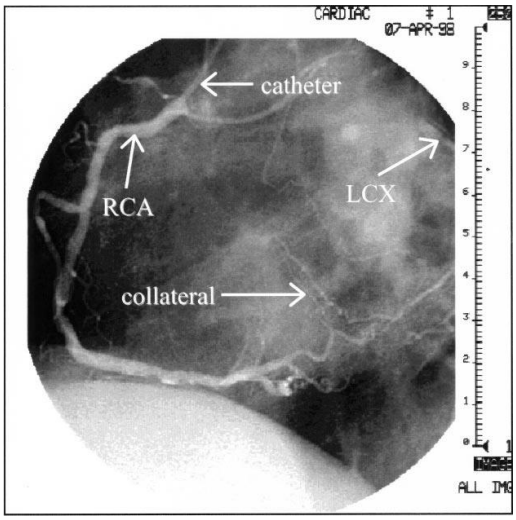

Figure 2.8: Figure showing a collateral flow
Reprinted from (Koerselman, van der Graaf, de Jaegere, & Grobbee, 2003), Copyright (2015) with permission from Circulation

When the stenosis severity increases, the collateral flow increases and therefore increased shear stress in the preexistent collateral arteries and vice versa in order to avoid trans-mural myocardial infraction. Thus the collateral flow rate is a direct indicator of Coronary artery disease (CAD) (C. Seiler, Stoller, Pitt, & Meier, 2013). In the presence of stenosis and collaterals, the total myocardial flow is equal to sum of epicardial and collateral flow.

2.6. Assessment of anatomical significance of stenosis severity:

2.6.1. Coronary angiography and CCTA

Coronary angiography is a radiological study and the most common technique used to study coronary artery disease. It provides a 2D image representation of the 3D vascular lumen of the arterial wall (Figure 2.9 A). A limitation of this technique lies in its inability to provide the functional or physiological significance of lesion especially those of intermediate stenosis whose diameter is between 45% - 70% with normal artery (W. Bob Meijboom, et al., 2008; Tobis, et al., 2007). Therefore, the assessment of an intermediate coronary artery stenosis severity still remains most difficult for cardiologists (Tobis, et al., 2007).

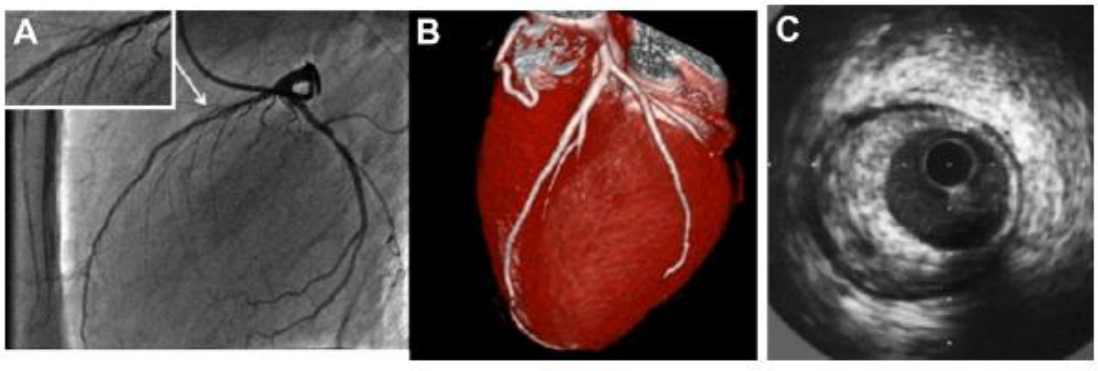

Figure 2.9: (A) Coronary angiography evaluation used to find anatomical significance of the stenosis (B) CCTA images used for the evaluation of severity of coronary artery stenosis (C) IVUS image shows stable and vulnerable plaque.

The eccentric lesions have maximum and minimum diameters, which differ significantly (apparently there are more than two diameters in a cross-section). In the conventional coronary angiography, it is extremely difficult to assess the severity of the stenosis, particularly, the arteries having multiple stenoses or diffused CAD. Further, coronary angiogram techniques overestimate or underestimate the severity of the stenosis. The 64-slice CCTA scanners have the ability to acquire the images of the complete coronary artery tree (Figure 2.9 B & Figure 2.10). Quantitative coronary angiography (QCA) is carried out after receipt of the CCTA images on an offline workstation to assess the anatomical significance of the stenoses (Kristensen et al., 2010; van Werkhoven et al., 2009). In the QCA, percent Area stenosis (AS), lesion length and percent diameter have been considered for the assessment of anatomical significance of the stenosis severity.

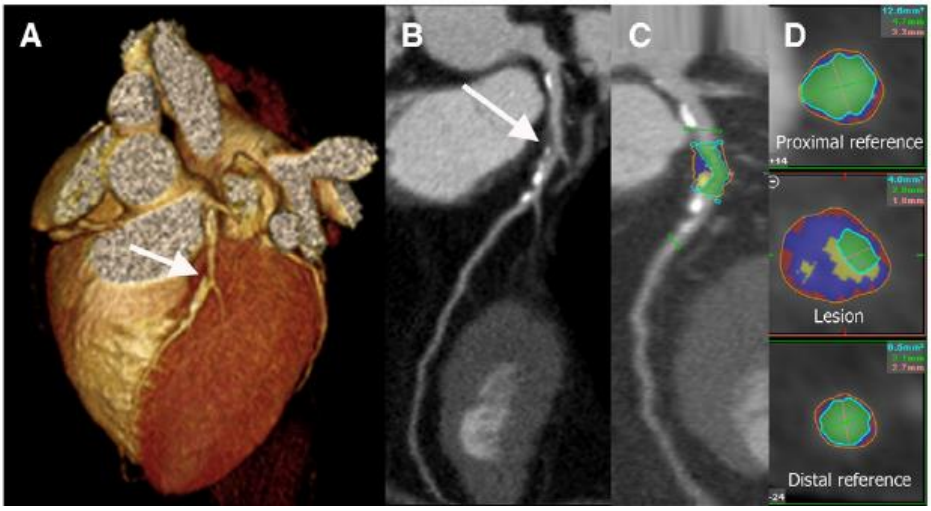

Figure 2.10: Three dimensional and curved multi-planar reconstruction of the left anterior descending artery (A, B). Vessel analysis using the plaque tool in a longitudinal plane (C) and transverse sections
Reprinted from (Kristensen, et al., 2010), Copyright (2015) with permission from Elsevier

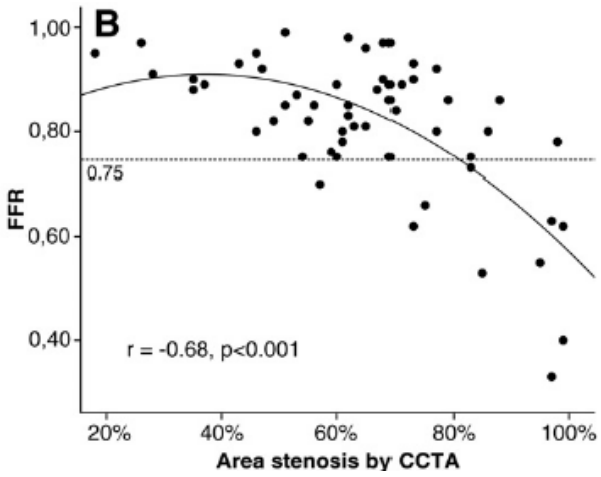

Figure 2.11: Correlation between % Area stenosis and FFR
Reprinted from (Kristensen, et al., 2010), Copyright (2015) with permission from Elsevier

There was discordance between anatomical and functional stenosis severity by considering lesion length and percent diameter alone. But there was a significant correlation between percent AS which is derived from CCTA images and FFR (Figure 2.11) (Kristensen, et al., 2010).

2.6.2. Intravascular ultrasound (IVUS)

Cross-sectional anatomical imaging can be obtained from the IVUS (Figure 2.9C). Since the IVUS offers greater sensitivity in terms of diagnosing the disease, it is widely used as a standard method for identifying anatomical atherosclerosis in vivo (Nissen & Gurley, 1991; Nissen & Yock, 2001). Regardless of the detailed anatomical and physiological information provided by the IVUS, there are some practical limitations, such as the inability to insert the catheter into the regions of excessively lengthy and complex vessels, calcified, non-calcified, fibrous stenosis, and in remarkably small arteries. Other limitations include non-uniform rotational distortion (NURD) with mechanical IVUS transducers and the distortion of the cross-sectional image if the IVUS catheter image plane is not perpendicular to the long axis of the vessel (Tobis, et al., 2007).

2.7. Hemodynamic parameters assessing functional significance of stenosis severity

Assessment of physiological severity of an intermediate stenosis in a single vessel or branched vessel using usual coronary angiogram or multi slice computed tomography is more complex (S.-J. Park et al., 2012; Tobis, et al., 2007). The true functional severity of coronary artery stenosis is assessed by pressure drop and flow (Gould, 2006; N. H. Pijls et al., 1996; N. H. Pijls, et al., 1995). Coronary flow reserve index and fractional flow reserve index are the two parameters that provide physiological information about the severity of the coronary artery stenosis. Among them, the FFR is currently used as a gold standard for the assessment of functional significance of stenosis severity.

2.7.1. Coronary flow reserve (CFR)

Coronary flow reserve (CFR) is defined as the ratio of hyperemic mean blood flow to the resting blood flow. The rate of flow through the coronary arteries is difficult to measure in the catheterization lab, but the flow velocity can be measured using the Doppler guide wire. This parameter usually called as coronary blood flow velocity reserve (CFVR). If the velocity distribution is uniform, the CFR is equal to CFVR (Shalman, Rosenfeld, Dgany, & Einav, 2002). Other non-invasive techniques used to assess the CFR are (i) Echocardiography (ii) Positron emission tomography (PET). If the severity of the stenosis increases, CFR value will decrease (Gould, Kirkeeide, & Buchi, 1990) and vice versa. A CFR value of 2.5 has been identified as being functionally significant (Serruys et al., 1997). Normal coronary blood flow reserve is even higher due to the dilatation of the arterial lumen (well above 3 and up to 5). The CFR value depends upon both, the epicardial and the micro-vascular resistance, and this

is also affected by myocardial chamber hypertrophy, diabetes, and age (Tobis, et al., 2007).

2.7.2. Fractional flow reserve (FFR)

Fractional flow reserve (FFR) is a well validated and is highly reproducible index for assessing functional significance of a coronary stenosis in most of the catheterization laboratory with sensitivity, specificity and diagnostic accuracy of 88%, 100% and 93% respectively (N. H. Pijls, et al., 1996). In a stenosed coronary artery (Figure 2.12), the FFR is defined as the ratio between the maximal achievable coronary flow in the stenotic coronary artery and the maximal flow or hyperemic flow in the same vessel if it were normal.

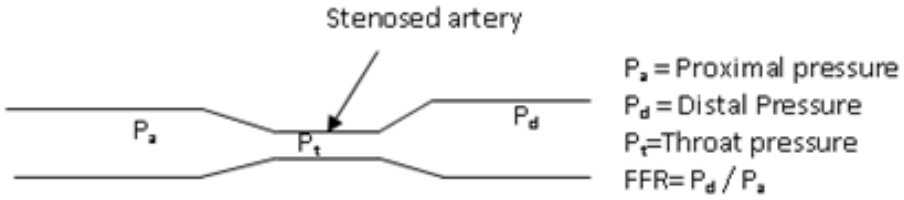

Figure 2.12: Simplified schematic representation of stenosis geometry. P_a and P_d are measured by guiding the catheter attached with a pressure sensor

Hyperemia is a condition that blood flow has been increased through stenotic vessel which is induced by vasodilator agent adenosine or papaverine. Myocardial fractional flow reserve (FFR_{myo}) is defined as the ratio between the distal pressure P_d (which is measured remarkably close to the distal stenosis) and the proximal pressure P_a (equivalent to mean aortic pressure) of the stenosis (N. H. Pijls, et al., 1996; Tobis, et al., 2007) and it has a value of 1 under no stenotic condition.

$$FFR_{myo} = \frac{P_d}{P_a} \tag{2.2}$$

The FFR is easy to measure during coronary intervention (Bernard De Bruyne et al., 2012). A suitable 0.014" diameter wire with pressure sensors located at an offset distance of approximately 3 cm from the tip is inserted across the stenosis and the absolute mean pressure P_a and P_d are recorded during maximal hyperemia. The arterial hyperemia is induced through intravenous infusion of vasodilator medications like adenosine (Tobis, et al., 2007). The FFR is linearly related to the maximum achievable blood flow (N. H. J. Pijls & Sels, 2012). A cut-off value FFR of 0.75 detects ischemia. Recent studies show that an FFR of less than 0.8 is functionally significant. If FFR < 0.75, then angioplasty or coronary artery bypass graft may be recommended (Hau, 2004; Kern & Samady, 2010; N. H. Pijls, et al., 1995). If FFR > 0.8, then, medical therapy may be recommended instead of surgical intervention and this may minimize unnecessary procedures. In the uncertainty region, the FFR value lies between 0.75 and 0.8.

The FFR measurement is also an extremely useful index for patients who suffer from multi-vessel disease. For patients with multi-vessel coronary disease, it is important to identify the culprit lesion which is responsible for ischemia. The FFR measurement is useful in this type of patients. The FFR is independent of blood pressure, heart rate, and contractility (N. H. Pijls, et al., 1995; N. H. J. Pijls, G. J. W. Bech, B. De Bruyne, & A. van Straten, 1997).

However, the FFR is not applicable to assess severity of serial stenoses. Since the physiological significance of each lesion is influenced by the presence of the other, a

more complex approach must be used to measure the severity of each stenosis in a vessel having serial stenoses. True FFR of the selected lesion is defined as the FFR of the selected lesion if the other lesions are physically removed (B. De Bruyne et al., 2000; N. H. Pijls et al., 2000).

Some of the limitations of FFR include, during hyperemic condition, myocardial resistances are minimal and remain constant and the central venous pressure (P_v) is assumed very small and hence neglected. FFR is completely dependent on the maximal hyperemic flow. Failure in achieving maximal hyperemic flow may not achieve the minimal microvascular resistance which will lead to underestimation of pressure drop and overestimation of FFR across the stenosis (N. H. Pijls, Kern, Yock, & De Bruyne, 2000).

2.8. Hemodynamic functional severity parameters derived from principles of fundamental fluid dynamics

Banerjee et al. (Banerjee et al., 2007) have developed diagnostic parameters such as a pressure drop coefficient (CDP), and Lesion flow coefficient (LFC) which are derived from the fundamentals of fluid mechanics in a coronary artery having a single stenosis.

2.8.1. Pressure drop coefficient (CDP)

CDP is defined as the ratio of mean trans-stenotic pressure drop ($\Delta\tilde{p}$) to proximal dynamic pressure. CDP uses pressure and flow measurements to assess stenosis severity and CDP has an advantage here, of being able to delineate epicardial stenosis and micro-vascular disease (Banerjee, et al., 2007).

$$CDP = \frac{\Delta \tilde{P}}{0.5\rho U^2_{Proximal}} \tag{2.3}$$

CDP depends on the geometry of the stenosis, flow rate, presence of the guide wire, and the flow pattern. Guide wire insertion affects viscous and momentum change losses. Further, Figure.2.13 (R. Banerjee et al., 2008) shows a linear correlation between FFR and CDP which is useful for identifying the functional significance of intermediate stenosis severity.

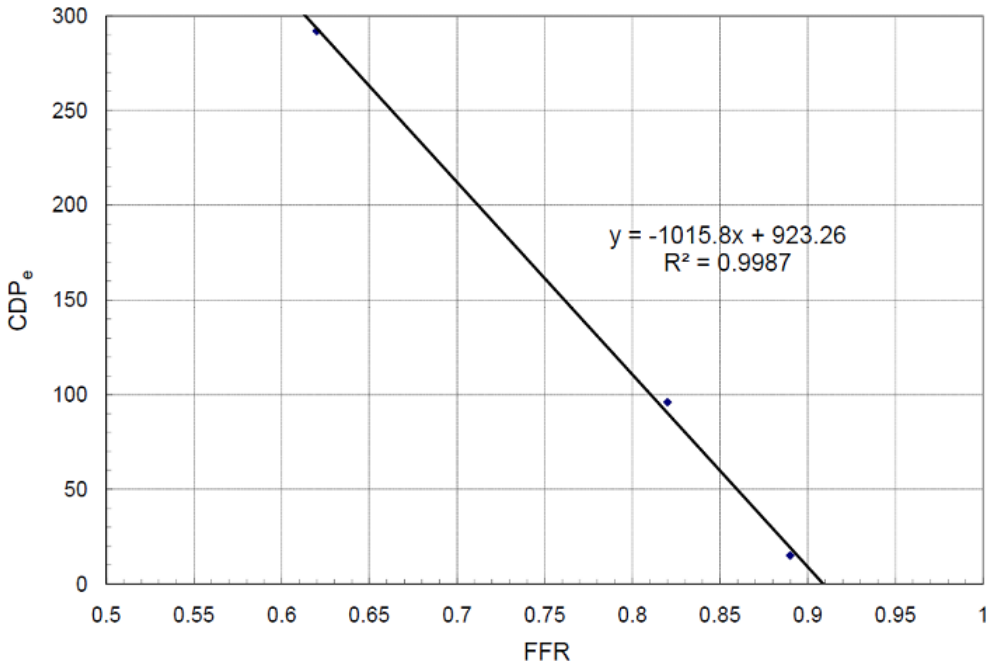

Figure 2.13: A relation between FFR and CDP (R. Banerjee, et al., 2008).

In the intermediate stenosis, FFR is limited to a small range (0.8 - 0.75) whereas, CDP has a wide range. Therefore, a better and more accurate threshold cut off value can be found for CDP after human clinical trials. The linear correlation indicates that the CDP could be a possible diagnostic tool to identify the stenosis severity.

2.8.2. Lesion flow coefficient (LFC)

Lesion flow coefficient ($\tilde{c}$) is a normalized and non-dimensional diagnostic parameter (Banerjee, et al., 2007) which combines hemodynamics and geometric parameters of coronary stenosis. In a stenosed artery, the LFC is defined as the ratio of percentage area stenosis to the square root of CDP evaluated at the site of stenosis at hyperemia. The LFC ranges from 0 to 1. Since the $\tilde{c}$ correlates well with FFR, it is also one of the factors to find coronary stenosis severity and has been proven for the porcine model by Sinha Roy et al. (Sinharoy et al., 2008). The cut-off value for the parameter is yet to be determined for the clinical evaluation.

2.9. Factors influencing coronary diagnostic parameters

Many studies have been performed in the uncertainty region during the past years. Insertion of sensor tipped guide wire (Sinha Roy, et al., 2006), downstream collateral flow (Peelukhana, et al., 2009) and other factors such as micro vascular resistance, aortic and coronary outflow pressure (Maria Siebes, et al., 2002), arterial wall compliance, plaque characteristics (Konala, et al., 2011) etc. have been significantly affecting the coronary diagnostic parameters.

2.9.1. Increasing doses of intracoronary adenosine

FFR is a well validated and highly reproducible for the assessment of functional severity of coronary artery stenosis. It is based on the change in the pressure gradient across the stenosis after the achievement of maximal hyperemia of the coronary microcirculation that may be obtained by either intracoronary bolus or intravenous

infusion of adenosine. (De Luca, Venegoni, Iorio, Giuliani, & Marino, 2011). Attainment of hyperemia is a primary pre- request for the accurate measurement of FFR to minimize the contribution of microvascular resistance (N. H. J. Pijls & Sels, 2012). With suboptimal microcirculatory coronary hyperemia might result in underestimation of the functional significance of the stenosis severity.

There are two routes of adenosine administration to measure FFR namely (i) Intravenous (ii) intracoronary. In vivo study reveals that the FFR decreases by higher doses of adenosine i.e. high doses of intracoronary adenosine increased the sensitivity of FFR in the detection of hemodynamically relevant coronary stenoses and vice versa (De Luca, et al., 2011; López-Palop et al., 2013).

2.9.2. Hemodynamic conditions (Coronary micro vascular resistance, aortic and venous pressure)

It is assumed that the measurement of FFR is independent of hemodynamics but external hemodynamic conditions affect the pressure-flow characteristics at hyperemia condition (Klocke, Mates, Canty, & Ellis, 1985). Also, stenosis resistance is flow dependent. Since the flow is determined by the pressure gradient and resistance, the common fluid dynamic equation can be used to evaluate the pressure gradient (Δp) across the stenosis is given by

$$\Delta P = A\tilde{Q} + B\tilde{Q}^2 \tag{2.4}$$

Where A is the coefficient of viscous pressure losses along the stenosis, and B is the coefficient for inertial pressure losses at the exit of the stenosis and $\tilde{Q}$ is the mean

hyperemic flow rate (Maria Siebes, et al., 2002). In the absence of collateral flow FFR is defined as

$$FFR = \frac{Q_s^{\max}}{Q_N^{\max}} = \frac{P_d - P_v}{P_a - P_v} \tag{2.5}$$

In a clinical settings, the P_v is the venous pressure assumed to be negligible. The FFR is approximated by

$$FFR \approx 1 - \frac{\Delta P}{P_a} \tag{2.6}$$

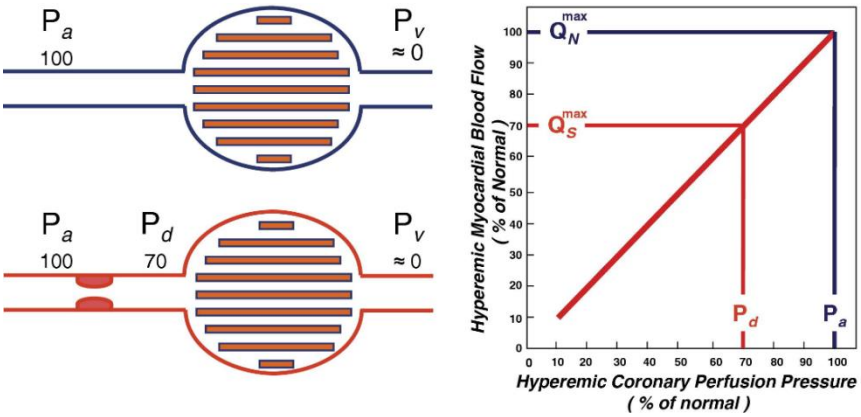

Figure 2.14: Concept of Fractional Flow Reserve Measurements
Reprinted from (N. H. J. Pijls & Sels, 2012), Copyright (2015) with permission from Elsevier

Increasing in stenosis severity, changes in aortic pressure, coronary microvascular resistance (R_{coro}) and out flow pressure(P_v) affect both the relative maximal flow and the corresponding pressure ratio representing FFR. For a given stenosis severity, increasing P_a or decreasing R_{coro} decreases the FFR (Maria Siebes, et al., 2002).

2.9.3. Lesion Length

Fractional flow reserve has become a gold standard in functional assessment of coronary artery stenosis severity. Lesion length is an important geometric variable that might affect the hemodynamics and hence the diagnostic parameters for a given percentage area stenosis severity (Brosh, Higano, Lennon, Holmes Jr, & Lerman, 2005;

Rajabi-Jaghargh, Kolli, Back, & Banerjee, 2011).The lesion throat length is directly related to the resistance for the coronary hyperemic flow and alters the pressure drop for a given percentage AS severity (Rajabi-Jaghargh, et al., 2011). A categorized cutoff lesion length value of 10 mm was identified as a sensitive predicting index for a categorized cutoff FFR value of 0.75 (Brosh, et al., 2005).

2.9.4. Guide wire flow obstruction

The true severity of artery stenosis can be assessed by pressure drop and flow. A sensor tipped guide wire inserted across the coronary stenosis causes a reduction in coronary flow (A. S. Roy et al., 2005) and increases both the losses of viscous and due to momentum change (Rajabi-Jaghargh, et al., 2011). The insertion guide wire alters and overestimates the hyperemic pressure drop (A. S. Roy, et al., 2005) which in turn leads to misinterpret the true functional severity of the stenosis. The insertion of guide wire increases the true percentage of area stenosis i.e. if the guide wire size increases, the percentage area stenosis increases and vice versa.

In the current clinical settings, an intracoronary pressure wire of diameter 0.014" is used to record the distal pressure under hyperemic condition, which is induced by micro-vascular vasodilator, adenosine or papaverine (N. H. J. Pijls & Sels, 2012). It is significant that insertion of guide wire increases the hyperemic pressure drop in moderate to intermediate stenosis severity whereas negligible effect found in hyperemic pressure drop for severe stenosis as compared to without guide wire (Rajabi-Jaghargh, et al., 2011). This might be due to the reduction in hyperemic flow rate as stenosis severity increases. Since the coronary diagnostic parameter FFR, and CDP and LFC contains hyperemic pressure data to evaluate the functional significance the stenosis

severity, the insertion of guide wire overestimate the hyperemic pressure drop and it masks the true functional severity of the stenosis.

2.9.5. Collateral flow

When there are functional collaterals present in the downstream to the stenosis, the total coronary flow increases which alters the hyperemic pressure drop and hence the coronary diagnostic parameters (Peelukhana, et al., 2009). In the presence of downstream collateral flow, the hyperemic pressure drop across the stenosis is lower than the pressure drop when there is no collateral flow. Since the coronary diagnostic parameters are derived from hyperemic pressure drop and flow, the collateral flow masks the true severity of the stenosis which might lead to misinterpretation of the functional significance of the coronary artery stenosis and measured FFR might wrongly lead to the postponement of the coronary interventional procedures, especially in patients with intermediate stenosis. Further, the CDP and LFC also affected which confirms that the true severity is masked due to the collateral flow.

2.9.6. Arterial wall-stenosis compliance (c)

Arterial compliance is the ratio of percentage diameter change and the difference between maximum pressure $(P_{\max})$ and minimum pressure $(P_{\min})$ measured in mmHg at systole and diastole respectively.

$$c = \frac{d_{\max} - d_{\min}}{d_{\min} \times (P_{\max} - P_{\min})} \times 100 \qquad (2.7)$$

Where d_{max} and d_{min} are the diameters (cm) at P_{max} and P_{min}, respectively (Konala, et al., 2011; Abhijit Sinha Roy, Back, & Banerjee, 2008)

Stenosis compliance is one of the factors for angina complaints, especially during periods of low microvascular resistance (M. Siebes et al., 2004). The arterial wall-stenosis compliance was caused by either calcification or smooth muscle cell proliferation (Konala, et al., 2011). Arterial compliance reduces with increasing age (Alfonso et al., 1994) and it becomes rigid (no compliance). The arterial wall-stenosis compliance masks the true severity of the stenosis. The variability in diagnostic parameters due to arterial wall –stenosis compliance had been studied in detail by Konala et al. (2011) and found that for a given stenosis geometry, the hyperemic pressure drop across the stenosis decreases as the wall compliance increases and hence the current clinical diagnostic parameter FFR increases. This increment in FFR leads the clinician to misdiagnose the severity of the stenosis and postponement of the coronary interventional procedure, especially for the intermediate stenosis severity. The misdiagnose region was found between 78.7%- 82.7% AS. Further, the CDP and LFC also affected which confirms that the arterial wall-stenosis compliance might lead to misinterpretation of stenosis severity.

2.9.7. Contractility and heart rate

From the in vivo study, the variation in contractility (CY) and heart rate (HR) alters the coronary diagnostic parameters (Kranthi K Kolli et al., 2011; K. K. Kolli et al., 2011; Kranthi K. Kolli et al., 2010). The fluctuation in cardiac contractility alters FFR and CDP significantly (Figure 2.15). The heart rate variations have no significant effect on FFR and CDP but marginal significance found on LFC (Figure 2.16)

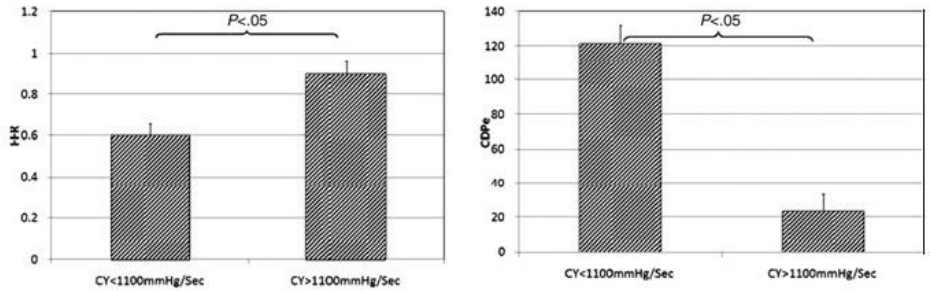

Figure 2.15: Influence of contractility on FFR and CDP
Reprinted from(Kranthi K. Kolli, et al., 2010), Copyright (2015) with permission from Elsevier

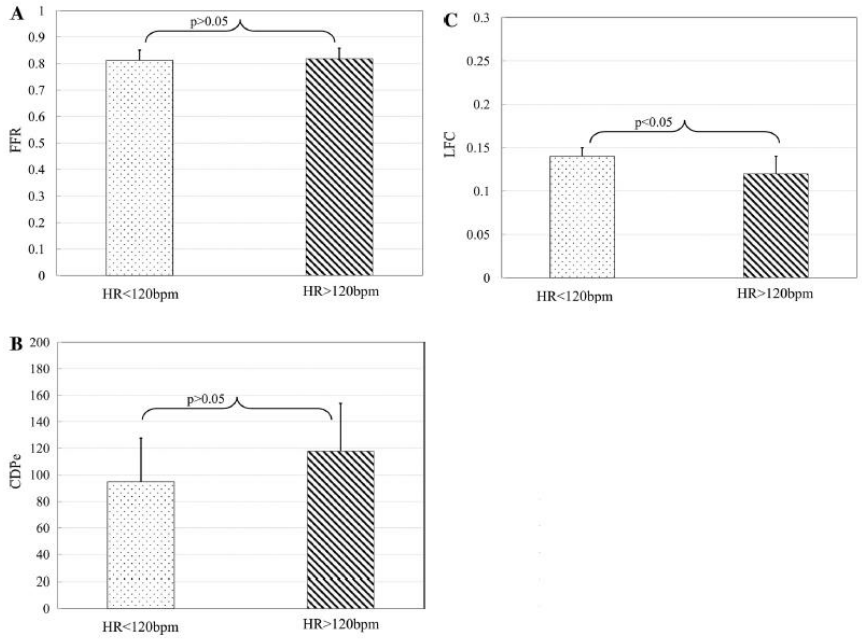

Figure 2.16: The influence of heart rate on (A) FFR (B) CDP and (C) LFC (Kranthi K Kolli, et al., 2011)

2.10. Computational Fluid Dynamics (CFD) on coronary flow

2.10.1. Coronary artery and stenosis modelling

3D models of coronary artery plays substantial role in the diagnosis and treatment of coronary artery diseases. Hemodynamic analysis in coronary artery can be performed using CFD method using either simulated models or realistic coronary artery geometry simulations (Lim & Kern, 2006; Shanmugavelayudam, Rubenstein, & Yin, 2010; Wellnhofer et al., 2010). Idealized solid models of coronary arteries and stenosis were

developed by using any one of the computer aided design software's such as Pro/ Engineer (Parametric Technology co., USA), SolidWorks (Dessault, SolidWorks Corp., France).

3D coronary model can be generated using CT angiography image data (Esses, Berman, Bloom, & Sosna, 2011). In CT workstation, the image data was saved in digital imaging and communication in medicine (DICOM) format. Reconstruction or segmentation of coronary artery was performed using post-image processing technique using any one of the image interpretation software's such as MATLAB, Mimics, Analyze, and Amira etc. The 3D segmented artery models were saved in STL format which is useful for further CFD analysis (Chaichana, Sun, & Jewkes, 2011)

2.10.2. Effect of stenosis on blood flow behavior

Blood mainly consists of plasma and red blood cells. When blood flows in the larger arteries, the shear rate is sufficiently high and it behaves like a Newtonian fluid (Berger & Jou, 2000). However, if the flow occurs in a narrowed stenosed artery, the red cell particles' interactions are more, and the shear rate will be less than 100 s^{-1}. The red cells tend to move outwards in the column of blood and thus, increase the viscosity of the blood. Under such conditions, blood behaves like a Non-Newtonian fluid (Johnston, Johnston, Corney, & Kilpatrick, 2006). The flow and shear rates are low in the outlet post-stenotically but are rather high in the inlet and bottlenecks of stenosis. It has been noted that patients with severe stenosis condition, hypertension and cerebrovascular diseases, blood behaves like non-Newtonian properties (Tu & Deville, 1996). There are five different types of non-Newtonian models from the literature and these are tabulated

in Table 2.2. The blood viscosity and shear stress as a function of strain of non-Newtonian models are given in the Figure 2.17.

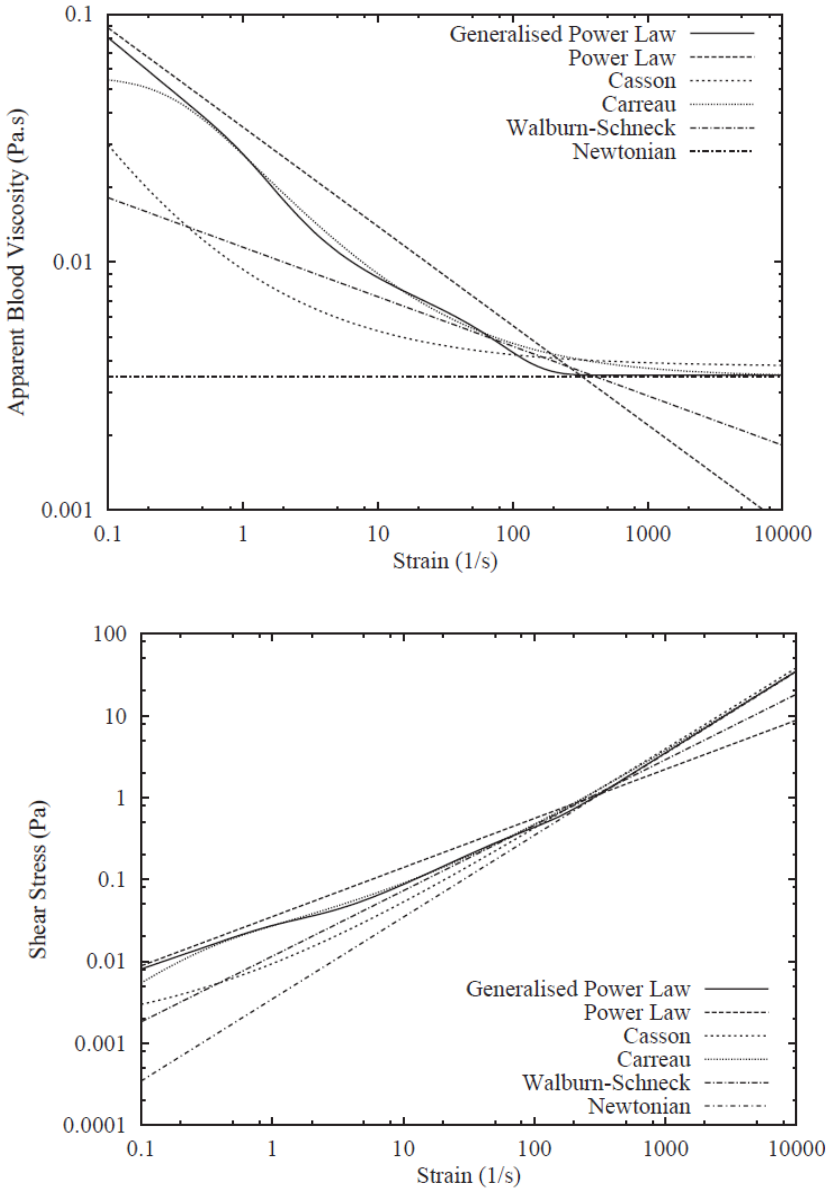

Figure 2.17: Viscosity and shear stress as a function of strain for different blood models
Reprinted from (Johnston, Johnston, Corney, & Kilpatrick, 2004), Copyright (2015) with permission from Elsevier

Table 2.2 : Non-Newtonian blood models

Blood model	**Effective viscosity**
Carreau model (Y. I. Cho & Kensey, 1991)	$\mu = \mu_\infty + (\mu_0 - \mu_\infty)[1+(\lambda\dot{\gamma})^2]^{(n-1)/2}$
Walburn–Schneck model (Walburn & Schneck, 1976)	$\mu = C_1 e^{C_2 H}\left(e^{C_4 (TPMA/H^2)}\right)\dot{\gamma}^{-C_3 H}$ Where $C_1 = 0.00797$, $C_2 = 0.0608$, $C_3 = 0.00499$, $C_4 = 14.5851\, g^{-1}$, Hematocrit $H = 40\%$ and sum of fibrinogen and globulin concentrations $TPMA = 25.91\, g\, l^{-1}$
Power Law (Y. I. Cho & Kensey, 1991)	$\mu = \mu_0(\dot{\gamma})^{n-1}$ Where $\mu_0 = 0.035$ and $n = 0.6$
Casson model (Fung, 1993)	$\mu = \left[\left(\eta^2 J_2\right)^{1/4} + 2^{-1/2}\tau_y^{1/2}\right]^2 J_2^{-1/2}$, Where $\lvert\dot{\gamma}\rvert = 2\sqrt{J_2}$, $\tau_y = 0.1(0.625H)^3$ and $\eta = \eta_0(1-H)^{-2.5}$ with $\eta_0 = 0.012P$ and $H = 0.37$
Generalized Power Law model (Ballyk, Steinman, & Ethier, 1994)	$\mu = \lambda\lvert\dot{\gamma}\rvert^{n-1}$, $\lambda(\dot{\gamma}) = \mu_\infty + \Delta\mu \exp\left[-\left(1+\frac{\lvert\dot{\gamma}\rvert}{a}\right)\exp\left(\frac{-b}{\lvert\dot{\gamma}\rvert}\right)\right]$, $n(\dot{\gamma}) = n_\infty - \Delta n \exp\left[-\left(1+\frac{\lvert\dot{\gamma}\rvert}{c}\right)\exp\left(\frac{-d}{\lvert\dot{\gamma}\rvert}\right)\right]$, Where $\mu_\infty = 0.035$, $n_\infty = 1.0$, $\Delta\mu = 0.45$, $\Delta n = 0.45$, $a = 50$, $b = 3$, $c = 50$, and $d = 4$

Coronary flow is complex and tt comprises a complex pattern of neuro-humoral and local regulation, where the surrounding cardiac muscles play an important role. The difference in the material properties of the arterial wall elasticity are due to various factors, namely calcified plaque, rigidity of the wall due to arteriosclerosis, and blockage due to smooth muscle cell proliferation. All of these influence both, the pressure and flow behavior.

A non-dimensional frequency parameter or the Womersley parameter ($\alpha = R\sqrt{\omega/\nu}$, where R is the artery radius, ω is the angular frequency, and ν is kinematic viscosity) highlights the relationship between the unsteady flow and viscous forces. The typical range of Reynolds number of blood flow in the body varies from 1 in small arterioles to approximately 4000 in the largest artery, the aorta (Ku, 1997). It is well-known that the Reynolds number and the frequency parameter value influence the pulsatile fluid flow. In a stenotic coronary flow, the pressure losses generally depends on orifice shape and the upstream Reynolds number (Ku, 1997). The mean proximal Reynolds number ($\tilde{\mathrm{R}}\mathrm{e} = 4\tilde{Q}/\pi d\nu$, where d is the proximal vessel diameter and ν is kinematic viscosity of blood) ranges from 100 to 230 and from 100 to 360 before and after coronary interventions for the pathophysiological flow, respectively.(A. S. Roy, et al., 2005).

2.11. Computational fluid dynamics advantages in coronary flow

Computational fluid dynamics (CFD) is a branch of fluid mechanics and has the ability to solve complex fluid flow problems by using numerical methods and algorithms. The CFD technique allows for the analysis of different clinical situations. It is useful in the study of coronary artery flows, instead of complicated and expensive in vivo

measurements enabling quantification of the hemodynamic of healthy and diseased blood vessels. For example, a full hemodynamic analysis can be done if the stenosis geometry, coronary flow, and coronary pressure, etc. are known. The CFD simulations can be used to provide missing data such as Wall Shear Stress (WSS) distribution, particle traces, Non-Newtonian importance factors, and other hemodynamic parameters to improve clinical decision-making and make it appropriate and accurate in both, the steady state and in transient simulations (Johnston, et al., 2004, 2006; Mallinger & Drikakis, 2002; Perktold et al., 1997). The computational approach has to be improved upon by considering anatomically correct geometric models, since a precise change in geometry can affect the flow field significantly.

The artery geometry, WSS, WSS gradient, and the oscillatory shear index are important risk factors in CAD. Since the coronary artery walls are small in size having approximately 3 mm in diameter, the CFD simulation is useful in assessing the risk factors (Knight et al., 2010). The impact of side branches of the coronary artery on WSS can be analyzed by using CFD technique. It was found that the WSS distribution was non-linear and depended on geometric shapes (Wellnhofer, et al., 2010).

Stenosis' severity is measured by considering the pressure gradient and velocity of blood. A small change in the pressure drop and flow will highlight an uncertainty or misinterpret the severity of the intermediate stenosis. In such conditions, the CFD technique proves to be a useful tool in the flow simulations undertaken to analyze the physical quantities.

In the current clinical settings, the invasive FFR is currently used as the gold standard to assess the functional significance of the severity of coronary stenosis by inserting

pressure or flow sensor tipped guide wire across the stenosis. The FFR can be measured non- invasively from the reconstructed CCTA images by the help of CFD analysis (Koo et al., 2011).

The CFD technique is also useful in finding the variability of the coronary diagnostic parameters due to the guide wire insertion, arterial wall compliance etc. as discussed in the section §2.9.

2.12. Motivation and significance of the study

Blood is a moving column with suspended cells. Normal endothelium did not allow passage of cells. However, it has been shown that atherosclerotic endothelium is highly permeable to white cells and platelets in the event of plaque rupture. Recells are also shown to enter to tunica media (Libby, Ridker, & Maseri, 2002).

One of the major limitations of the well published studies is that the coronary artery wall is impervious to blood. From the literature, it is clear that all the human tissues are porous in nature (Chakravarty & Sannigrahi, 1998; Dabagh, Jalali, Konttinen, & Sarkomaa, 2008; Khakpour & Vafai, 2008; Prosi, Zunino, Perktold, & Quarteroni, 2005) and the plaque region mainly includes a large lipid core and a thin fibrous cap (Tang et al., 2009). It is useful to study the pulsatile non-Newtonian blood flow through stenotic arteries taking into account of blood transport through the porous arterial wall, and to investigate the effect of porous media on the diagnostic parameters. Hence, It is highly desirable to study the effect of porous media of the stenosed artery wall to the coronary physiological diagnostic parameter for a given stenosis severity and identify a

region of misdiagnosis when assessing the stenosis severity using CCTA image analysis.

Similarly, the artery wall curvature augments the flow resistance in addition to the blockage. The curvature further decreases the pressure at the site of stenosis for a given stenosis severity. Hence it is highly desirable to study the influence of artery wall curvature on the coronary diagnostic parameter FFR, and CDP and LFC for a given stenosis severity from straight artery to curved artery and identify a region of misdiagnosis when assessing the anatomical significance of stenosis severity using FFR as a standard parameter.

Coronary artery bifurcation angulation variations distal to the stenosis affects the flow through LAD and LCX. Hence it is highly desirable to study the influence of artery wall bifurcation angulation on coronary diagnostic parameter FFR, and CDP and LFC for a given stenosis severity and identify a region of misdiagnosis when assessing the stenosis severity in-vitro using FFR as a standard parameter.

3. NUMERICAL METHODS

3.1. Introduction

Computational fluid dynamics (CFD) is the analysis of systems involving fluid flow, heat transfer and associated phenomena such as chemical reactions by means of computer-based simulation. Apart from the CFD technique and the finite volume method used in the discretization of mass, momentum and turbulence, this chapter also discuss the characteristics of the fluid, boundary conditions and discretization of the numerical method used in the simulations are presented.

3.2. Finite volume method

In the finite volume method, the computational domain is subdivided into large number of control volumes in which the conservation equations are applied. The conservation equation in the form of control volume integration as a starting point is given in equation 3.1

$$\int_{CV} \frac{\partial(\rho\phi)}{\partial t} dv + \int_{CV} div(\rho\phi u) dv = \int_{CV} div(\Gamma grad\phi) dv + \int_{CV} S_{\phi} dv \qquad (3.1)$$

This equation consists of various transport process such as the rate of change and convective term on the left side of the equation and diffusion term and source terms on the right side of the equation. By applying Gauss's divergence theorem, volume integral of the convective and diffusive terms are rewritten as

$$\int_{CV} div(a)dv = \int_{A} n.a\, dA \tag{3.2}$$

$n.a$ is the component of vector *a* in the direction of the vector ***n*** normal to surface element d*A*. The equation (3.1) can be written as

$$\frac{\partial}{\partial t}\left(\int_{CV} \rho\phi\, dV \right) + \int_{A} n.(\rho\phi u)\, dA = \int_{A} n.(\Gamma grad\ \phi)\, dA + \int_{CV} S_{\phi} dv \tag{3.3}$$

It is common practice to set up control volumes near the edge of the domain in such a way that the physical boundaries coincide with the control volume boundaries (Versteeg & Malalasekera, 2007).

3.3. Computational blood flow model

Blood exhibits Newtonian effects only in larger arteries whereas non-Newtonian effect in small arteries and capillaries. It will be assumed that the flow of blood is incompressible and governed by the Navier Stokes equations.

$$\rho\left(\frac{\partial v}{\partial t} + v.\nabla v \right) = -\nabla.\tau - \nabla p \tag{3.4}$$

and the continuity equation for incompressible flow is

$$\nabla.v = 0 \tag{3.5}$$

Here $\vec{v}$ is the three dimensional velocity vector, t the time, ρ the blood density, p the pressure and τ the stress tensor. In this work, a non-Newtonian blood is assumed to follow the Bird-Carreau model and the blood viscosity μ given in poise (P) as a function of shear rate $\dot{\gamma}$ given in s^{-1} is given by

$$\mu = \mu_{\infty} + (\mu_0 - \mu_{\infty})[1 + (\lambda\dot{\gamma})^2]^{(n-1)/2} \tag{3.6}$$

Where, λ (Time constant) = 3.313s, n (Power law index) = 0.3568, μ_0 (Low shear viscosity) = 0.56 P and μ_{∞} (High shear viscosity) = 0.0345 P. The density of the blood (ρ) is assumed as $1050\ kg/m^3$. It should be noted that the above equations are useful for both incompressible laminar and turbulent flow. Analytical solutions of the Navier-Stokes equations exist for only a few laminar flow cases, such as pipe and annulus flows or boundary layers. Turbulent flows are modeled by using various turbulence modeling schemes.

3.4. Turbulence modeling

Two equation turbulence models such as $k-\varepsilon$ and $k-\omega$ models are widely used. In the $k-\varepsilon$ model k is the turbulence kinetic energy and ε is the turbulence eddy dissipation (the rate at which fluctuation in velocity dissipates). In the $k-\omega$ turbulence model, k is the turbulent kinetic energy and ω is the turbulent frequency (Wilcox, 1994). The k-ω model has a capability to solve the near wall treatment for low Reynolds computation. Since the flow through stenosed artery during hyperemia condition become turbulent. In this work the standard k-ω model and k-ω based Shear Stress Transport (SST) have been discussed in detail.

3.4.1. Standard (k-ω) model

$$\frac{\partial \rho}{\partial t} + \frac{\partial}{\partial x_i}\left(\rho u_i\right) = 0 \tag{3.7}$$

$$\frac{\partial}{\partial t}\left(\rho u_i\right) + \frac{\partial}{\partial x_j}\left(\rho u_j u_i\right) = \frac{\partial}{\partial x_j}\left(-\rho \delta_{ji} + \tilde{\tau}_{ji}\right) \tag{3.8}$$

$$\frac{\partial}{\partial t}\left(\rho k\right) + \frac{\partial}{\partial x_j}\left(\rho u_j k\right) = \tau_{ij}\frac{\partial u_i}{\partial x_j} - \beta^* \rho \omega k + \frac{\partial u}{\partial x_j}\left[\left(\mu + \sigma^* \mu_T\right)\frac{\partial k}{\partial x_j}\right] \tag{3.9}$$

(Kaye et al.)

$$\frac{\partial}{\partial t}\left(\rho \omega\right) + \frac{\partial}{\partial x_j}\left(\rho u_j \omega\right) = \alpha \frac{\omega}{k}\tau_{ij}\frac{\partial u_i}{\partial x_j} - \beta \rho \omega^2 + \frac{\partial}{\partial x_j}\left[\left(\mu + \sigma \mu_T\right)\frac{\partial \omega}{\partial x_j}\right] \tag{3.10}$$

$$\hat{\tau}_{ij} = 2\mu\left(S_{ij} - \frac{1}{3}\frac{\partial u_k}{\partial x_k}\delta_{ij}\right) + \tau_{ij} \tag{3.11}$$

$$\tau_{ij} = 2\mu_T\left(S_{ij} - \frac{1}{3}\frac{\partial u_k}{\partial x_k}\delta_{ij}\right) + -\frac{2}{3}\rho k \tau_{ij} \tag{3.12}$$

$$\mu_T = \alpha^* \rho k / \omega \tag{3.13}$$

$$S_{ij} = \frac{1}{2}\left(\frac{\partial u_i}{\partial x_j} + \frac{\partial u_j}{\partial x_i}\right) \tag{3.14}$$

In Eqs. (3.7 - 3.14), t is the time, x_i is position vector, u_i is velocity, ρ is density, *p* is pressure, μ is molecular viscosity, and $\hat{\tau}_{ij}$ is the sum of molecular and Reynolds stress tensors. Also, δ_{ij} Kronecker delta, *k* is the turbulence kinetic energy, ω is the turbulent frequency τ_{ij} is Reynolds stress tensor, and μ_T is eddy viscosity. The six parameters $\alpha^*, \alpha, \beta^*, \beta, \sigma^*$ and σ are closure coefficients whose values are given below

$$\alpha^* = \frac{\alpha_0^* + \mathrm{Re}_T / R_k}{1 + \mathrm{Re}_T / R_k} \tag{3.15}$$

$$\alpha = \frac{5}{9}\frac{\alpha_0 + \mathrm{Re}_T / R_\omega}{1 + \mathrm{Re}_T / R_\omega}\left(\alpha^*\right)^{-1} \tag{3.16}$$

$$\beta^* = \frac{9}{100}\frac{5/18 + \left(\mathrm{Re}_T / R_\beta\right)^4}{1 + \left(\mathrm{Re}_T / R_\beta\right)^4} \tag{3.17}$$

$$\beta = \frac{3}{40},\ \sigma^* = \sigma = 1/2 \tag{3.18}$$

$$\alpha_0^* = \beta/3,\ \alpha_0 = 1/10 \tag{3.19}$$

$$R_\beta = 8,\ R_k = 6,\ R_\omega = 2.7 \tag{3.20}$$

Where Re_T is the turbulence Reynolds number defined by

$$\mathrm{Re}_T = \frac{\rho k}{\omega \mu} \tag{3.21}$$

3.4.2. Shear-Stress Transport (SST) k-ω (or k-ω-SST) model

The $k-\omega$ based SST model accounts for the transport of the turbulent shear stress and gives highly accurate predictions of the onset and the amount of flow separation under adverse pressure gradient (F. Menter, Kuntz, & Langtry, 2003; F. R. Menter, 2009) .

$$\frac{\partial(\rho k)}{\partial t} + \frac{\partial(\rho U_i k)}{\partial x_i} = \tilde{P}_k - \beta^* \rho k \omega + \frac{\partial}{\partial x_i}\left[\left(\mu + \sigma_k \mu_t\right)\frac{\partial k}{\partial x_i}\right] \tag{3.22}$$

$$\frac{\partial(\rho \omega)}{\partial t} + \frac{\partial(\rho U_i \omega)}{\partial x_i} = \alpha \frac{1}{\nu_t}\tilde{P}_k - \beta \rho \omega^2 + \frac{\partial}{\partial x_i}\left[\left(\mu + \sigma_\omega \mu_t\right)\frac{\partial \omega}{\partial x_i}\right] + 2(1 - F_1)\rho \sigma_{\omega 2}\frac{1}{\omega}\frac{\partial k}{\partial x_i}\frac{\partial \omega}{\partial x_i} \tag{3.23}$$

The turbulent eddy viscosity is defined as

$$v_t = \frac{a_1 k}{\max(a_1 \omega, SF_2)};\ S = \sqrt{2S_{ij}S_{ij}} \tag{3.24}$$

$$P_k = \mu_t \frac{\partial U_i}{\partial x_j}\left(\frac{\partial U_i}{\partial x_j} + \frac{\partial U_j}{\partial x_i}\right) \tag{3.25}$$

$$\tilde{P}_k = \min\left(P_k, 10 \cdot \beta^* \rho k \omega\right) \tag{3.26}$$

Where F_1 and F_2 are blending function which are equal to zero away from the surface and are defined by

$$F_1 = \tanh\left\{\left\{\min\left[\max\left(\frac{\sqrt{k}}{\beta^* \omega y}, \frac{500v}{y^2 \omega}\right), \frac{4\rho\sigma_{\omega 2} k}{CD_{k\omega} y^2}\right]\right\}\right\}^4 \tag{3.27}$$

$$F_2 = \tanh\left[\left[\max\left(\frac{2\sqrt{k}}{\beta^* \omega y}, \frac{500v}{y^2 \omega}\right)\right]^2\right] \tag{3.28}$$

$$CD_{k\omega} = \max\left(2\rho\sigma_{\omega 2}\frac{1}{\omega}\frac{\partial k}{\partial x_i}\frac{\partial \omega}{\partial x_i}, 10^{-10}\right) \tag{3.29}$$

where, k is the turbulence kinetic energy, ω is the turbulence frequency, y is the distance to the nearest wall, S is the strain rate, ρ is the density and U_i is the flow velocity. Constants are computed from the $k-\varepsilon$ and the $k-\omega$ model through $\alpha = \alpha_1 F_1 + \alpha_2(1-F_1)$ The model constants are $\beta^* = 0.09$, $\alpha_1 = 5/9$, $\beta_1 = 3/40$, $\sigma_{k1} = 0.85$, $\sigma_{\omega 1} = 0.5$, $\alpha_2 = 0.44$, $\beta_2 = 0.0828$, $\sigma_{k2} = 1$, $\sigma_{\omega 2} = 0.856$.

3.5. Overview of ANSYS CFX

ANSYS CFX is general purpose Computational Fluid Dynamics (CFD) software. It has a combination of advanced pre and post processing solver capabilities. It has the following features(ANSYS, 2012)

- Reliable and robust coupled solver
- Integration with problem definition, analysis and presentation of results
- It has advanced menus and interactive setup process

ANSYS CFX is capable of modelling

- Steady and transient flows,
- Laminar and turbulent flow for Newtonian and non-Newtonian fluid
- Multiphase flows etc.
- Heat transfer and thermal radiation
- Buoyancy flow
- Subsonic and supersonic flows
- Combustion
- Particle tracking

3.6. The structure of ANSYS CFX

ANSYS CFX consists of four software modules that take a geometry and mesh and pass the information required to perform a CFD analysis (Figure 3.1).

CFX pre is used to define simulations. Mesh geometry can be imported for analysis and applying flow physics, boundary condition, initial values and solver parameters. CFX solver solves all the solution variables for the simulation specified in CFX- pre. CFX

solver manager control the CFD task such as start/stop the CFX solver, monitor the progress of the solution etc. The last part of the ANSYS CFX is ANSYS CFD-Post which provides interactive post processing graphics to analyze the simulation results.

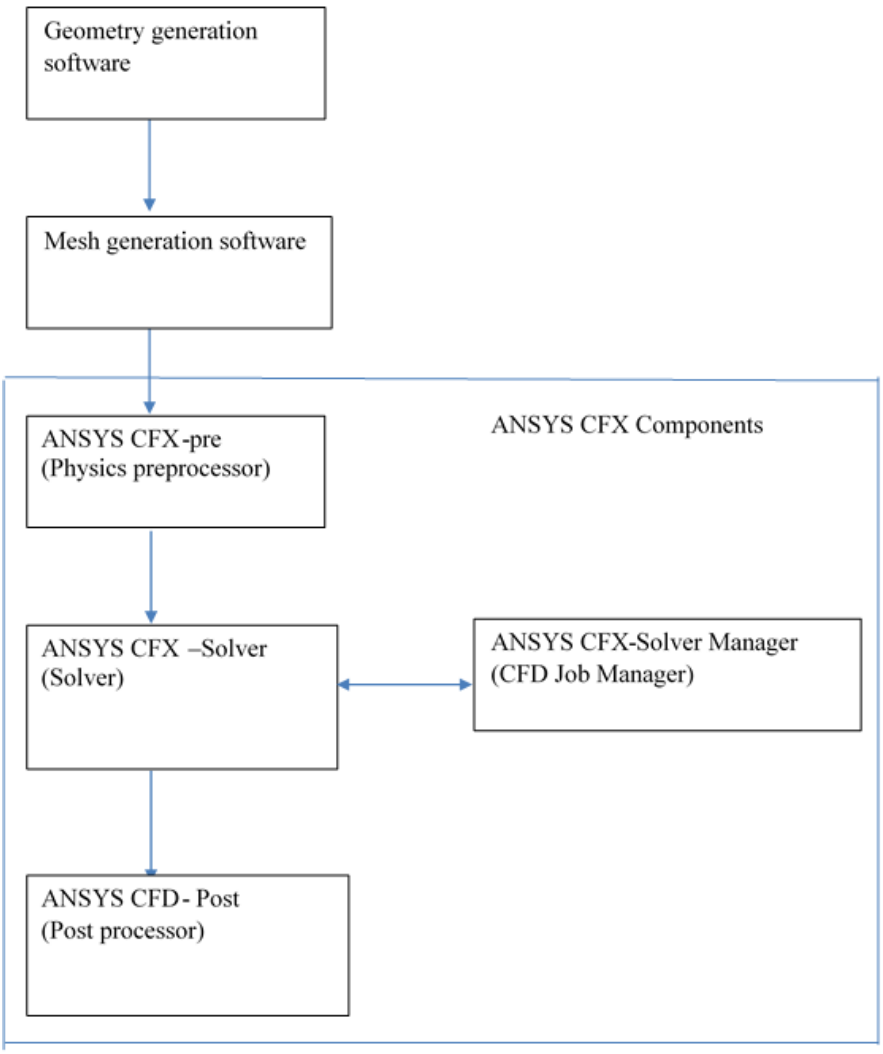

Figure 3.1: Overview of ANSYS CFX

3.7. Mathematical flow modelling and meshing

In this study, coronary artery models with stenosis were created in ANSYS work bench 14.0. The stenosed arterial models of 70% (moderate), 80% (intermediate) and 90% (severe) Area Stenosis (AS) were developed for the computational fluid dynamic analysis. Under hyperemic conditions the possible variations in the diagnostic

parameter FFR, and CDP and LFC due to the following factors have been studied in detail under three severity conditions.

(i) porous stenosed artery model by comparing with Rigid stenosed artery (RA) model

(ii) Curved stenosed artery wall model with straight artery

(iii) Bifurcated artery wall model with various angulation in Left Coronary Artery (LCA) model

The mathematical flow modelling or geometry of the above models have been explained in detail in chapters 4, 5 and 6 and the possible region of misinterpretation of stenosis severity in the clinical anatomical assessment was found using FFR as a standard parameter.

Meshing of the flow domains were done using CFX mesh which is a mesh generator aimed at producing high quality meshes which further can be used in computational fluid dynamics simulations. CFD requires meshes that can resolve boundary layer phenomena and satisfy more stringent quality criteria than structural analysis. The computational domains were initially meshed with structured hexahedral elements. The maximum and minimum elements size was determined by the mesh element size control. The quality of the mesh was tailored by a process called inflation near fluid wall interface. The inflation control is used for resolving the mesh near-wall region to capture the boundary layer effects. The near-wall region boundary layer effects give rise to velocity gradients which are greatest normal to the face. Quality of mesh was checked by inspecting various parameters such as skewness, orthogonal quality, element quality etc. In this work the quality of the mesh determined from skewness

mesh metric which is one of the primary quality measures of mesh. The elements greatly skewed can decrease the accuracy and disrupt the solution. In quantifying the quality of each grid, values of equi-angle skew and equi-volume skew of 0–0.25 are considered excellent, 0.25–0.5 are good and 0.5–0.75 are fair(Thakker & Hourigan, 2005). In our study we obtained more than 75% of the grid could be in excellent and the remaining could be good (Figure 3.2)

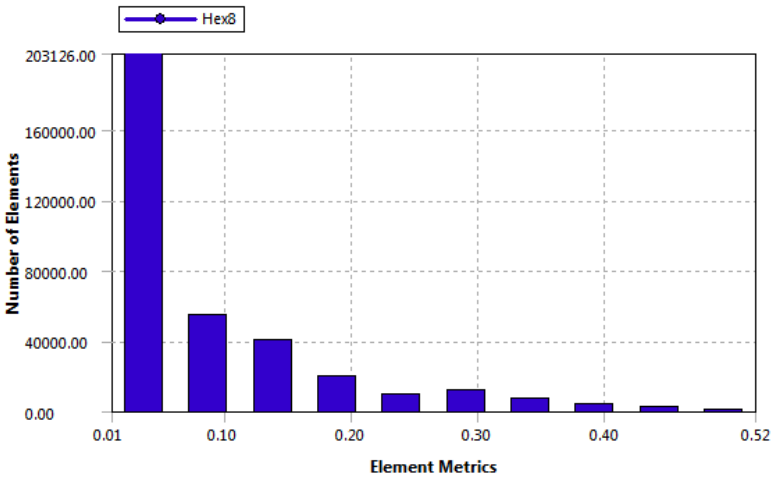

Figure 3.2: Mesh metrics

3.8. Domains

Regions of fluid flow and/or heat transfer in CFX are called domains. Fluid domains are the region of fluid flow whereas solid domains are regions occupied by conducting solids in which volumetric sources of energy can be specified (ANSYS, 2010). Porous domains are similar to fluid domains, but are used to model flows where the geometry is too complex to resolve with grid.

3.9. Overview of domain interfaces

Domain interfaces provide a way of connecting meshes or domains together. The domains can be connected through interfaces. Through different types of domain interfaces, energy may flow through, for example fluid solid interface, fluid porous

interface, solid porous interface etc. In this work fluid porous interface has been adapted and it will be described in the chapter 4.There are three interface models are available in the CFX namely

(i) Translational periodicity: In this case, two sides of the interface must be parallel to each other such that single translation transformation can be used

(ii) Rotational periodicity: In this case, two sides of the periodic interface can be mapped by a single rotational transformation about the axis and

(iii) General connection: It is a powerful way to connect the region. A general connection can be used to apply a frame change or connecting non matching grids or fully transient sliding interfaces between domains.

3.10. Boundary conditions

The following boundary conditions have been applied to solve the governing time averaged equations (3.4 – 3.5). Furthermore, in the SST turbulence models, the turbulence is specified by percentage of turbulence intensity with reasonable assumption with appropriate length scale.

The following combination of boundary conditions are valid in the CFX

(i) Velocity/Mass flow at an inlet; Static pressure at an outlet which is the most robust boundary condition.

(ii) Static pressure at an inlet; velocity/Mass flow rate at an outlet which is robust boundary condition.

(iii) Opening boundary

An opening boundary condition allows the fluid to cross the boundary surface in either direction, i.e. fluid can flow into or out of the domain simultaneously an opening boundary condition might be used.

(iv) Wall

If the solid wall boundary is impermeable to the fluid flow then a no-slip condition can generally be imposed. This is the most pertinent type of boundary condition. The fluid velocity is zero at the wall. For the wall which is permeable to the fluid flow, slip condition applied between domain interface (Fluid- porous interface) (Beavers & Joseph, 1967) where shear stress at the wall is zero ($\tau=0$).

3.11. Benchmark case for validation of software

In recent years Computational Fluid Dynamics (CFD) simulations are increasingly used in simulated and realistic coronary artery models with stenosis to find the pressure drop across the stenosis and hence to evaluate functional significance of the stenosis under hyperemic flow condition. Under hyperemic flow condition, the shear layer instability occurs in the flow due to dynamic variation of heart and heart rate, and irregularities in plaque anatomy (Mallinger & Drikakis, 2002). This can make the flow turbulent and it requires accurate simulation of low Reynolds number turbulent flows using the Reynolds Averaged Navier- Stokes (RANS) equations of fluid dynamics. The k-ε turbulence model is not suitable where the amount of flow separation from the smooth surfaces under adverse pressure gradient whereas k-ω model is more appropriate for low Reynolds turbulent flow modelling (I. ANSYS, 2009). In order to obtain accurate numerical simulation and results, it is necessary to validate the results obtained from numerical simulations against the experimental data. For this reason, the bench mark validation case has been done for guide wire flow obstruction effect on pressure drop across the stenosis and hence the coronary diagnostic parameters in-vitro experimental setup

3.11.1. Simulation of guide wire measurement of stenosis severity in vitro experimental setup

A 3-D model replicate of coronary artery model with stenosis employed experimentally by Banerjee et al (Banerjee, Peelukhana, & Goswami, 2014) to study the pressure drop across the stenosis and hence the diagnostic parameter was considered for the benchmark validation. In this experimental work, the coronary test section consists of converging, throat and diverging part. Dimensions of coronary test sections for 80% AS are given in Table 3.1.This geometry was well validated with clinical data in several occasion (Ashtekar, Back, Khoury, & Banerjee, 2007; R. Banerjee, et al., 2008). In this benchmark validation, the CFD analysis was carried out with the coronary artery model used by Banerjee et al (Banerjee, et al., 2014) by assuming blood was non-Newtonian fluid which follow Carreau model. The flow was assumed to be pulsatile. Experiments of Banerjee et al. (Banerjee, et al., 2014) uses a guide wire of diameter 0.014" to measure the pressure drop across the stenosis. The hyperemic flow rate was found from the clinical data (Wilson et al., 1988) which was used in their experiment to evaluate FFR and CDP. The experimental mean hyperemic flow rate was 135 ml/min in the case of intermediate stenosis severity (80% AS) and it was set in this simulation. These results could be used as a benchmark case for validation of the CFX simulations.

In addition to achieve the goal of validation of CFX simulation solver for computing pressure drop across the stenosis to find the functional significance of the stenosis severity, this study focuses on the effect of mesh density, and laminar and $k-\omega$ SST model on the accuracy of results.

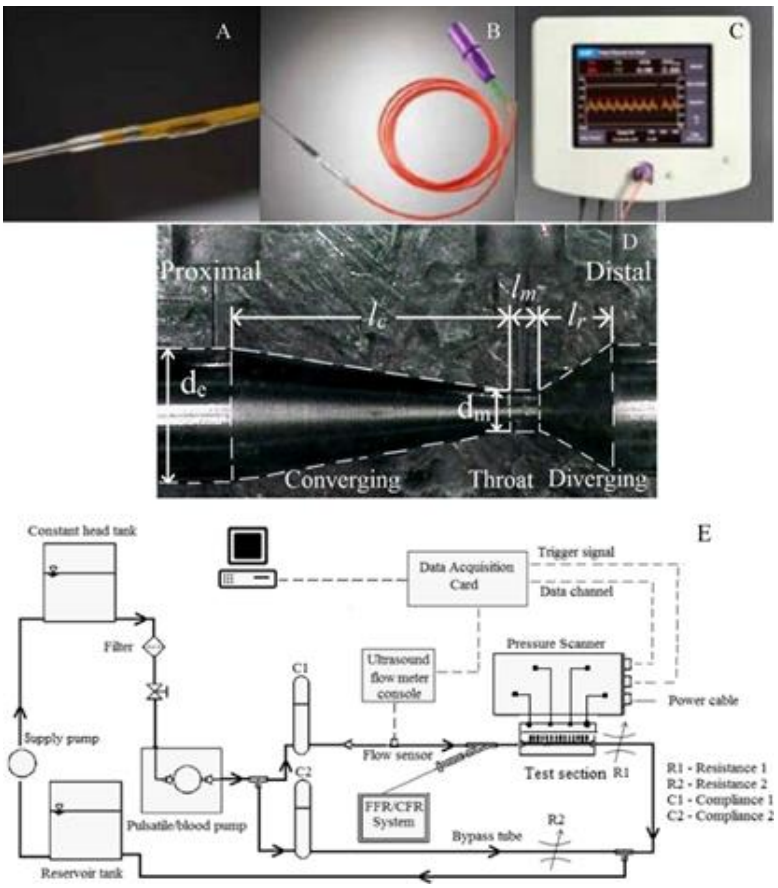

Figure 3.3: Experimental setup of coronary artery model
Reprinted from (Banerjee, et al., 2014), Copyright (2015) with permission from Elsevier

3.12. Results and discussion benchmark simulation

A mesh independent study was performed and finalized mesh of max size 0.00018 m was used for carrying out the computational study. Figure 3.4 shows the surface stream line velocity at different time steps. From this numerical study, transient time average pressure drop was found and hence the FFR, CDP and LFC were evaluated and compared with numerical experimental results.

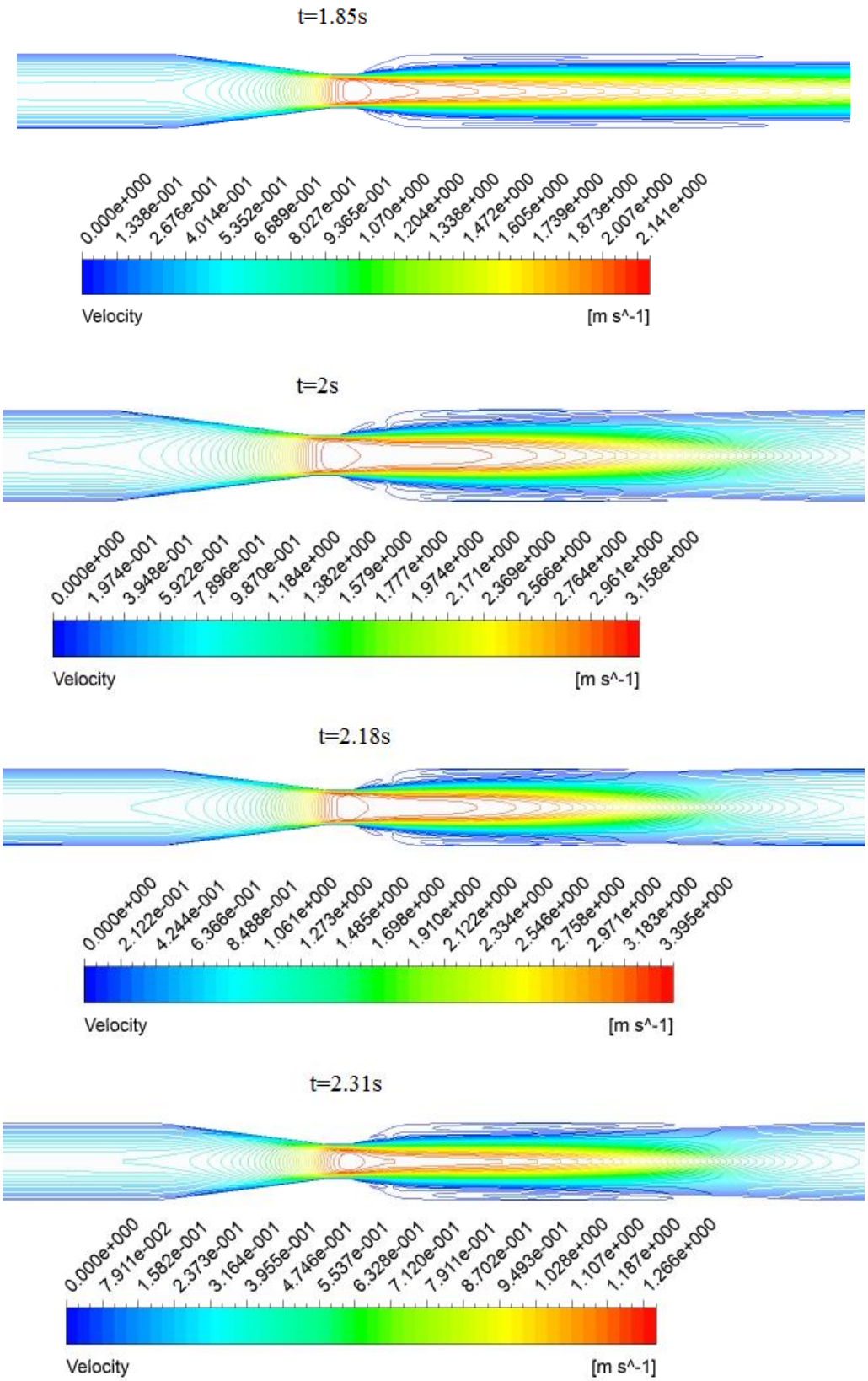

Figure 3.4: Velocity contour at different time steps

3.12.1. Pressure drop comparison

Figure 3.5 shows the pressure drop comparison of our results using $k-\omega$ SST models with the experimental results of Banerjee et al (Banerjee, et al., 2014) and found that there is a good agreement between $k-\omega$ SST turbulence model and experimental data for the intermediate stenosis severity condition. Many studies shows that the laminar flow is observed in the stenosis free vessels (Boutsianis et al., 2004; Goubergrits et al., 2008) whereas turbulence could be generated at the site of downstream to the stenosis in the case of intermediate/ severe stenosis (Stein & Sabbah, 1976; Varghese & Frankel, 2003).

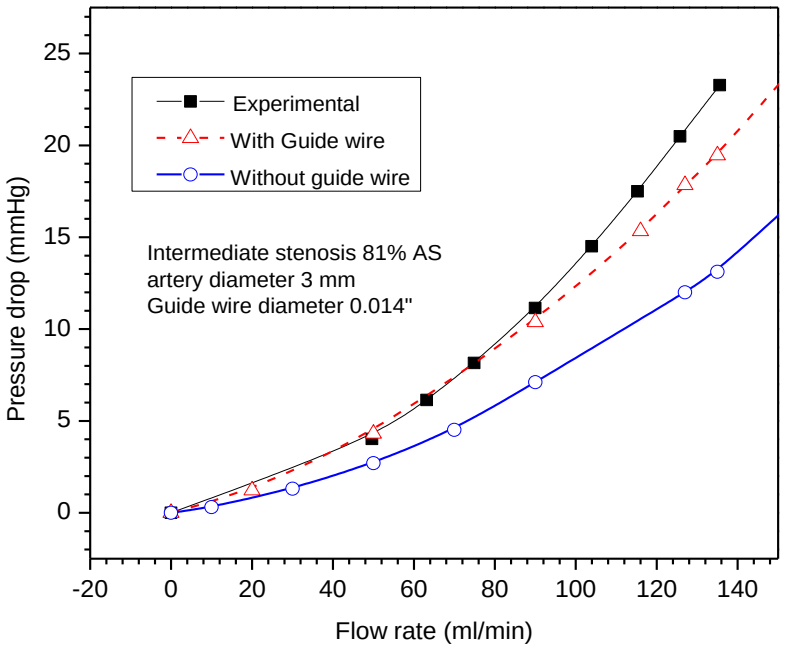

Figure 3.5: Results of Experimental data (Banerjee, et al., 2014) and computational data of with and without guide wire

In this study, the laminar model is not suitable for hyperemic flow condition when the stenosis severity increases. The simulations conducted in this section demonstrate that a suitable low Reynolds turbulence model ($k-\omega$ SST) and critical mesh elements can

model the hyperemic flow condition with acceptable accuracy in the coronary stenotic model.

3.12.2. FFR and CDP comparison

Under hyperemic flow condition, the FFR and CDP was evaluated and it can be seen that there is a good agreement of our numerical results with experimentally found value (Banerjee, et al., 2014).

4. EFFECT OF POROUS MEDIA OF THE STENOSED ARTERY WALL TO THE CORONARY PHYSIOLOGICAL DIAGNOSTIC PARAMETER: A COMPUTATIONAL FLUID DYNAMIC ANALYSIS

4.1. Introduction

A progressive narrowing in the arterial system of human or animal heart is known as stenosis, which impairs blood flow to the heart muscle and eventually results in atherosclerotic plaque formation and life threatening myocardial infarction (Naghavi et al., 2003). Assessment of physiological severity of an intermediate stenosis in a single vessel or branched vessel using usual coronary angiogram or multi slice computed tomography is more complex (S. J. Park et al., 2012; Tobis, et al., 2007).

The true functional severity of coronary artery stenosis is assessed by pressure drop and flow (Gould, 2006; N. H. Pijls, et al., 1996; N. H. Pijls, et al., 1995). Coronary flow reserve index (N. H. Pijls, et al., 1995) (CFR; ratio of hyperemic flow to the flow at resting conditions) and fractional flow reserve index (N. H. J. Pijls & Sels, 2012) (FFR; ratio of distal coronary pressure to aorta pressure under hyperemic condition) are the two parameters that provide physiological information about the severity of the coronary artery stenosis so that appropriate therapy can be initiated to the patient during cardiovascular intervention. The CFR is not an independent physiological significance index, and it is highly dependent on the hemodynamic conditions such as myocardial chamber hypertrophy, diabetes and age (Banerjee, et al., 2009; Tobis, et al., 2007). In contrast to CFR, the FFR has a value of 1 for every patient under no stenotic condition (N. H. Pijls, G. J. Bech, B. De Bruyne, & A. van Straten, 1997).

In the current era, Fractional Flow Reserve (FFR) is used as a gold standard for the assessment of functional significance of stenosis severity and to decide upon the percutaneous coronary intervention (PCI) procedure which is required or it can be safely deferred. The hyperemic flow condition is induced by a vasodilator agent such as adenosine or papaverine. A 0.014 inch diameter guide wire with the pressure sensor at its tip is advanced across the stenosis to measure distal pressure.

Assessment of the functional significance in the moderate and severe stenosis severity will not lead to the clinician for the misdiagnosis whereas assessment of the functional significance of the intermediate stenosis is a challenge for the clinician. When assessing functional significance of the stenosis, a possible misdiagnosis on the stenosis severity causes postponement of surgical treatment and can lead to death. This misdiagnosis on the severity of the stenosis may happen for the intermediate stenosis

The FFR does not contain any empirical relations, but it simply depends on measurable quantities of distal pressure and proximal pressure. Pressure drop-flow $(\Delta p - Q)$ relation and FFR in the stenosis region have been studied by many researchers by considering the arterial wall as rigid (R. Banerjee, et al., 2008; Banerjee, Back, Back, & Cho, 2003; Rajabi-Jaghargh, et al., 2011). However, variations in the values of FFR due to porous stenotic arterial wall have not been previously studied.

Recently proposed non dimensionless diagnostic parameters, pressure drop coefficient (CDP) and Lesion Flow Coefficient (LFC) which are derived from fundamental fluid mechanics based on coronary pressure and flow (Sinharoy, et al., 2008) may be useful to improve the functional assessment of coronary stenosis severity. Recent meta-analysis was done by Kolli, et al (K. K. Kolli et al., 2014) by comparing results of FFR

and CFR of the same lesions and found an optimal cut-off value of CDP corresponding to the clinically used cut off value of FFR=0.8 ,FFR=0.75 and CFR= 2.0 by plotting receiver operating curve. The cut off value to detect FFR< 0.8 and FFR < 0.75 was at CDP 27.1 and CDP 27.9, respectively.

In this chapter the effect of porous media of the stenosed arterial wall under plaque rupture condition on the diagnostic parameters FFR, CDP and LFC has been considered. Under porous media consideration, an uncertainty region, where possible misdiagnosis of physiological significance of stenosis severity in the intermediate stenosis need to be found for better clinical outcome for the patients who are suffering from coronary artery disease.

The shear stress in the blood flow, plays a substantial role that ultimately determines the location of atherosclerotic plaques. One of the major limitations of the well published studies is that the coronary artery wall is impervious to blood. From the literature, it is clear that all the human tissues are porous in nature (Chakravarty & Sannigrahi, 1998; Dabagh, et al., 2008; Khakpour & Vafai, 2008; Prosi, et al., 2005) and the plaque region mainly includes a large lipid core and a thin fibrous cap (Tang, et al., 2009). The normal arterial wall consists of endothelium, intima, internal elastic lamina (IEL), media and adventitia (Ai & Vafai, 2006). It is believed that the permeability of endothelium wall increases with deposition of cholesterol due to the damaged or inflamed arterial wall.

Blood is a moving column with suspended cells. Normal endothelium did not allow passage of cells. However, it has been shown that atherosclerotic endothelium is highly

permeable to white cells and platelets in the event of plaque rupture. Re-cells are also shown to enter to tunica media(Libby, et al., 2002; Libby & Theroux, 2005).

It is useful to study the pulsatile non-Newtonian blood flow through stenotic arteries taking into account of blood transport through the porous arterial wall, and to investigate the effect of porous media on the diagnostic parameters, FFR, CDP and LFC. In this chapter, a 3D computational rigid stenosed artery (RA) and porous stenosed artery (Fluid Porous Interface-FPI) models have been considered. For the given percentage area stenosis, we examine the pressure drop across the stenosis and estimate the value of FFR in both models for identifying the possible misdiagnosis region. The CDP and LFC variations are also studied in the RA and FPI models. A finite volume software CFX14.0 (ANSYS inc) was used for flow simulations.

4.2. Literature Review

4.2.1. Porous medium: a back ground

A porous medium is characterized by solid matrix and void spaces, where a small fluid flows called interstitial flow due to pressure gradients. A porous medium is characterized by its dimensionless parameter porosity (ε), permeability (K) and its constituents. The porosity is defined as the ratio of void space to total volume of the medium and the permeability is a measure of conductivity for the fluid flow in the porous medium and its unit is m^2.

4.2.2. Darcy model

The earliest flow transport model in porous media is Darcy model. Hendry Darcy revealed a linear proportionality between the flow velocity and the applied pressure gradient across the porous medium

$$u = -\frac{K}{\mu}\frac{\partial P}{\partial x} \tag{4.1}$$

where u, P, μ and K are the Darcy velocity (the average of the fluid velocity over the cross section), fluid pressure, dynamic viscosity of the fluid and the permeability of the porous medium, respectively. The permeability depends on the geometry of the medium. In 3D form, Eq. (4.1) can be written as

$$\vec{V} = -\frac{\underline{\underline{K}}}{\mu}\nabla P \tag{4.2}$$

where $\underline{\underline{K}}$ is a permeability, a second order tensor. The terms ∇P and $\vec{V}$ are pressure gradient and Darcy velocity vectors. Darcy model has been widely used in biomedical studies such as tumors, perfused muscle tissues, flow in soft connective tissues etc.

Darcy model neglects the boundary effects or the inertial forces on the fluid flow and heat transfer through porous media (Vafai & Tien, 1981). So, a number of models have been proposed. One of the models is Darcy- Forchheimer model which accounts for inertial effects and it is given by

$$\nabla p = -\frac{\mu}{K}V + c_F K^{-\frac{1}{2}}\rho|V|V \tag{4.3}$$

where c_F is a dimensionless parameter related to inertial effects. The second term of the right side of the equation called Forchheimer term has been added to account for

inertial effects. The transition from Darcy-flow to Darcy–Forchheimer flow depends on the permeability-based Reynolds number. This Reynolds number is defined as

$$\mathrm{Re}_K = \frac{u_P \sqrt{K}}{\nu} \tag{4.4}$$

Where $u_P, \sqrt{K}$ and ν are pore velocity, permeability and kinematic viscosity, respectively.

4.2.3. Brinkman model

The Brinkman's model is stated as shown below and it was developed by Brinkman (Brinkman, 1949)

$$\nabla p = -\frac{\mu}{K} v + \bar{\mu} \nabla^2 v \tag{4.5}$$

The first and second terms of the right side of the equation are the viscous term which is the Darcy term and momentum diffusion term with $\bar{\mu}$ being the effective dynamic viscosity of the medium, respectively. The Eqn. (4.5) is a general form of volume averaged Stokes equation. Brinkman simply took $\bar{\mu} = \mu$, but for the isotropic porous medium, the $\bar{\mu}$ is not the same as the dynamic viscosity μ due to the tortuosity and dispersion of viscous diffusion (Ochoa-Tapia & Whitaker, 1995). Bear and Bachmat (Bear & Bachmat, 1990) showed that the effective viscosity is related to the porosity through the following relation,

$$\frac{\bar{\mu}}{\mu} = \frac{1}{\varepsilon} \lambda^* \tag{4.6}$$

Where ε and λ^* are the porosity and tortuosity. It is important to note that the Brinkman model cannot be rigorously justified, except when the porosity is close to unity. Brinkman model has been effectively utilized in several biomedical research works (Dash, Mehta, & Jayaraman, 1996).

4.2.4. Generalized flow transport model

If the fluid inertia is not negligible then the form drag exerted by the fluid on the solid becomes significant. The generalized flow transport model in porous media which takes into account various pertinent effects was derived by Vafai and Tien and is given by the following equation (Vafai & Tien, 1981)

$$\frac{\rho_f}{\varepsilon}\left[\frac{\partial\langle V\rangle}{\partial t}+\langle(V.\nabla)V\rangle\right]=-\nabla\langle P\rangle^f+\frac{\mu}{\varepsilon}\nabla^2\langle V\rangle-\frac{\mu}{K}\langle V\rangle-\frac{\rho_f F\varepsilon}{K^{1/2}}\left[\langle V\rangle.\langle V\rangle\right]J \tag{4.7}$$

where μ, ρ_F, ε, K and F are fluid dynamic viscosity, fluid density, porosity, permeability and the dimensionless inertia term coefficient, respectively. The parameters J and $\langle P\rangle^f$ are a unit vector oriented along the velocity vector V and the average pressure inside the fluid, respectively. The quantities $\langle V\rangle$, and $\langle(V.\nabla)V\rangle$ are the local volume average of V and $(V.\nabla)V$, respectively, associated with the fluid. This generalized model contains the convective terms. This generalized model is referred to as the Brinkman–Forchheimer–Darcy equation. The F term is replaced by c_F, a dimensional parameter related to inertial effects called Forchheimer coefficient.

4.2.5. Transport in porous media-governing equations

A porous medium, being a heterogeneous system made of a solid matrix and voids filled with a fluid, can be treated as a continuum by proper implementation of the role of each phase in transport phenomena. In this section, the governing equations for fluid flow through porous media will be introduced.

4.2.6. Porous momentum model

The momentum loss models available in CFX solver are (i) Isotropic Loss Model and (ii) Directional Loss Model. In this momentum loss models there are two loss terms involved namely viscos loss and inertial loss. Isotropic and directional loss models are useful for modeling porous momentum losses either with or without the volume effect of porosity. Permeability and loss coefficients are useful to formulate the momentum loss through an isotropic region. In the directional loss model, the momentum source through anisotropic porous region such as honeycomb or perforated plate can be modeled.

4.3. Methodology

4.3.1. Stenosed coronary artery: a mathematical modelling

In this chapter, stenosis geometry was considered as trapezoidal as shown in Figure 4.1. The fluid porous interface (FPI) geometry and rigid artery (RA) geometry were created in ANSYS work bench 14.0. The axial direction is along the z axis. Stenoses do not have any specific shape. Lesion dimensions (Table 4.1) are taken from Konala et al.(Konala, et al., 2011) and Rajabi et al. (Rajabi-Jaghargh, et al., 2011). Stenosis regions consist of converging (of length l_c), throat (of radius r_m and length l_m) and

diverging (of length l_r) sections. Moreover, proximal and distal radius is assumed to be identical ($r_e = r_d$). Three stenotic models 70% (moderate), 80% (intermediate) and 90% (severe) Area Stenoses (AS) have been considered here for both RA and FPI models. Adequate proximal and distal length was taken to ensure for accurate determination of the pressure drops due to the lesion and for the convergence of the calculations.

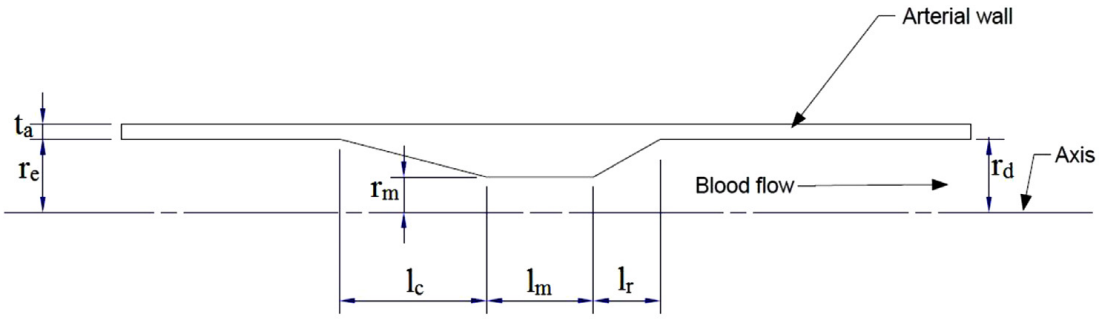

Figure 4.1: Schematic drawing showing lesion geometry (Dimensional values are given in Table 1)

Table 4.1: Artery wall and stenosis geometry. All dimensions are in mm

Area stenosis (AS) (%)	t_a	r_e=r_d	r_m	l_c	l_m	l_r
70	1	1.5	0.82	6	3	1.5
80	1	1.5	0.67	6	1.5	1.5
90	1	1.5	0.47	6	0.75	1.5

4.3.2. Arterial wall modelling

Fluid flow was modeled through a homogeneous porous stenotic artery wall. In this work, Darcy-Forchheimer model, which accounts for the inertial effects. The governing momentum loss equations can be written as (Khakpour & Vafai, 2008).

$$\nabla p = -\frac{\mu}{K}V + c_F K^{-\frac{1}{2}}\rho|V|V \tag{4.8}$$

where ∇p is the pressure gradient, μ is fluid kinematic viscosity, K is the permeability of the wall, V is the superficial velocity vector, c_F is a dimensionless parameter related to inertial effects and ρ is a fluid density. In our study, we set the thickness of the arterial wall which is represented by t_a= 1 mm (Konala, et al., 2011), K= 2×10^{-14} cm^2 (Prosi, et al., 2005) porosity ε = 0.15 (Prosi, et al., 2005) $C_F = \frac{-1.75}{\sqrt{150\times\varepsilon^3}}$ (X. Liu, Fan, & Deng, 2010)

4.3.3. Computational blood flow model

It will be assumed that the flow of blood is incompressible and governed by the Navier-Stokes equations. The blood flow through the coronary artery was assumed to be incompressible, unsteady, and governed by the Navier-Stokes equation.

[

$$\rho\left(\frac{\partial v}{\partial t} + v.\nabla v\right) = \nabla.\tau - \nabla P \tag{4.9}$$

and the continuity equation for the incompressible flow is given by

$$\nabla.v = 0 \tag{4.10}$$

where v is the three-dimensional velocity vector, t the time, ρ the blood density, P the pressure and τ the stress tensor. In this study, the blood is assumed to be non-Newtonian and following the Carreau model (Johnston, et al., 2006) whereas the blood

viscosity μ given in poise *(P)* as a function of the shear rate $\dot{\gamma}$ given in s^{-1} is expressed as

$$\mu = \mu_{\infty} + (\mu_0 - \mu_{\infty})[1 + (\lambda\dot{\gamma})^2]^{(n-1)/2} \tag{4.11}$$

Where λ = 3.313s; n= 0.3568, μ_0 = 0.56 P, μ_{∞} = 0.0345 P, and the blood density (ρ) is assumed as $1050\ kg/m^3$.

4.3.4. Meshing

The computational domain, a 3-D computational coronary artery models for simulation are The computational domain of a 3-D coronary artery models were initially meshed with structured hexahedral elements as shown in Fig. 4.2(a) & (b).

(a) (b)

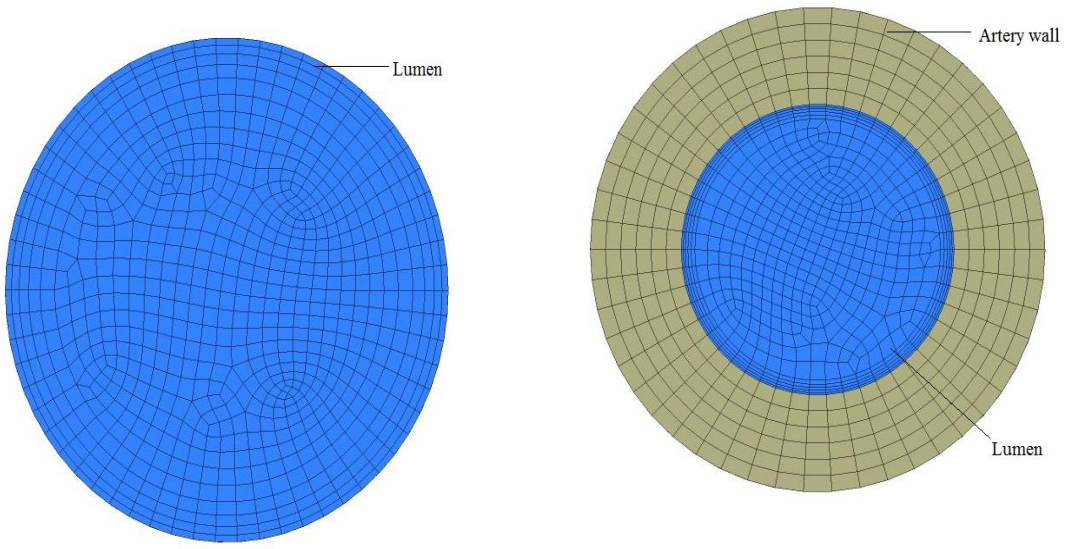

Figure 4.2 (a) & (b): Computational mesh used for numerical study in the RA and FPI models respectively

The maximum and minimum element size determined by the element size and mesh control. The quality of the mesh was tailored by a process called inflation near fluid wall interface. The inflation control is used for resolving the mesh near the wall region to capture flow effects for viscous problem. In the near wall region boundary layer effect give rise to velocity gradients which are greatest normal to the face.

The total numbers of elements vary from 200,000 to 250,000. The accuracy of simulation of the flow is dependent on the quality of the mesh. Quality of mesh was checked by inspecting various parameters such as skewness, orthogonal quality, element quality etc. In this work the quality of the mesh determined from skewness mesh metric which is one of the primary quality measures of mesh quality which was discussed in chapter 3 in the section 3.7.

4.3.5. Boundary conditions

Adequate distal length was ensured for accurate determination of the pressure drops due to the lesion and for the convergence of the calculations. Flow entry and exit from the calculation domain was assumed to be normal to the inlet and outlet surfaces. A transient parabolic velocity u (t) (Banerjee, et al., 2003; Sinha Roy, et al., 2006) (Figure 4.3) was applied at the inlet, and stress free boundary condition was set at the outlet (Sinha Roy, et al., 2006). The post stenotic velocity waveform was characterized by augmentation of the systolic velocity component and a relatively small diastolic velocity component. These characteristics distinctly contrasted with normal coronary artery flows, i.e., a diastolic-predominant pattern wave form (Kajiya et al., 1987).

Both RA and FPI cases were solved with same inlet and outlet boundary conditions. For RA model, no slip boundary condition was applied at the wall. For FPI model, general grid interface (Naghavi, et al.) mesh connection was adopted for the fluid and porous domains. At the interface between porous and lumen region, slip condition has been imposed (Chakravarty & Datta, 1992) and on other wall surfaces, the no-slip boundary condition was applied. The velocity profile for 70%, 80% and 90% AS was obtained from the mean hyperemic flow rate ($\tilde{Q}$) 175, 165 and 115 ml/min (Konala, et al., 2011) respectively.

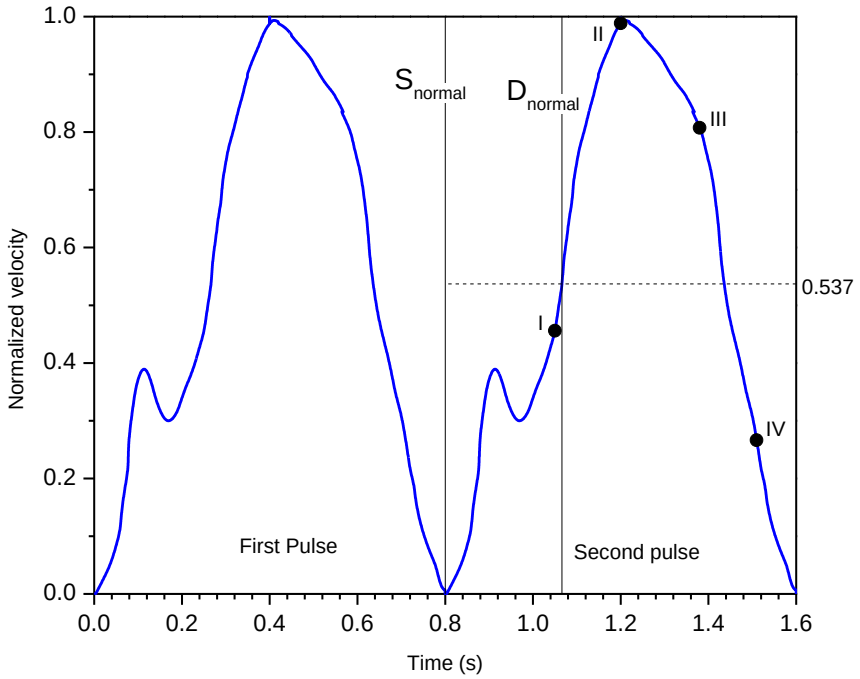

Figure 4.3: Normal Coronary flow wave form $\bar{u}/\bar{u}_{p-t}$ versus t. Where S_{normal} indicates the beginning of systole and D_{normal} indicates the beginning of diastole. The peak diastolic velocity corresponds to a normalized velocity of 1.0, so that the ratio of mean to peak veloc ity $\bar{u}/\bar{u}_{p-t}$ is 0.537.

The proximal mean Reynolds number $\left(2\tilde{Q}/\pi\nu r_e\right)$ and throat Reynolds number $\left(2\tilde{Q}/\pi\nu r_m\right)$ was calculated and reported in Table 4.2 with the kinematic viscosity ν as $0.035\,cm^2/s$ (Banerjee, et al., 2003).

4.3.6. Numerical methodology

In all the three stenotic models, there are possibilities of shear layer instabilities secondary to heart rate variability and irregularities in plaque anatomy (Banerjee, et al., 2003; Mallinger & Drikakis, 2002; Rajabi-Jaghargh, et al., 2011) at hyperemic flow conditions. This can make the flow turbulent. Since the turbulence is going to be a low Reynolds turbulence, shear stress transport (SST) turbulence model belongs to $k-\omega$ model family was adopted for the flow modeling which is more accurate and robust in overcoming near wall treatment errors for low Reynolds turbulence computations (Jozwik & Obidowski, 2010; Kagadis et al., 2008). The CFD simulation was run first with steady-state flow analysis and followed by transient flow analysis with the results from the steady-state analysis as the initial guess (Jozwik & Obidowski, 2010). The sequencing of steady-state and transient analysis was set up through simulation control and configuration. The following values of parameters at the inlet and outlet were taken, namely:

- Velocity at the inlet: 0.413 m/s, 0.389 m/s and 0.271 m/s corresponds to 70%, 80% and 90% AS respectively. (Velocity values are calculated from the corresponding mean hyperemic flow rate).
- Stress free boundary condition at the outlet.

The transient flow analysis was run for 640 time steps (0.005 s per time step) representing 4 cycles (0.8 s each) of pulsatile flow with each time step converging to a residual target of 1×10^{-5} and we found the results to be repeatable. In all cases, without guide- wire condition was considered. Subsequently a mesh independent study was performed with the elements varies from 250,000 to 500,000 to ensure the computed shear stress values differed by less than 0.3%.

4.4. Result

In both RA and FPI models, the pressure drop was analyzed first and then the effect of porous media of the arterial wall on the diagnostic parameter was analyzed for misinterpretation.

4.4.1. Rigid artery (RA model) and Pressure drop

Figure 4.5 shows the magnitude of axial pressure drop $p - p_e$ along the stenosis at various time I (0.25,1.05,1.85 and 2.65s), II (0.4,1.2,2.0 and 2.8s), III (0.58,1.38,2.18 and 2.98s) and IV(0.71,1.51,2.31 and 3.11s) during the cardiac cycle for 70%, 80% and 90% AS where p_e is the reference pressure measured at the entrance (Z=0). From the general profile of the pressure distribution, major pressure drop occurs across the convergent region due to wall friction and momentum changes in the fluid flow. In the throat region, the pressure drop further increases due to additional area restriction and additional momentum changes. In the divergent region, the flow decelerates along with pressure rise and flow separation. Pressure recovery occurs in the distal region due to density and viscosity of blood. For a given time point in the cardiac cycle, the pressure drop distribution along the axis increases as % AS increases. Due to shear layer instability distal to the stenosis for the 80% and 90%AS, the pressure recovery at time point II is highly unstable than in the 70% AS.

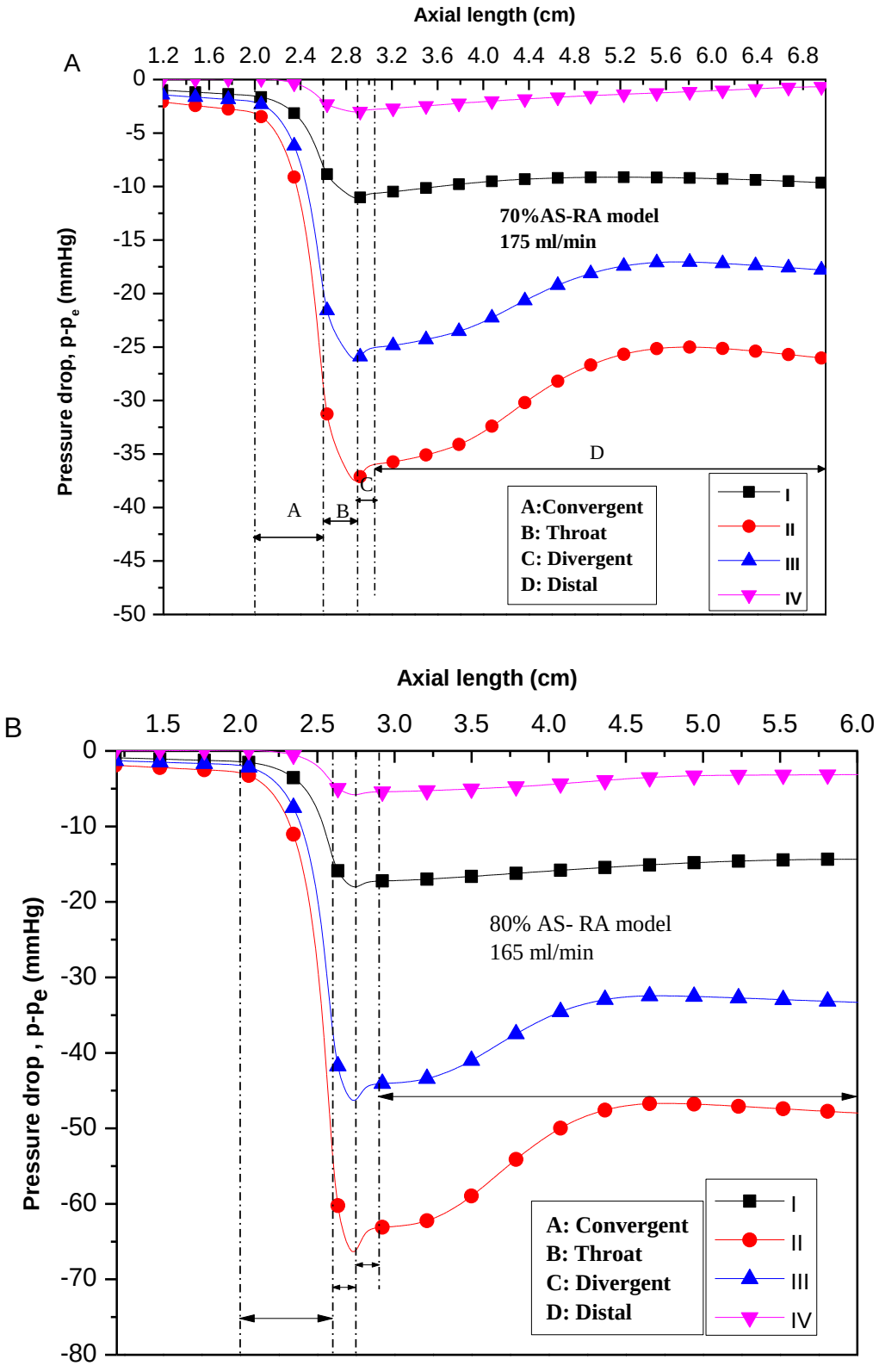
A
Axial length (cm)
1.2 1.6 2.0 2.4 2.8 3.2 3.6 4.0 4.4 4.8 5.2 5.6 6.0 6.4 6.8
0 -5 -10 -15 -20 -25 -30 -35 -40 -45 -50
Pressure drop, p-pe (mmHg)
70%AS-RA model
175 ml/min
A
B
C
D
A:Convergent
B: Throat
C: Divergent
D: Distal
I
II
III
IV
B
Axial length (cm)
1.5 2.0 2.5 3.0 3.5 4.0 4.5 5.0 5.5 6.0
0 -10 -20 -30 -40 -50 -60 -70 -80
Pressure drop , p-pe (mmHg)
80% AS- RA model
165 ml/min
A: Convergent
B: Throat
C: Divergent
D: Distal
I
II
III
IV

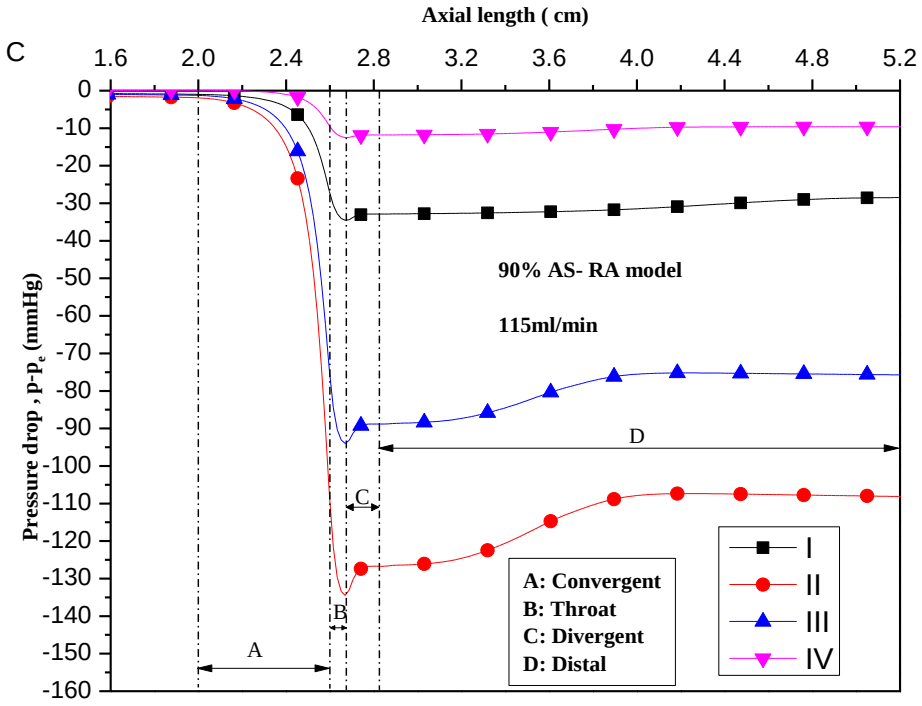

Figure 4.4: Axial pressure drop p-pe along the axis of the stenosis in 70%, 80% and 90% AS in RA model

Figure 4.5 shows the overall transient pressure drop $\Delta p_{RA} = p_a - p_r$ (where p_a is the pressure measured at 3 mm proximal to the start of converging portion and p_r is the distal recovery pressure) which was taken during the cardiac cycles 3 and 4 for the moderate stenosis and there is no significant difference in the pressure drop found in the cycles 3 and 4 to ensure the accurate results with numerical data being reported for the third and fourth cycles. At hyperemia, the time averaged pressure drop $\Delta\tilde{p}_{RA} = \tilde{p}_a - \tilde{p}_r$ (including the pressure recovery) for 70%, 80% and 90 AS was calculated and are reported in Table 2. For RA model, an increase in AS from 70% to 80% resulted in a 9.33 mmHg increase in $\Delta\tilde{p}$ whereas from 80% to 90% AS $\Delta\tilde{p}$ increased by 26.31 mmHg. The calculated $\Delta\tilde{p}_{RA}$ was in close agreement with the study done by B.C Konala et al.(Konala, et al., 2011) in the rigid artery with rigid plaque with the absence of guide wire.

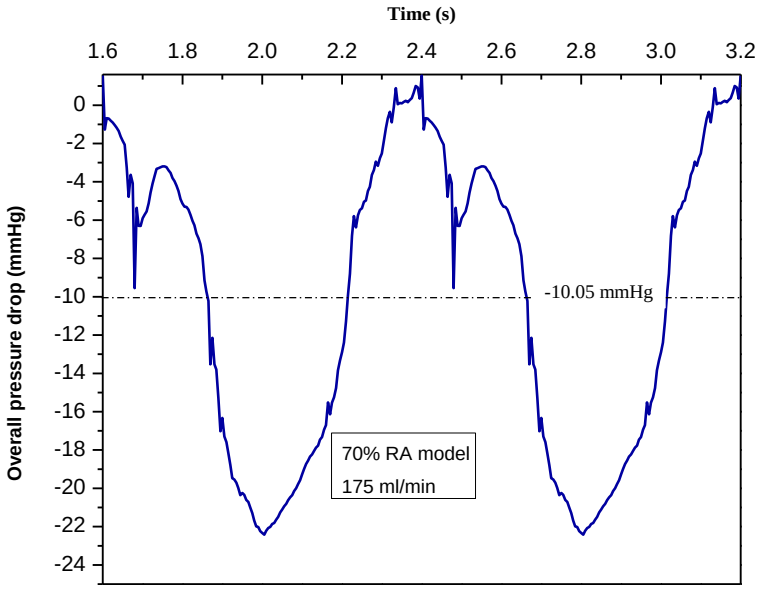

Figure 4.5: Overall pressure drop across the stenosis during the cardiac cycle at hyperemic flow in 70% AS RA model.

4.4.2. Porous stenotic artery (FPI model) and Pressure drop

Figure 4.6 shows the magnitude of axial pressure drop as a function of axial distance $p - p_e$ at time I, II, III, IV during the cardiac cycle for 70%, 80% and 90% AS.

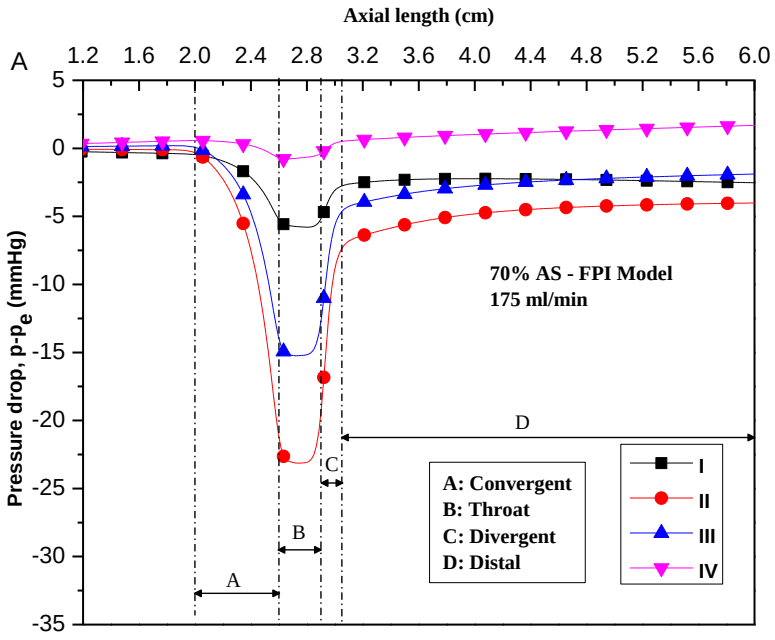

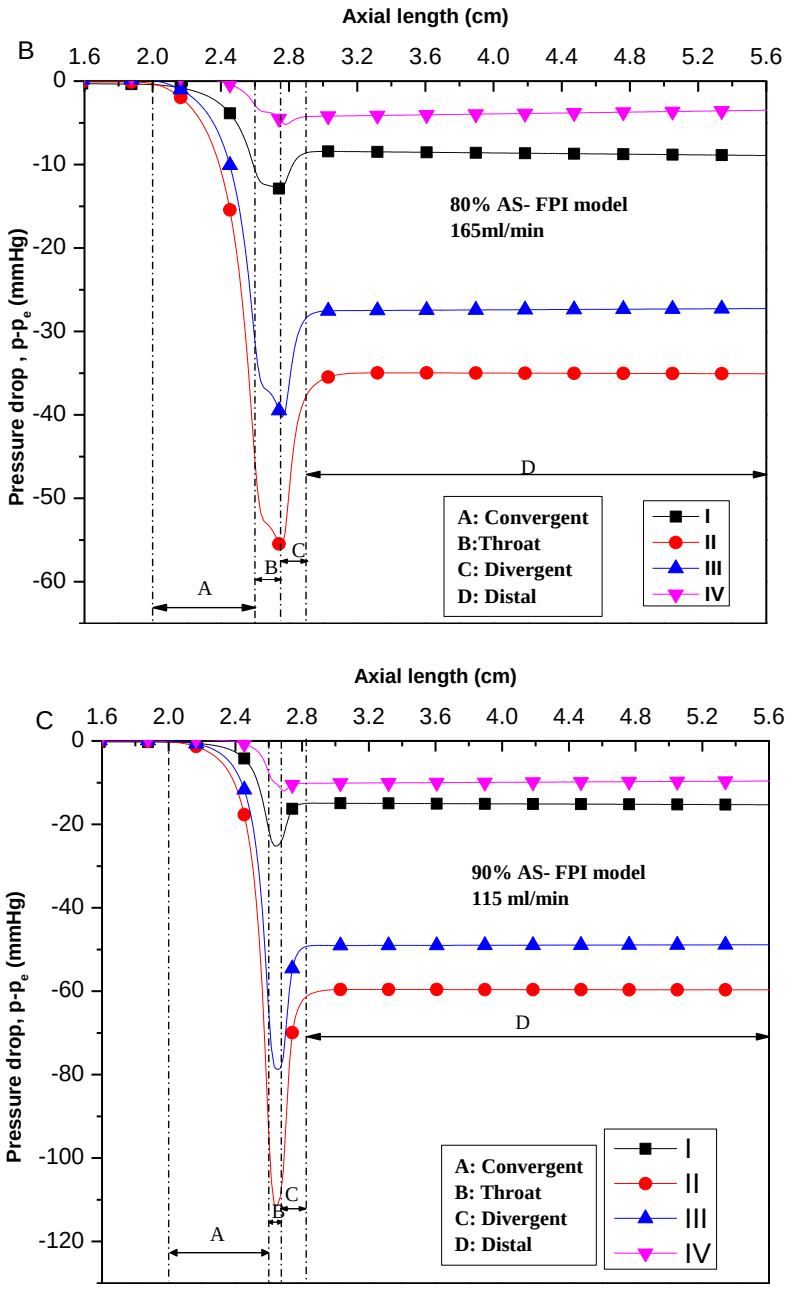

Figure 4.6: Axial pressure drop p-pe along the axis of the stenosis in 70%, 80% and 90% AS in RA model

At hyperemia, the time averaged pressure drop $\Delta\tilde{p}_{FPI} = \tilde{p}_a - \tilde{p}_r$ for 70%, 80% and 90% AS was calculated and are reported in Table 4.2. Due to the porous media of an arterial wall in the FPI model, the distal pressure recovery length occurred earlier than in the RA model. A bar graph (Figure 4.7) compares the pressure drop between FPI and RA models for the three different stenotic conditions.

Table 4.2: Results from computational analysis for RA and FPI models

RA and FPI models				RA model			FPI model		
% Area stenosis	Hyperemic flow $(\tilde{Q})$ ml/min	Proximal $\tilde{\mathrm{Re}}$	Throat $\tilde{\mathrm{Re}}$	$\tilde{P}_a$ mmHg	$\Delta\tilde{P}$ mmHg	FFR_{RA}	$\tilde{P}_a$ mmHg	$\Delta\tilde{P}$ mmHg	FFR_{FPI}
70	175	354	610	88.89	10.05	0.89	78.92	1.67	0.98
80	165	333	747	90.97	19.39	0.79	85.73	15.73	0.82
90	115	232	742	91.74	45.7	0.5	73.36	28.38	0.61

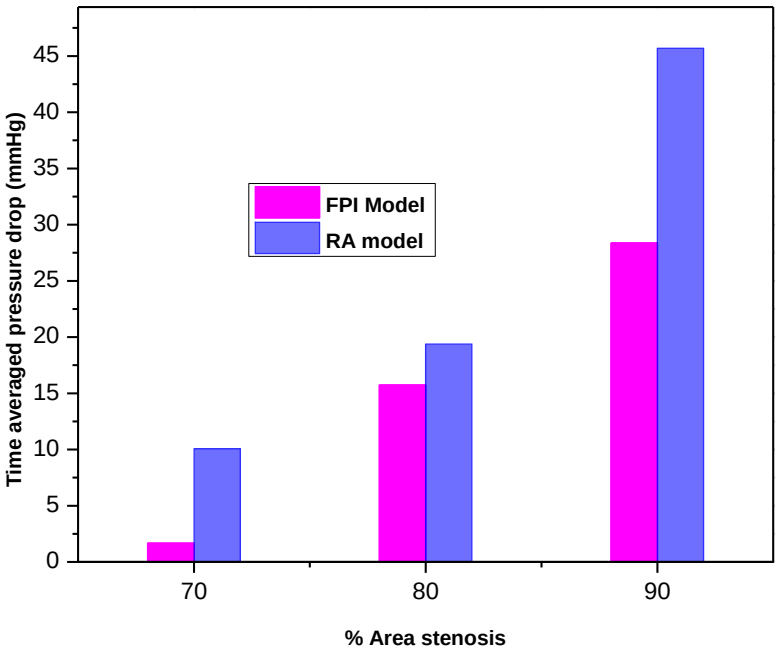

Figure 4.7: Bar graph showing the variation of time averaged pressure drop across a given stenosis in FPI, RA models.

As expected, a nonlinear relationship was observed in $\Delta\tilde{p}$ as the stenosis severity increases in both RA and FPI models. This could be characterized by the non-linear nature of momentum changes on account of area constriction and vary with a second power of flow rate (Banerjee, et al., 2007). From the computed $\Delta\tilde{p}$ in RA and FPI models, a nonlinear pressure drop decrements are observed in all the three stenotic conditions in the FPI model than in the RA model.

4.4.3. FFR calculations for RA and FPI models:

Having obtained the time averaged pressure drop $\Delta\tilde{p}$ and the pressure proximal to stenosis $\left(\tilde{p}_a\right)$ from this computational study, FFR $\left(=\frac{\tilde{p}_d}{\tilde{p}_a}=1-\frac{\Delta\tilde{p}}{\tilde{p}_a}\right)$ can be calculated (Table 2).

4.4.4. Effect of porous media of the artery wall on coronary diagnostic parameter- FFR

The values of FFR for the RA model, obtained in this study are in close agreement with available numerical results in the absence of guide wire condition which was done by B.C Konala et al. (Konala, et al., 2011) (Figure 4.8). In the study of Konala et al. the effect of porous media of the arterial wall on the diagnostic parameter have not been considered. Hence, the present study focuses on the effect of porous media on FFR. For both RA and FPI models, FFR values decreases as % AS increases. An inverse non-linear second degree polynomial fit approximation (Dupouy et al., 2005; Kristensen, et al., 2010) was used to plot the computed values of % AS and FFR as shown in Figure 4.9. To estimate the uncertainty % AS region for the possible misdiagnosis, a horizontal line representing the cut-off value was drawn at FFR=0.75 (Konala, et al., 2011; Kristensen, et al., 2010). This horizontal line intercepted the FFR - % AS lines for RA and FPI models at 81.89 % and 83.61 % AS, respectively. In the range of 81.89% - 83.61 % AS, FFR values for FPI model were higher than the RA model. Thus, in this region a possible misdiagnosis might lead to postponement of coronary intervention if the clinical decision is purely based on angiographs as it happens in many under developed and developing countries, instead of actual FFR measurement

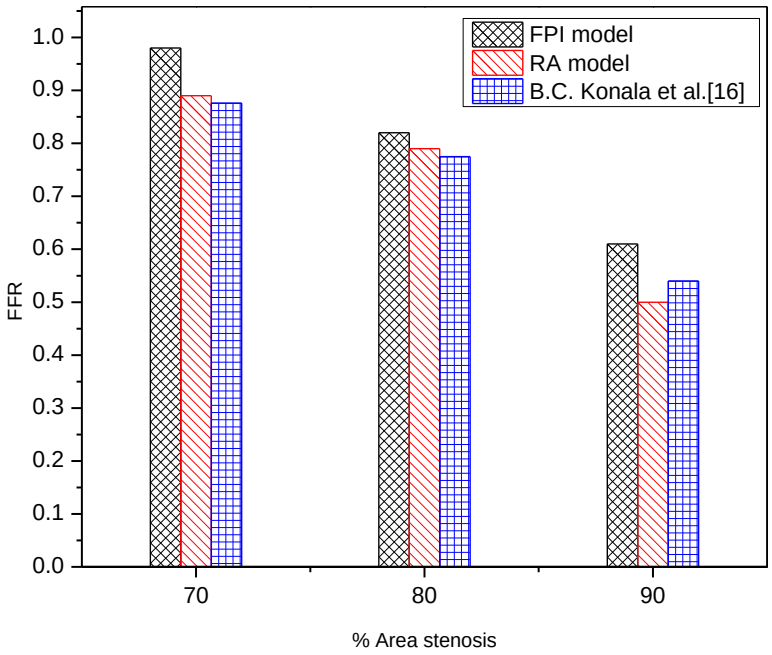

Figure 4.8: Bar graph showing the variation of FFR in the simulated FPI and RA models with B.C. Konala et al.study (Konala, et al., 2011)

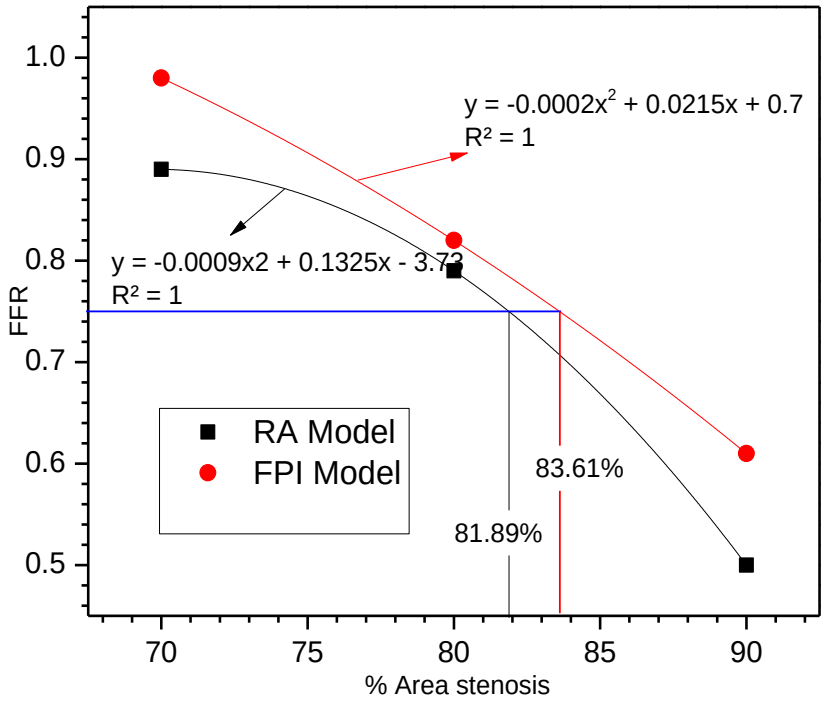

Figure 4.9: Variation of FFR values in FPI and RA models. A non-linear trend line was fitted to FFR data for the FPI and RA models. Based on the FFR cut-off value of 0.75 and using the non-linear trend lines, a region of uncertainty was found to be 81.89% - 83.61%

4.4.5. CDP and LFC in RA and FPI models

CDP

At hyperemia, the CDP is a dimensionless parameter derived from fluid dynamics principles by considering time-averaged pressure drop ($\Delta\tilde{p}$) and the velocity proximal to the stenosis (Banerjee, et al., 2007; Konala, et al., 2011).

$$\text{CDP} = \frac{\Delta\tilde{p}}{0.5\rho U_e^2} \tag{4.12}$$

where $\Delta\tilde{p} = (\tilde{p}_a - \tilde{p}_d)$ (N/m^2) and U_e is the mean proximal velocity (m/s).

LFC

At hyperemia, LFC is a normalized and non-dimensional diagnostic parameter ranging from 0 to 1, and is the ratio of percentage AS and the square root of CDP evaluated at the site of stenosis (Banerjee, et al., 2007).

$$\text{LFC} = \frac{percentage\ \ AS}{\sqrt{\Delta\tilde{p}/0.5\rho U_m^2}} \tag{4.13}$$

where U_m is the mean velocity at the site of stenosis (m/s).

4.4.6. Effect of porous media on CDP and LFC

The CDP and LFC values were calculated in both RA and FPI models. In both models, the CDP and LFC values shows a nonlinear increment with percentage AS .

For RA model, the CDP value increased from 14.96 to 32.54 which is twofold increment in 70% AS to 80% AS. Further increment of stenosis severity from 80%AS to 90% AS the CDP value elevated to 158.02 which is 4.86 fold increment.

Similar nonlinear increment were found in FPI models. For FPI models, the CDP value increased from 2.49 to 26.4 in 70%AS to 80%AS. Similarly, the CDP value elevated to

98.133 as the stenosis severity increased to 90%AS. Similar variations in LFC are found in FPI model. The cut off value of LFC yet to be finalized for the clinical evaluation.

4.5. Discussion:

The FSI modeling capabilities include a coupling between solid - fluid boundaries, which is useful in modeling blood circulation problems such as arteriosclerosis, aneurysms, grafts, endovascular stents, or heart valves. The porous medium modelling is suitable for analyzing bio mass and bio heat transport phenomena across and within biological tissues. In our study, blood is transported mainly in the artery lumen but some could be transported through the wall layers due to the effect of wall permeability and porosity. The critical assessment in the diagnosis of severity of coronary artery stenosis is the study of fluid flow and pressure variation within the coronary artery. To study the effect of wall interaction on the flow and pressure field, we compare the pressure drop and hence the diagnostic parameter obtained from the models having porous wall and the model with rigid wall for the cases of 70%, 80% and 90% percentage AS. The result shows that fluid wall interaction has significant effect on the findings.

In general, the influence of porosity and permeability of the wall reduces the local wall shear stresses (Tripathi, 2013) which increases the filtration of blood from the lumen into the artery. In our study, the axial pressure drop $\Delta\tilde{p}$ in the FPI model was lower than the one obtained from the RA model during a cardiac cycle in all the cases. Similarly, FFR which is currently a functional significant diagnostic tool for the coronary artery disease (CAD) was also affected by the porous media of the arterial wall.

Figure 4.9 shows a significant variation in the FFR values in the FPI model as compared with RA model. The FFR values vary around the cut-off value of 0.75 due to porosity and permeability of the stenosed arterial wall. For AS < 81.89%, the FFR value for the FPI and RA models were well above the cut-off value of 0.75. For AS > 83.61 %, the FFR values for both models were below the cut-off value of 0.75. Thus, the FFR values greater or lower than the cut-off value will not lead to misdiagnosis in both FPI and RA models. However, in the region of uncertainty (81.89-83.61% AS) might lead to misinterpretation of the severity of the coronary artery stenosis.

From this study, it is observed that the porous media of the arterial wall plays a substantial role in the FFR measurement in addition to the plaque size, shape and its components. The variations in the diagnostic parameter due to the porous media might lead to misinterpretation in the assessment of functional severity of intermediate stenosis. This might wrongly lead to the postponement of coronary interventional procedure.

There are some limitations that should be addressed in our study. First, the computational simulation does not fully reflect the realistic physiologic situation as the coronary wall moves during the cardiac cycle.

Second, a smooth surface 3D model is considered rather than a realistic model to capture the physiologic variation in pressure drop in the stenosed arteries.

Third, the porous medium of an arterial wall for the computational analysis considered as a homogeneous porous medium whereas the artery wall consists of many layers having different permeability and porosity.

Fourth, the significance of FFR as functional assessment of the ischemic potential of a stenosis not only resides on theory, but also on clinical research demonstration. The gray zone does depend from this empirical FFR validation, but it could be difficult to validate in vivo. However, we believe our data will help the researchers to design future studies using a realistic coronary artery model and thus can overcome the limitations of the "gray zone" the cut-off value on FFR.

4.6. Conclusion:

For a given percentage area stenosis, the porous stenotic arterial wall affects the flow properties and hence the changes in diagnostic parameter FFR. In clinical settings, due to the effect of porous media of the stenosed arterial wall, there is a possibility of misinterpretation of diagnosis on stenosis severity in patients with intermediate stenosis. From the well-established cut-off value of FFR = 0.75, we found a region of uncertainty of stenosis severity between 81.89% and 83.61% AS in a single vessel CAD by plotting a second degree polynomial non-linear approximate correlation between FFR-% AS. The FFR "gray zone" was only a 5% difference i.e. 0.75 to 0.80 and we expect a smaller difference in percentage of area stenosis. Our mathematical model does signify a proof of concept and these need to be tested in human arteries. We speculate that this difference is likely to be higher due to the irregular appearance of the atherosclerotic plaque and thus the computed area difference is likely to be larger and may be clinically relevant. In addition to the plaque size, shape and its components, we conclude that the porous stenotic arterial wall also determines the cut-off value of FFR. For a given percentage area stenosis, the porous stenotic arterial wall affects the flow properties and hence the changes in diagnostic parameter.

5. INFLUENCE OF WALL CURVATURE ON THE CORONARY DIAGNOSTIC PARAMETERS AND EVALUATION OF REGION OF UNCERTANITY IN THE ANATOMICAL ASSESSMENT OF STENOSIS SEVERITY

5.1. Introduction

The study of blood flow in a progressive narrowing arterial system has generated great interest because the atherosclerotic plaque formation results in life-threatening myocardial infarction. Tortuous coronary arteries and its clinical importance are still unclear. It is widely accepted that plaque development and progression are influenced by many factors, such as static pressure, wall shear stress, blood viscosity, flow velocity, etc.(Goldsmith & Karino, 1995; B. Liu, 2007). The flow patterns such as sudden changes in velocity, direction, or both are responsible for the formation of complex spiral secondary flow and recirculation. These flow patterns are strongly influenced by the vascular geometry irregularity at vessels branch, aortic T-junctions, curve, and change in diameter (Huang, Yang, & Lan, 2010; Wang & Li, 2011). The curvature or the radius of curvature is defined as the degree of artery vessel deviation from being straight at a given point, which refers to the radius of a circle that mathematically best fits the curve at that point (Wang & Li, 2011). Thus, a coronary vessel with a small radius bends more sharply than a vessel with a large radius. From a macroscopic perspective, these vessels differ from each other in dimension and shape. Therefore, investigations regarding the physiological diagnostic parameters in curved arteries with different angles of curvature are significant.

Assessing the functional significance of intermediate stenosis severity remains a challenge for cardiologists (Tobis, et al., 2007). In the current clinical setting, fractional flow reserve (N. H. J. Pijls & Sels, 2012) (FFR, which is the ratio of the distal pressure to the aorta pressure under maximal hyperemia) is a clinically well-proven parameter for measuring the functional severity of stenosis. Numerous clinical trials showed that stenosis with FFR < 0.75 require coronary intervention in single-vessel coronary artery disease (CAD) (N. H. Pijls, et al., 1995), whereas stenoses with FFR > 0.8 in multi-vessel CAD are not associated with exercise-induced ischemia (N. H. J. Pijls & Sels, 2012; Tonino et al., 2009). This finding indicates that the gray zone for FFR is between 0.75 and 0.80, which is categorized under the intermediate area of stenosis (AS = area of the blockage because of stenosis/area of the lumen free from stenosis). In the current clinical evaluation, a cut off value of 0.8 was used in Fractional flow reserve versus Angiography for Multi-vessel Evaluation 1 (FAME1) and FAME2 study and shown to be clinically valid(Melikian et al., 2010). The recently proposed functional and anatomic parameters pressure drop coefficient (CDP) and lesion flow coefficient (LFC), which are derived from the basic fluid dynamic principles (Banerjee, et al., 2007), are useful in diagnosing stenosis severity.

Recent technological advances in multi-detector row computed tomography (MDCT) have improved image quality considerably, and coronary CT angiography (CCTA) has become an integral part of the diagnostic work-up in patients suspected for CAD (Abdulla et al., 2007). The CCTA technique is a non-invasive and quality image can be obtained quickly. The functional or physiological significance is more valuable than the anatomical significance of CAD. In recent times, the true physiological significance of coronary artery stenosis severity is assessed by pressure drop and flow (MacCarthy et al., 2005; N. H. Pijls, et al., 1996; N. H. J. Pijls & Sels, 2012).

The insertion of guide wire (Sinha Roy, et al., 2006), downstream collateral flows (Peelukhana, et al., 2009), arterial wall compliance and plaque characteristics (Konala, et al., 2011), and aortic and coronary outflow pressure (Maria Siebes, et al., 2002) have been found to significantly affect the FFR value. The above-mentioned cases have led to misinterpretation of the functional severity of stenosis in the gray zone. Several experimental, analytical, and computational simulation analyses conducted on the hemodynamic changes in stenotic arteries and computing the severity of stenosis have been reported by many researchers in an axisymmetric stenotic straight tube(R. Banerjee, et al., 2008; Konala, et al., 2011; Sinha Roy, et al., 2006). A limited number of research focused on the influence of the curved stenosed arterial wall on physiological diagnostic parameters and the evaluation of region of misinterpretation in-vitro assessment using FFR as a standard parameter. Hence, it would be highly desirable to construct 3D computational curved rigid arteries with various stenosis severities 70% (moderate), 80% (intermediate), and 90% (severe) with various angles of curvature models for the investigation under transient physiological hyperemic flow conditions.

In this chapter, for a given percentage area stenosis severity (percentage AS = 100% × (reference lumen – minimum lumen area)/reference lumen), the physiological coronary diagnostic parameter variations such as fractional flow reserve (FFR), pressure drop coefficient, and lesion flow coefficient owing to stenosed coronary arterial wall curvature are investigated. FFR is the current gold standard to assess the functional significance of coronary stenosis severity. From the clinical perspective, the pressure drop across the stenosis and FFR in curved artery models were analyzed and a possible uncertainty region was found owing to curved stenosed artery wall by correlating % AS and FFR.

5.2. Literature review:

5.2.1. Influence of artery wall curvature on hemodynamics

The coronary artery geometry varies from person to person and it has shape of straight and curved artery. The flow is uniform in the straight sectional artery whereas the flow is skewed in the curved artery without any obstruction. If the obstruction exists due to stenosis, the flow will be disturbed in both kind of arteries. Artery wall curvature plays substantial role on the intraluminal flow and wall shear stress in the presence or absence of a luminal obstruction. The flow characteristics such as flow separation, secondary flow, wall shear stress and pressure drop characteristics vary dramatically along the length and circumference of the artery owing to curvature of the artery (Figure 5.1 and Figure 5.2) (B. Liu, 2007).

From the study done by Liu (B. Liu, 2007), when the stenosis located at the inner wall of the curved artery and its severity reaches a certain level, the blood flow pattern in the downstream of the stenosis has changed dramatically as compared to that of a curved artery with no stenosis. If the stenosis severity increases in a curved artery the flow separation area is larger at the downstream and the reversed flow occurred and stronger near the inner wall of the curved artery.

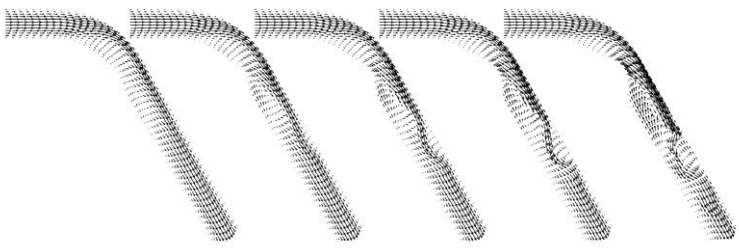

Figure 5.1: Comparison of the effect of stenosis 19%, 36%, 44%, 51% and 64% at the minimum flow rate during diastole
Reprinted from (B. Liu, 2007), Copyright (2015) with permission from Elsevier

5.2.2. Dynamic curvature variation on hemodynamics

Realistic modeling of the deforming geometry is important in determining which locations in the coronary arteries are subjected to low and oscillating wall shear stresses, flow patterns that have been associated with atherogenesis (Santamarina, Weydahl, Siegel, & Moore, 1998). The tortuosity of the coronary artery alters the shear stress when the flow through lumen and may trigger platelet formation in micro vessel. From the vitro dynamic flow model done by S.Schilt et al.(Schilt, Moore Jr, Delfino, & Meister, 1996), the velocity profile skewed to the outer wall when the fluid flow through curved artery and also modulated with the shape of dynamic change of curvature. The maximum skewness occurs when the radius of curvature changed from minimum to maximum value.

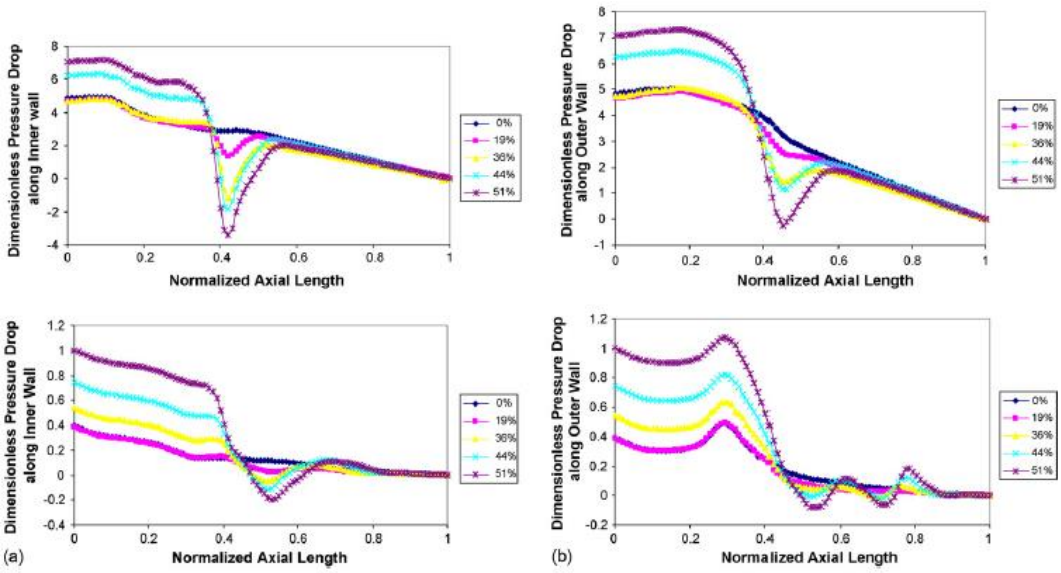

Figure 5.2: Dimensionless pressure drop of the blood flow in curved arteries with different size of stenosis along the inner wall (a) and along the outer wall (b), at systolic peak and at the minimum flow rate during diastole (B. Liu, 2007)
Reprinted from (B. Liu, 2007), Copyright (2015) with permission from Elsevier

The flow patterns such as wall shear stress may be important in determining the localization of atherosclerosis. X. Wang, X.Li demonstrated the flow velocity and shear stresses in a curved vessel by applying fluid wall interaction (Figure 5.3) and compared their findings with rigid wall flow (Wang & Li, 2011). From their findings, peak stress increased in the curved vessel when the curvature of the vessel increased, and increased with decrease of wall flexibility. Figure 5.4 (a&b) shows the axial velocity plot at the cross section of the straight wall portion and curved wall portion, respectively. From Figure 5.5 (a&b) time varying maximum stress occurs before the maximum inlet velocity along the outer wall and inner wall of the artery model. The inner side wall shear stress is maximum than the outer side wall of the curved artery in the cardiac cycle. Coronary atherosclerosis generally formed along the inner arc of the curved vessel. So it is highly desirable to see the effect of arterial wall curvature on the coronary diagnostic parameters.

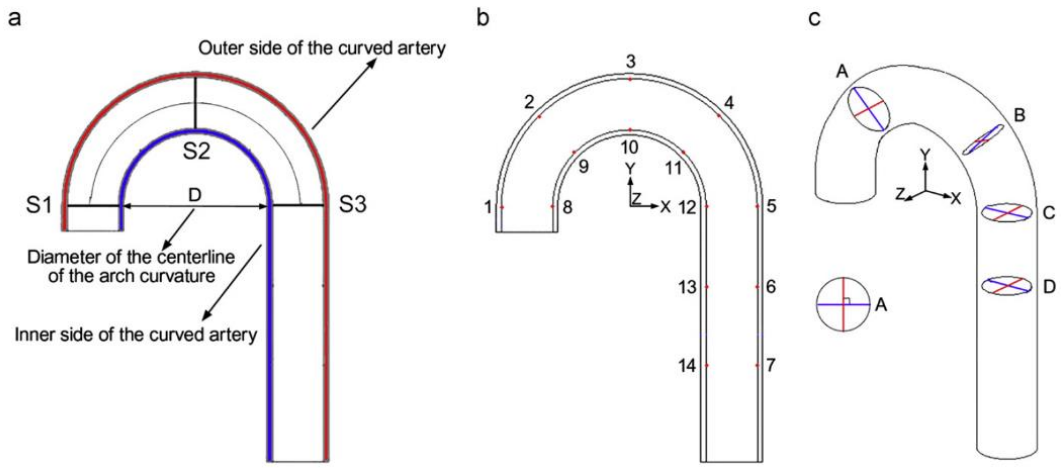

Figure 5.3: Curved artery models (a) location of cross section (b)point of interest and (c) cross sectional plane
Reprinted from (Wang & Li, 2011), Copyright (2015) with permission from Elsevier

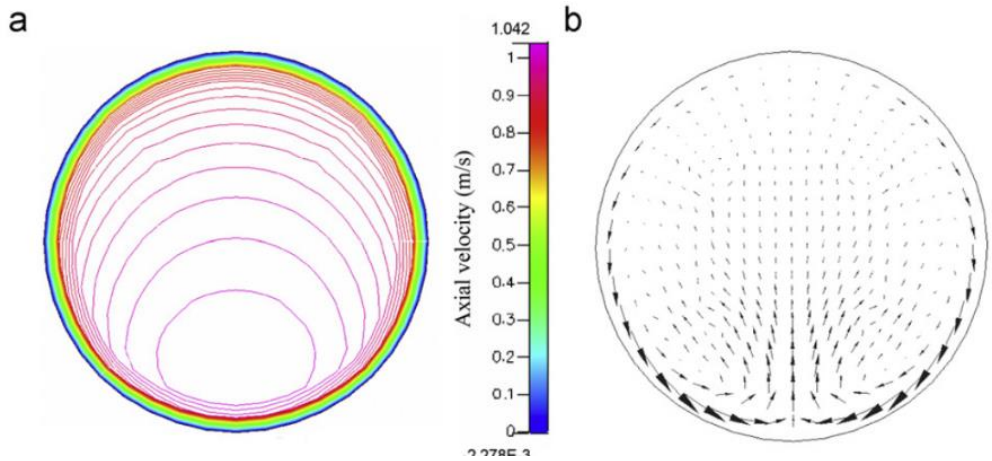

Figure 5.4: Axial velocity plot (a) at section S1 and (b) at S2
Reprinted from (Wang & Li, 2011), Copyright (2015) with permission from Elsevier

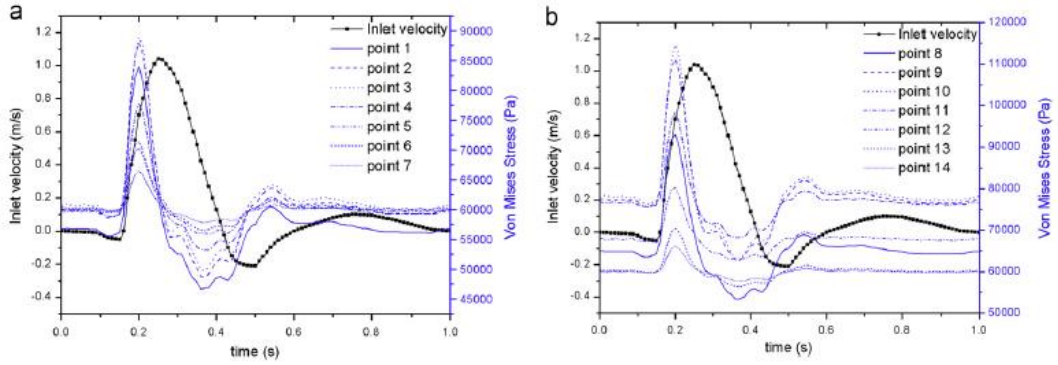

Figure 5.5: Time variation of Von Mises stresses at the point of interest
Reprinted from (Wang & Li, 2011), Copyright (2015) with permission from Elsevier

5.3. Methodology

5.3.1. Stenosis geometry

For this analysis, 70%, 80%, and 90% AS were used in the curved artery models with different angles of curvature. The general geometrical form of an ideal model of the curved stenosed rigid artery is shown in Figure 5.6. The internal diameter of the unobstructed artery is 3 mm. The angles of curvature (θ°) for the curved arteries are 0° (straight section), 30°, 60°, 90°, and 120° (Yao, Ang, Yeo, & Sim, 2000). Stenosis, a

duplicate geometry of Dash et al.(Dash, Jayaraman, & Mehta, 1999) has been developed in a concentric method with a length of L (10 mm) and is given by,

$$\frac{\tilde{\eta}(\tilde{z})}{a} = 1 - \frac{h}{a}\sin\pi\left(\frac{\tilde{z}-d}{L}\right), \quad d \le \tilde{z} \le d + L, \tag{5.1}$$

where $\tilde{\eta}(\tilde{z})$ is the radius of the stenosis, a is the radius of an artery (1.5 mm), $\tilde{z}$ is measured along the axis of the artery, and h is the maximum projection of the stenosis into the lumen. A categorized cut-off lesion length value of 10 mm is a sensitive prediction index for a categorized cut-off FFR value of 0.75 (Brosh, et al., 2005).

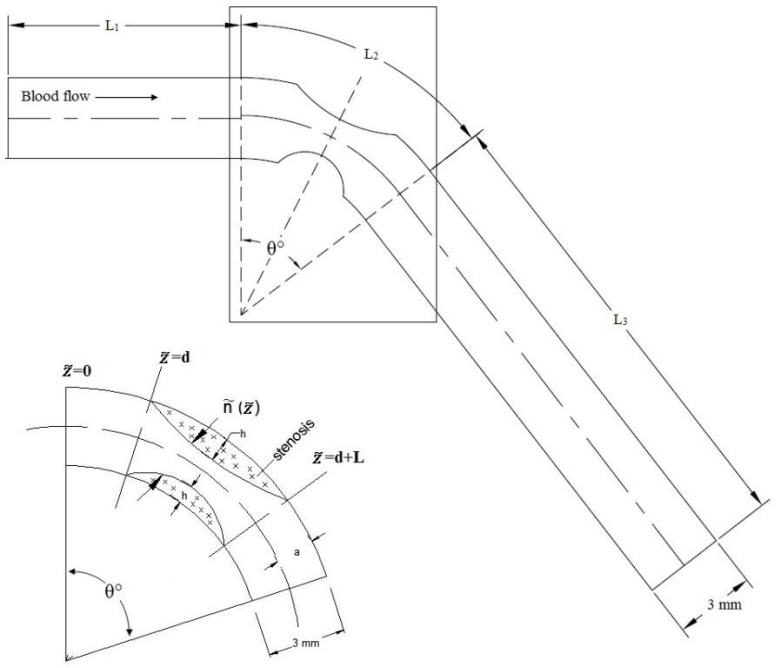

Figure 5.6: The schematic diagram of the curved artery with stenosis

To provide complete assessment of the curvature effect, three different locations such as central, proximal and distal positions of the stenosis at the bend have been taken into consideration. For all the curvature models, the fixed length of L_2 (18 mm) and L_3 (60 mm) are the axial length of the curved section and straight distal length immediately after the curve, respectively. L_1 is the straight entrance length prior to the curve. The L_1

(minimum axial length of 18 mm) have been varied depending on the location of the stenosis at the bend to maintain the length of L_1+d as constant in all the curvature models, where d is the axial distance between the start of curvature and the start of stenosis at the bend.

5.3.2. Mathematical formulation

The blood flow through the coronary artery is assumed to be incompressible, unsteady, and governed by the Navier–Stokes equation. The blood is assumed to be non-Newtonian and follows Carreau model. The details are given in the section §3.3 of chapter 3.

5.3.3. Boundary conditions

The post stenotic velocity waveform was characterized by augmentation of the systolic velocity component and a relatively small diastolic velocity component. These characteristics distinctly contrasted with normal coronary artery flows, i.e., a diastolic-predominant pattern wave form (Kajiya, et al., 1987). In order to ensure a realistic 3D numerical analysis, transient pressure *p(t)* (Konala, et al., 2011; Tang, et al., 2009) and velocity *u(t)* (Young I Cho, Back, Crawford, & Cuffel, 1983; Konala, et al., 2011) were applied at the inlet and outlet (Figure 5.7), respectively. No slip condition was applied at the arterial wall. The velocity profiles for 70%, 80%, and 90% AS were obtained from the mean hyperemic flow rate $(\tilde{Q})$ of 175, 165, and 115 mL/min (Konala, et al., 2011; A. S. Roy, et al., 2005), respectively which was explained in the Chapter 4 section 4.3.5.

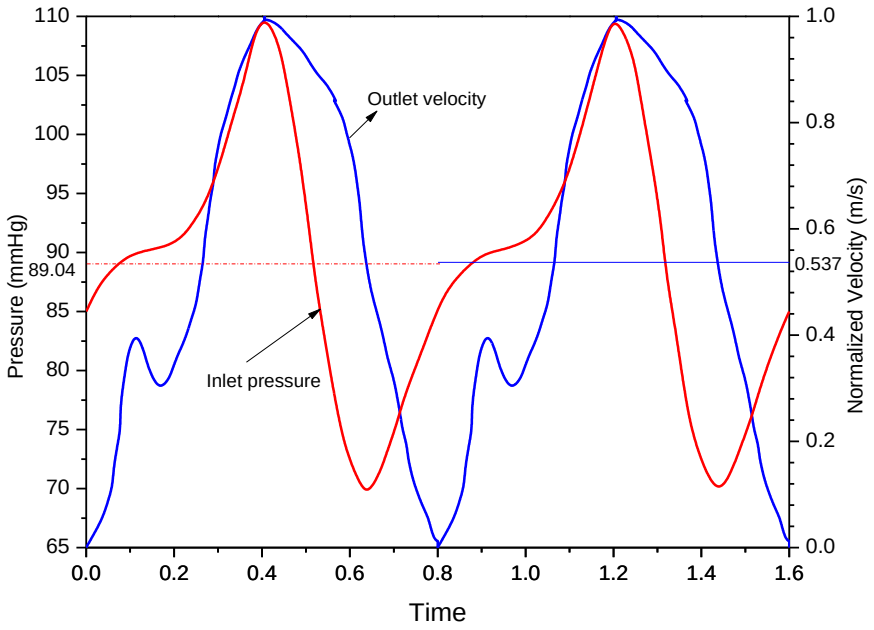

Figure 5.7: Physiological pressure (Konala, et al., 2011; Tang, et al., 2009) and velocity applied at the inlet and outlet (Young I Cho, et al., 1983; Konala, et al., 2011), respectively. The peak velocity corresponds to a normalized velocity of 1.0, so that the ratio of mean to peak veloc ity $\bar{u}/\bar{u}_{p-t}$ is 0.537.

A shear stress transport turbulence (SST) model of the k-ω model family was adopted for flow modeling because of its accuracy and robustness in overcoming the near-wall treatment errors for low Reynolds turbulence computations (Jozwik & Obidowski, 2010). The CFD simulation was first run with steady-state flow analysis and then with transient flow analysis based on the results of the steady-state analysis as the initial estimate (Jozwik & Obidowski, 2010).

For the steady-state analysis, the values of the following parameters at the inlet and outlet were recorded:

- Mean physiological pressure at the inlet: 89.04 mmHg for 70%, 80%, and 90% AS models.
- Mean velocity at the outlet: 0.413, 0.389, and 0.271 m/s corresponding to 70%, 80% and 90% AS, respectively.

5.3.4. Numerical methodology

The computational domains were initially meshed with hexahedral elements as shown in Figure 5.8.

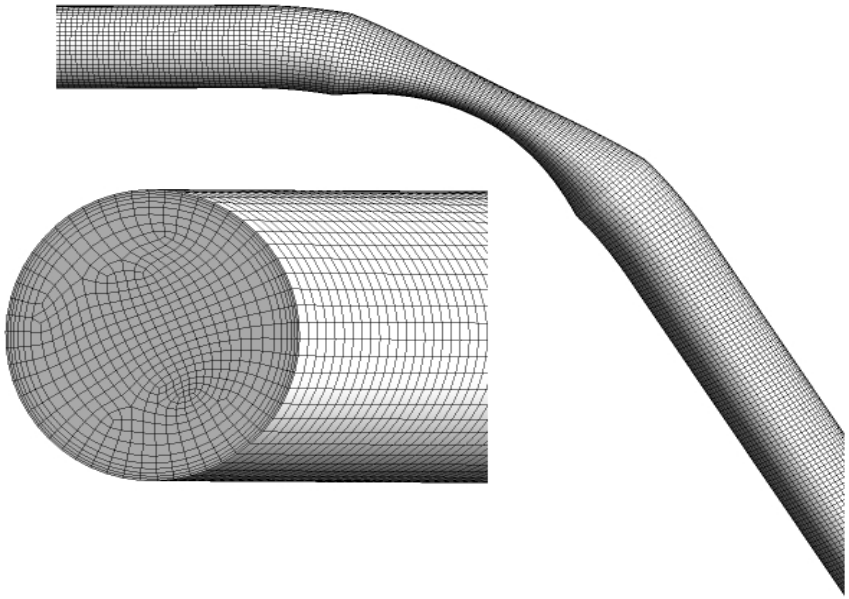

Figure 5.8: Computational mesh used for numerical study in the curved stenotic artery model

The total number of elements varied from 200,000 to 250,000 for 70%, 80%, and 90% AS models. Quality of mesh was checked by inspecting various parameters such as skewness, orthogonal quality, element quality etc. as explained in the section §4.5.1 of chapter 4 A finite volume software CFX 14.0 (ANSYS CFX, Canonsburg, PA) was used for the flow simulation. Adaptive time stepping method was used where the initial time step was set to 0.001 s and the minimum and maximum time step was between 0.001 and 0.01 s. The increase and decrease in the time step occurred after six target loops with the factor of 1.5 and 0.5, respectively. To ensure that the flow was periodic, the transient flow analysis was run for four cycles (0.8 s each) of pulsatile flow with each time step converging to a residual target of 1×10^{-4}. In all the cases, without-

guide-wire condition was considered. Subsequently, a mesh-independent study was performed with the elements varied from 250,000 to 350,000 to ensure that the computed wall shear stress differed by < 0.3%.

5.4. Results

To examine the influence of angle of curvature on blood flow for the possible uncertainty region of stenosis severity, a computational simulation was used in 0°,30°,60°,90° and 120° curved stenosed artery wall models. For each curvature wall model, three cases of AS, 70%, 80% and 90% were investigated. From all the curvature models, the pressure drop across the stenosis was analyzed first, and then the FFR, CDP and LFC were analyzed from the pressure drop. The FFR- %AS was related for the various angle of curvature models and a region of interest where the possible misinterpretation of stenosis severity in the visual assessment of CCTA was found from the correlation by applying the FFR cut off value. The pressure drop and functional diagnostic values obtained in this study were transient time averaged quantities under hyperemic flow conditions.

5.4.1. Pressure drop in curved arteries

In all the curvature models, $\tilde{p}_a$ was measured at 3 mm before the arterial wall began to bend, and $\tilde{p}_d$ was measured at the distal recovery pressure along the axis of the coronary artery. The overall transient pressure drop $\Delta p = p_a - p_d$ which was taken during the cardiac cycles 3 and 4 and there is no significant difference in the pressure drop found between the cycles 3 and 4 to ensure that the accurate results with numerical

data being reported for the third and fourth cycles. Fig.4 shows the overall transient pressure drop in 0° and 120° curvature wall models, having 80% AS.

The time averaged pressure drop $\Delta\tilde{p} = \tilde{p}_d - \tilde{p}_a$ under various angles of curvature conditions for 70%, 80%, and 90% AS are reported in Table 5.1. The pressure drop increases as the percentage of stenosis severity increases for a given angle of curvature. However, $\Delta\tilde{p}$ increases in a non-linear manner as the angle of curvature increases for a given percentage of AS in any rigid wall plaque model. The bar graph presented in Figure 5.10 shows a nonlinear variation in $\Delta\tilde{p}$ as the angle of curvature was varied as 0°, 30°, 60°, 90° and 120° for a given percentage AS. A negligible pressure drop variations were found as the stenosis location changed from upstream to central position and central to downstream position at the bend for a given percentage AS and for the given angle of curvature. All $\Delta\tilde{p}$ data and the coronary diagnostic parameters, which are derived from $\Delta\tilde{p}$ are reported in the following sections were obtained with the stenosis located centrally at the bend. As the angle of curvature changes from 0° to 120°, the corresponding $\Delta\tilde{p}$ increases from 8.09 mmHg to 11.98 mmHg (48.08%), 17.49 mmHg to 23.04 mmHg (31.73%), and 40.92 mmHg to 49.8 mmHg (21.7%) in 70%, 80%, and 90% AS, respectively. This finding indicates that the presence of the curvature elevates the flow resistance in addition to the resistance caused by the stenotic lesion. Therefore, the major pressure drop is due to the stenosis, which is higher at the region of the minimal area of cross section. The curvature of the arterial wall also contributed to the pressure drop across the stenosis.

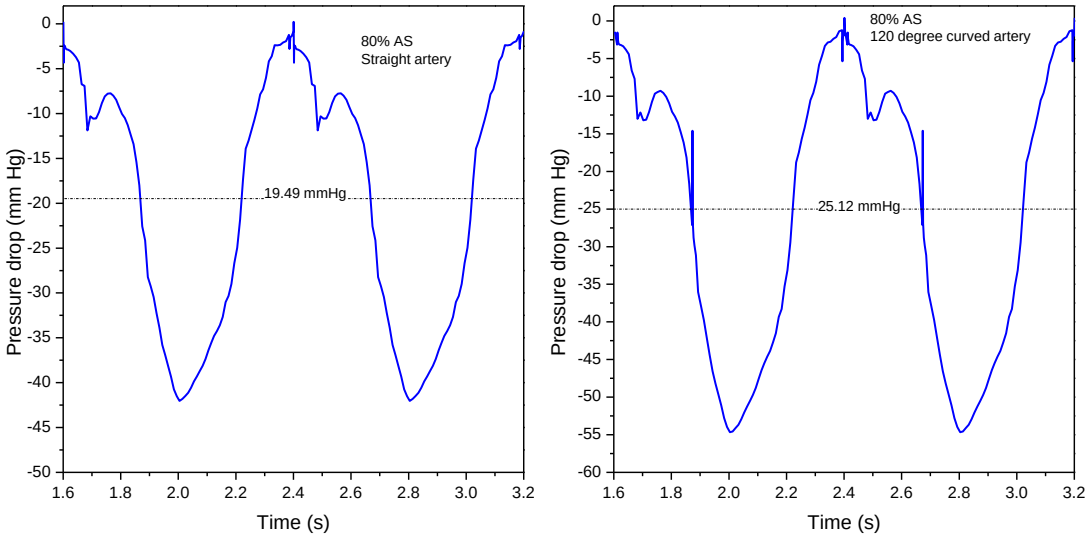

Figure 5.9: The overall transient pressure drop in straight and 120° stenosed curved artery having 80% AS

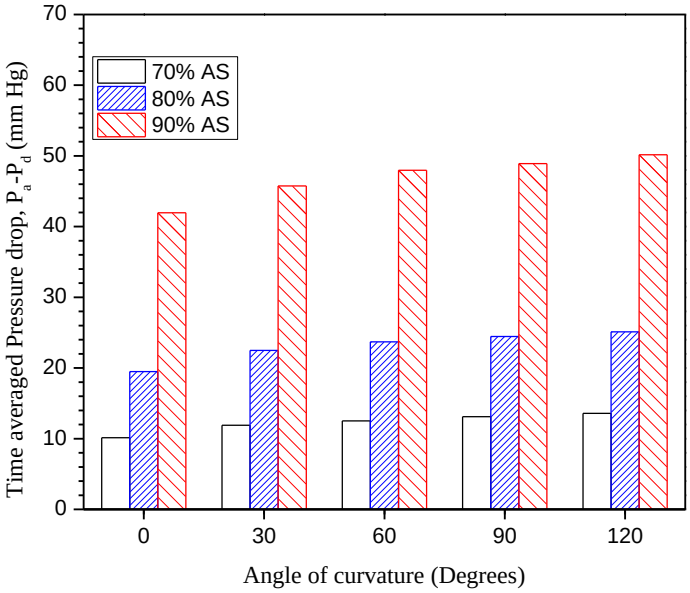

Figure 5.10: Variation of time averaged pressure drop across the stenosis with angle of curvature.

Table 5.1: Results from Computational analysis

Angle of curvature θ°	70% AS			80% AS			90% AS		
	$\tilde{P}_a$ mmHg	$\Delta\tilde{P}$ mmHg	FFR	$\tilde{P}_a$ mmHg	$\Delta\tilde{P}$ mmHg	FFR	$\tilde{P}_a$ mmHg	$\Delta\tilde{P}$ mmHg	FFR
0 (Straight section)	87	8.09	0.91	87.04	17.49	0.8	88	40.92	0.54
30	87.28	10.12	0.88	87.35	20.79	0.76	88	44.71	0.49
60	87.13	10.8	0.88	87.31	22.18	0.75	88	47.35	0.46
90	87.29	11.35	0.87	87.27	22.69	0.74	88.02	47.88	0.46
120	86.79	11.98	0.86	87.11	23.04	0.74	87.99	49.8	0.43

5.4.2. Effect of curvature of the stenosed arterial wall on the diagnostic parameters

5.4.2.1. FFR

The FFR value decreases as the percentage of AS increases. The FFR value decreases considerably when the angle of curvature of the artery increases in any given AS percentage and are reported in Table1. As the angle of curvature changes from 0° to 120°, the FFR decreases from 0.91 to 0.86 (5.49%), 0.8 to 0.74 (7.5%), and 0.54 to 0.43 (20.37%) in 70%, 80%, and 90% AS, respectively. This finding indicates that the presence of the curvature decreases the FFR. A more significant effect is observed when the severity changes from intermediate to severe stenosis. A best-fit approximation is plotted against the computed FFR values (Figure 5.11). This approximation includes the non-linear correlation (R^2) of 0.97, 0.98, and 0.98 for 70%, 80%, and 90% AS, respectively.

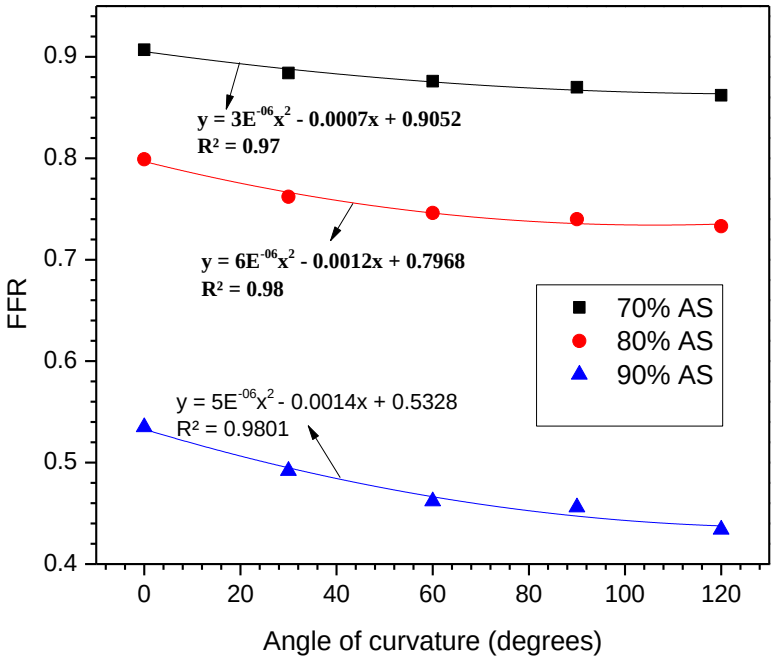

Figure 5.11: Variation of FFR values with the angle of curvature in 70%, 80% and 90% AS models. A non-linear trend line was fitted to FFR data with angle of curvature.

A best fit linear approximation (Konala, et al., 2011) was used to plot the computed values of percentage AS and FFR, as shown in Figure 5.12. To estimate a region of uncertainty, a horizontal line representing the cutoff value corresponding to FFR=0.8 and FFR=0.75 was drawn (Konala, et al., 2011; Kristensen, et al., 2010). This horizontal line corresponding to FFR=0.75 intercepted the FFR–percentage AS lines for 0° and 120° curvature models at 79.06% and 76.10% AS, respectively. For FFR =0.8 the interceptions were at 76.31% and 73.66% AS for 0° and 120° curvature models, respectively. The following discussion and conclusion are based on the cut off value of 0.75 for FFR.

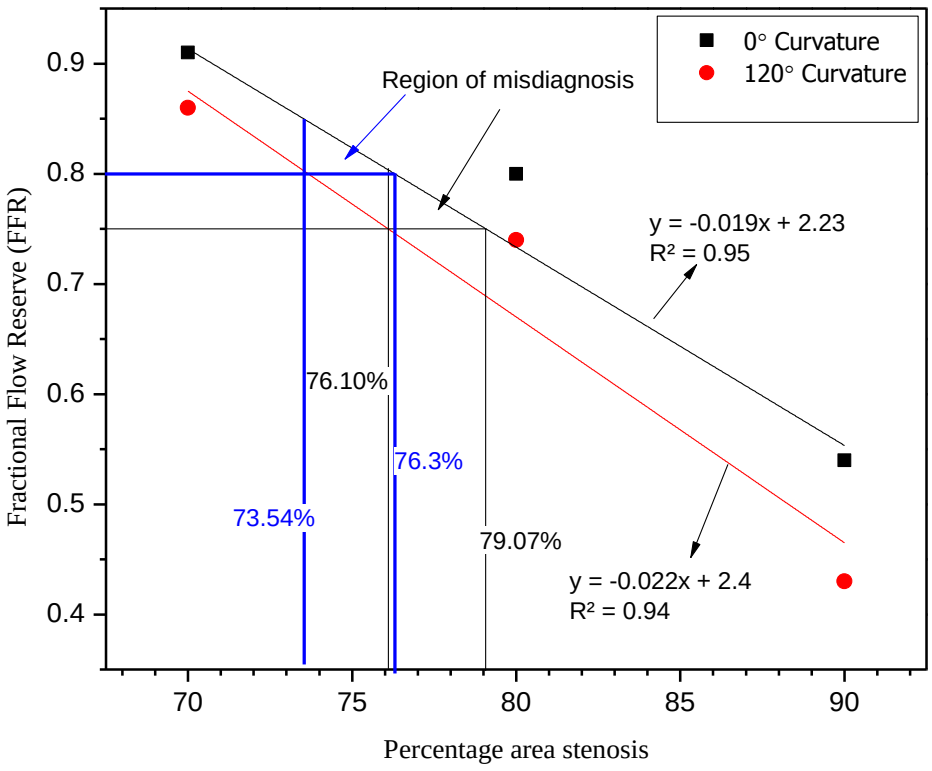

Figure 5.12: Variation of FFR values with the angle of curvature. A linear trend line was fitted to FFR data for 0° and 120° curvature models. Based on the FFR cut-off value of 0.75 for single vessel stenosis and using the non-linear trend lines, a region of uncertainity region was found to be 76.10 – 79.06% AS

5.4.2.2. CDP and LFC

The values of CDP and LFC are computed using the pressure, flow, and lesion geometry. For a given arterial wall curvature, the CDP and LFC values increased non-linearly with the percentage AS. Furthermore, a nonlinear increment in the CDP values and a nonlinear decrement in the LFC values were observed as the angle of curvature of the arterial wall ncreased for a given percentage AS (Figure 5.13 & Figure 5.14).

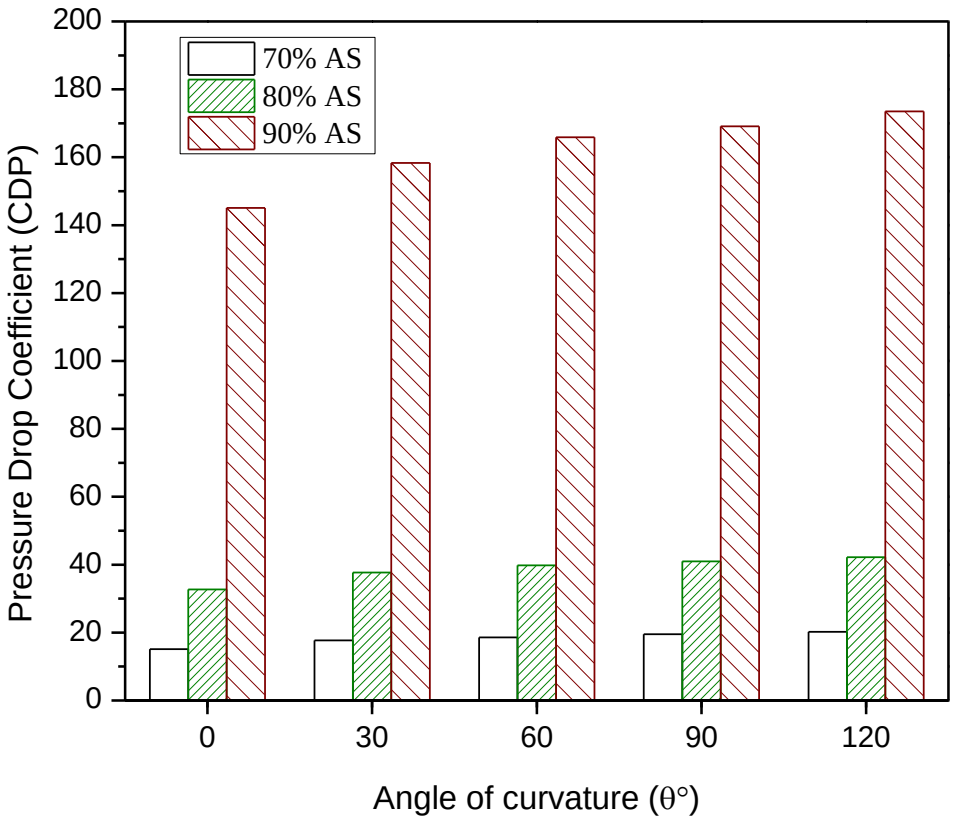

Figure 5.13: Variation of CDP with angle of curvature in 70%, 80% and 90% AS models

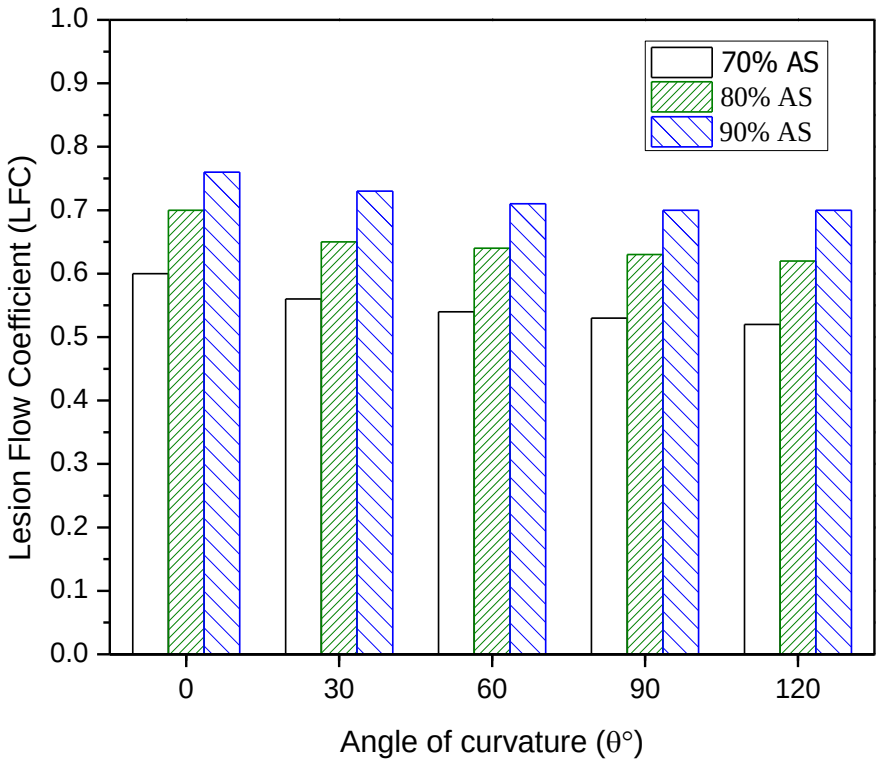

Figure 5.14: Variation of LFC with angle of curvature in 70%, 80% and 90% AS models

The computed CDP and LFC values are reported in Table 1. In 70% AS, the CDP value increased from 15.1 to 20.2 (33.77%) as the angle of curvature varied from 0° to 120°, whereas the LFC decreased from 0.6 to 0.52 (13.33%). A similar nonlinear increasing trend in the CDP values and a decreasing trend in the LFC values were observed in 80% AS; under this severity condition, the CDP value increased from 32.7 to 42.2 (29.05%) and the LFC value decreased from 0.7 to 0.62 (11.43%). Similarly, in 90% AS, the CDP value increased from 145.1 to 173.5 (19.57%), whereas the LFC value decreased from 0.76 to 0.7 (7.89%).

5.5. Discussion

The vascular geometry is a combination of curved vessels (Wang & Li, 2011) and straight vessels (R. K. Banerjee et al., 2008; Banerjee, et al., 2003). The dynamic variation of a coronary artery geometry is owing to heart motion during each cardiac cycle in the cardiovascular system (Prosi M Fau - Perktold, Perktold K Fau - Ding, Ding Z Fau - Friedman, & Friedman; Schilt, et al., 1996). Nosovitsky et al. (Nosovitsky, Ilegbusi, Jiang, Stone, & Feldman, 1997) reported that coronary artery curvature exerts an important impact on the intraluminal flow and shear stress in the presence or absence of a luminal obstruction. Wang et al. (Wang & Li, 2011) showed that wall shear stress was high in the regions of curvature, indicating that the risk region of the artery mostly appeared in the curved part. The primary purpose of the present study was to reveal the variability in FFR, CDP, and LFC values for a given percentage AS owing to the curvature of the arteries, and to identify a region of a possible misinterpretation in the intermediate stenosis severity when assessing anatomical significance of stenosis severity using CCTA assessment by applying in-vivo measurement of FFR, which could lead the clinician to decide upon coronary intervention around the clinically used cutoff value of 0.75 (Konala, et al., 2011).

To study the effect of stenosed curved artery vessel wall on the flow and pressure field, we compared the pressure drop, and hence, the diagnostic parameters obtained from the models having various angles of curvature for the cases of 70%, 80%, and 90% AS. The results showed a nonlinear increment of pressure drop with an increase in stenosis severity. This was owing to the change in the momentum as the flow velocity increased across the stenosis. For a given percentage AS, the axial pressure drop $\Delta\tilde{p}$ was higher in 120° curved artery than that in the 0° curved artery (straight section) during a cardiac

cycle, similar to that observed by Yao et al. and Dash et al. (Dash, et al., 1999; Yao, et al., 2000). This is owing to the occurrence of secondary flow as a result of centrifugal pressure gradient along the curved artery, which tends to push the flow in the curving plane towards the outer wall Figure 5.15. Thus, the bend of an artery restricts the flow, in addition to area constriction, causing additional head loss.

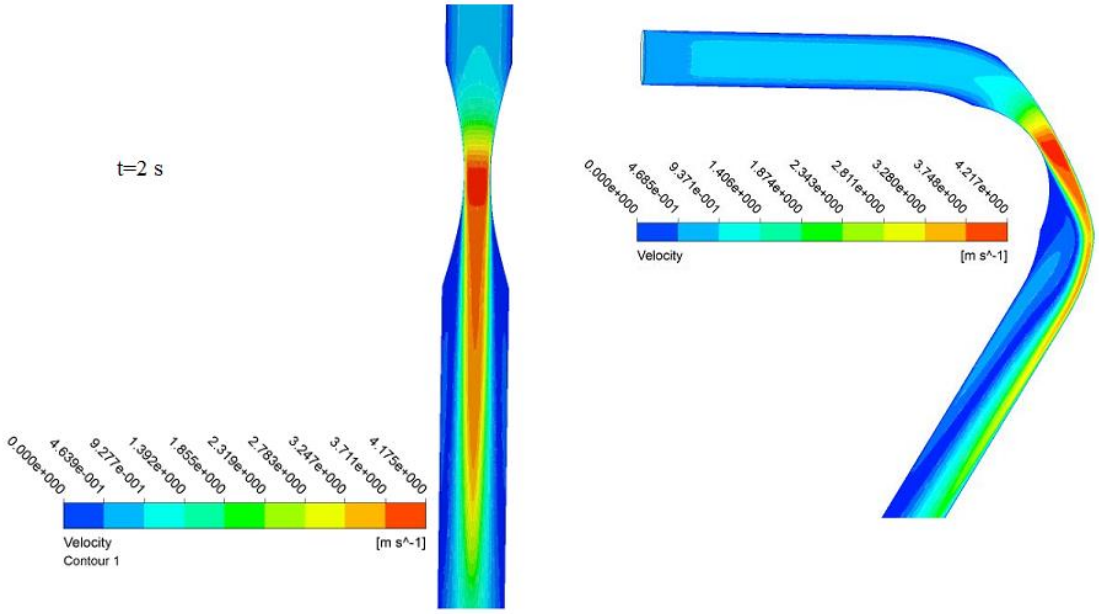

Figure 5.15: Development of secondary flow in straight and curved artery model

The FFR, which is derived from pressure drop across the stenosis, decreased as the percentage AS increased, which, in general, is consistent with that reported in a previous in vivo study (Banerjee, et al., 2009). Furthermore, for a fixed percentage AS and flow, the FFR was affected owing to the curvature of the artery. Figure 5.15 shows significant variations in FFR as it decreased with the increase in the angle of curvature of the arterial wall under all the three severity models. The values of pressure drop and FFR obtained in this study in the straight stenosed artery wall models (0°) from all severity cases were in close agreement with the available numerical results obtained by Konala et al. in the absence of guide wire condition (Konala, et al., 2011) in the rigid

artery with rigid plaque model (Figure 15.16(a)&(b)). However, in the study by Konala et al. (Konala, et al., 2011), the impact of artery wall curvatures on the FFR was not considered. Hence, the present study focused on the curved stenotic artery wall and their effect on FFR.

The FFR value varied around the cutoff value corresponding to 0.75 owing to the curvature of the artery wall and thus a region of uncertainty was found to be 76.10–79.07% AS. For AS < 76.10%, the FFR values were well above the cutoff value of 0.75, whereas for AS > 79.07%, the FFR values were below the cutoff value of 0.75, irrespective of the given range of angles of curvature. It should be noted that, for the intermediate stenosis (80%) AS, the FFR values for a 0° curvature is 0.8, whereas for the curved arteries it is less than 0.8 (varied between 0.76 and 0.74; Table 1). Since the FFR is decreasing (but, not increasing) for curved cases, the chance of misdiagnosis (i.e., not being treated) is impossible. In other words, the FFR outcome for curved arteries in comparison to straight arteries is more conservative. Further, if the combination of stenosis and curvature leads to an FFR below 0.75, then such an artery needs to be treated anyway. Our curved stenosed arterial wall models demonstrated that the variation in the angle of curvature significantly affects the FFR for a given percentage AS.

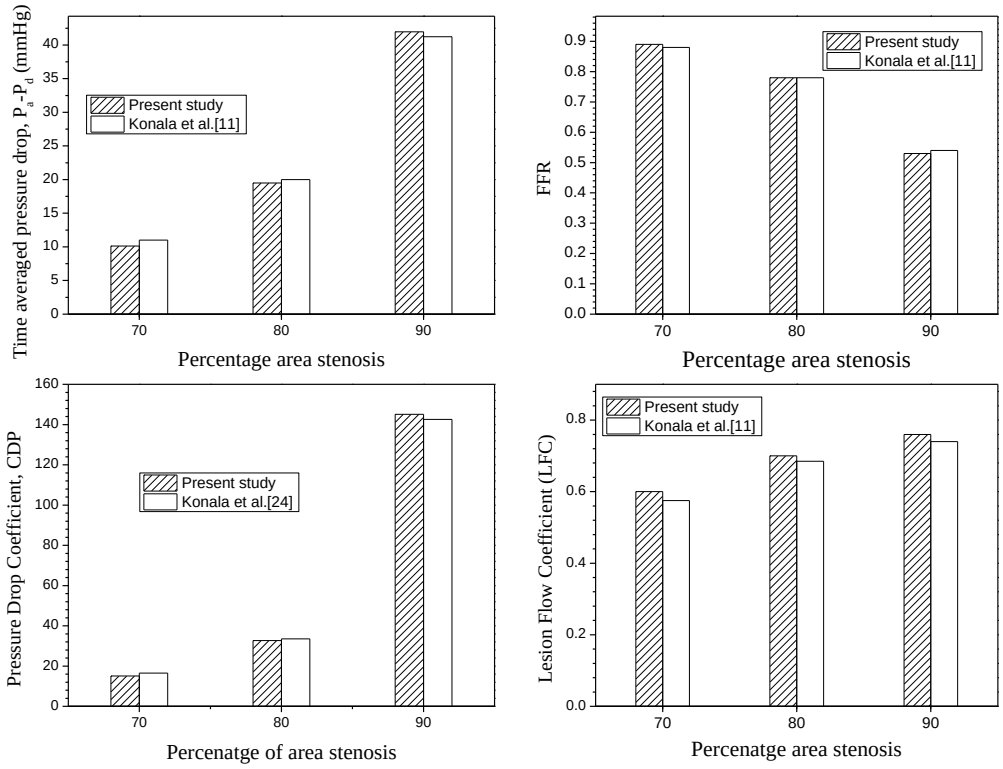

Figure 5.16: Comparison of numerically obtained ,FFR, CDP, LFC values with B.C Konala et al. (Konala, et al., 2011) study in the straight section of the stenotic coronary artery models for the 70% , 80% and 90% AS

Few studies have shown to be a poor correlation between percent diameter stenosis obtained from CCTA images and FFR (W. B. Meijboom et al., 2008; Wijpkema et al., 2007). But from the recent study done by Kristensen et al., percent area stenosis obtained from CCTA appeared to be clinically useful and is significantly correlated with physiological diagnostic parameter FFR by applying automated quantitative algorithm (Kristensen, et al., 2010). The FFR obtained from all the curvature models for a given percentage of stenosis are closely concurred with the digitized data obtained from the study done by Kristensen et al. (Kristensen, et al., 2010). This variations in FFR due to curved artery will notably impact on the anatomical assessment of intermediate stenosis severity. From the numerical study, it should be noted that the percentage difference between the FFR of the intermediate stenosis (80% AS) for the 0° and 120° curvature was 7.5%. Thus, the contribution of bend, in relation to the stenosis

severity, on the FFR and pressure drop, particularly for the 80% AS, is marginal and is probably near the diagnostic uncertainty of measurements during the catheterization procedure. In other words, curvature effect can't be ignored during the anatomical assessment of stenosis severity irrespective of the fact that the straight artery could result in an FFR greater than 0.75. Similar to $\Delta\tilde{p}$ and FFR, variations in CDP and LFC were observed in 70%, 80%, and 90% AS in various angle of curvature models (Figure 5.13 and 5.14). Recent meta-analysis study shows that clinical cut-off value of CDP to detect FFR < 0.8 and FFR < 0.75 was at CDP > 27.1 and CDP > 27.9, respectively (K. K. Kolli, et al., 2014). However, the cutoff value for LFC has not yet been decided for clinical evaluation (Peelukhana, et al., 2009)

There are some limitations of the present study. The factors that influence the diagnostic parameters such as arterial wall compliance (Konala, et al., 2011), multiple bend, dynamic curvature variation owing to heart motion (Yang et al., 2008), wall roughness, and lesion eccentricity were not considered. Furthermore, in future studies, realistic coronary artery model needs to be used, which will overcome the limitations to analyze the influence of curvature on the coronary diagnostic parameters.

5.6. Conclusion

This computational fluid dynamics simulation study investigated the effects of the angle of curvature on the coronary diagnostic parameters in 70%, 80%, and 90% AS coronary artery models under hyperemic flow conditions. In the case of intermediate stenosis severity and from numerical study it is clearly shown that the FFR values varies around the cut-off value of 0.75 owing to variations in hemodynamic conditions, which could lead to a dilemma for the clinician in distinguishing intermediate lesions that require

stenting or simply need appropriate medical therapy when assessing anatomical assessment stenosis severity by using CCTA images. For a given percentage AS, the curvature of the stenosed arterial wall affected the intraluminal flow, and hence, changes in the diagnostic parameter FFR. These variations in the diagnostic parameters elevate the stenosis severity during the measurement of functional significance of stenosis. From the physiological evaluation of stenosis severity in a curved arterial wall, the assessment of % AS using CCTA images for the clinical decision making can lead to underestimation of the stenosis severity and postponement of coronary interventional procedure. From the well-established cutoff value of FFR=0.75 (Konala, et al., 2011) for single vessel CAD, we found a region of uncertainty in evaluating functional significance of stenosis severity between 79.07 and 76.10% AS in a curved stenosed artery by plotting a linear approximate correlation between FFR and percentage AS. We speculated that this difference could possibly be higher owing to severe coronary tortuosity and irregular appearance of atherosclerotic plaque, and thus, the computed uncertainty region is likely to be larger and may be clinically relevant. We also found that the CDP value increased and the LFC value decreased as the angle of curvature changed from straight section to curved section for a given percentage AS. However, further in vivo studies and validations are required to fix the cutoff value for LFC, similar to FFR. However, further in-vivo and vitro studies and validations are required to correlate anatomical significance and functional significance of stenosis severity by considering the artery wall curvature. In addition to the plaque size, shape, and its components, the curvature of the arterial wall influence on the visual assessment of stenosis severity.

6. INFLUENCE OF VARIABLE ANGULATION OF ARTERIAL WALL ON CORONARY DIAGNOSTIC PARAMETERS

6.1. Introduction

Geometrical appearance of the Left Coronary Artery (LCA) differs from the Right Coronary Artery (RCA). The LCA has a short main stem, which divides into two main branches called Left Anterior Descending (LAD) and Left Circumflex (LCX) forming an angle, with many side branches as shown in Figure 6.1 (Chaichana, et al., 2011; Giannoglou, Antoniadis, Koskinas, & Chatzizisis, 2010). The angulation between the two coronary side branches differ from each other in dimension and shape (Figure 6.2) and thus the angulation between the coronary side branches have significant effects on blood flow which was potential risk for the development of atherosclerosis (Chaichana, et al., 2011; Wiwatanapataphee, Wu, Siriapisith, & Nuntadilok, 2012). Chaichana, et al. (Chaichana, et al., 2011) showed that with wider angulation, the flow become disturbed and reduced wall pressure from left main stem to the bifurcated regions. A bifurcation lesion is a coronary artery narrowing that may occur adjacent to, and/or involving the origin of a significant side branch. There is a good correlation between plaque formation and the angulation of coronary bifurcation (Sun & Cao, 2011) and mostly originate in the LCA bifurcation. There are many procedure to treat bifurcation lesions (Lefèvre et al., 2000; Yamashita et al., 2000) but still not clear that which side branch lesion to be treated first after stenting the main branch lesion. Angiographic evaluation of the functional significance of the stenosis severity in jailed side branch lesions overestimate the functional significance of the lesion and FFR may be useful in

treating bifurcation lesions and it is both safe and feasible (Koo et al., 2005). Recent non-dimensional parameters CDP and LFC are useful in determining the functional significance of the stenosis in the bifurcation lesions which have been explained in Chapters 4 and 5.

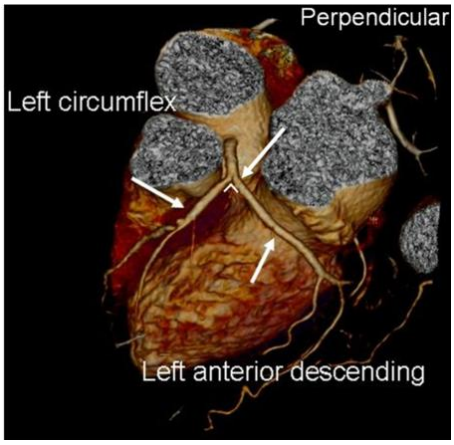

Figure 6.1: LCA and side branches
Reprinted from (Chaichana, et al., 2011), Copyright (2015) with permission from Elsevier

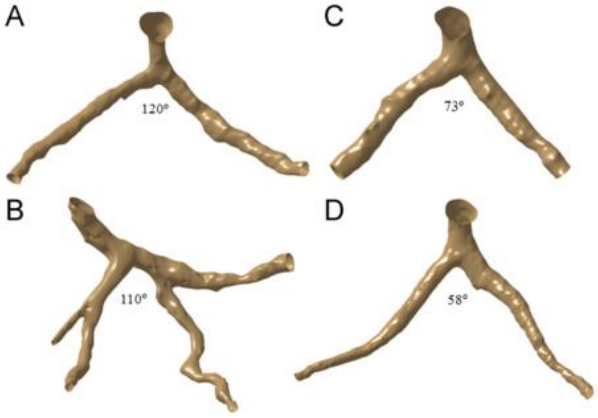

Figure 6.2: Patients realistic coronary artery models with different bifurcation angle
Reprinted from (Chaichana, et al., 2011), Copyright (2015) with permission from Elsevier

There are many factors which influence on FFR measurement and they are discussed in the previous Chapters 2, 4 and 5. It is noted that an artery bifurcation plays a substantial role for contributing the pressure distribution in the side branches. The side - branches

are stealing flow from the main vessel similar to collaterals. Since the diagnostic parameters are derived from pressure drop across the stenosis under hyperemic condition, it is useful to study the variations of pressure drop in the stenosed coronary bifurcated artery with variable angulation between LAD and LCX using CFD analysis. It is expected that the geometry and flow through Coronary Artery Branches play a substantial role in evaluating physiological significance of stenosis severity for the bifurcated lesion

6.2. Literature review

6.2.1. Flow behavior in bifurcated artery

The effect of coronary bifurcation angulation variation plays substantial role on the flow behavior. The branching also contributing to a reduction in the pressure distribution and an increase in the wall shear stress (Wiwatanapataphee, et al., 2012). Plaque may develop due to higher shear stress region which may occur at the bifurcation. Study shows that a direct correlation exists between bifurcation angulations and dimensional changes and development of plaque (Sun & Cao, 2011). From the numerical investigation on the flow through bifurcated artery, a laminar flow occurs at small angled model whereas turbulence flow occurs at wide angled model under peak systolic phase (Chaichana, Sun, Wong, Tu, & Hamza, 2010). CFD has been widely used in the coronary artery models due to the difficulty of measuring hemodynamic parameters such as wall shear stress, wall pressure and flow changes directly into the coronary arteries and can provide alternate ways to diagnose the CAD (Shanmugavelayudam, et al., 2010). Generally, outlet velocity or pressures of the side branches are unavailable. Murray's law predict the percent distribution of total flow rate through side branches which correlates flow rate and diameter of the branched vessel and it can be written as

$$\frac{q_{D1}}{q_{D2}} = \left(\frac{d_{D1}}{d_{D2}}\right)^3 \tag{6.1}$$

Where q_{D1} and q_{D2} ml/min are flow through the diameters d_{D1} and d_{D2} mm of the branches, respectively.

Groen et.al showed that Murray's law (outflow ratio) reasonably applicable when the percentage area stenosis less than 65% and for the stenosis greater than 66% it was invalid by comparing Murray's law with measured values in the carotid bifurcation using phase-contrast MRI in patients with varying degrees of stenosis (Groen et al., 2010).

6.2.2. Medina classification of bifurcation lesion

Coronary bifurcation lesions have been one of the most challenging lesion subsets in the field of percutaneous coronary intervention (PCI). Treating bifurcation lesions are associated with higher procedural cost, lower procedural success rate, higher restenosis, higher complication rate and worse outcome when compared with PCI of simple coronary artery lesions (Latib & Colombo, 2008; Park & Koo, 2012). Coronary lesions located at a bifurcation give a wide range of angiographic and anatomical morphologies depending upon the location of the plaque in the LCA. Medina has proposed a simple lesion classification consisting of a binary value (1, 0) as shown in Figure 6.3. There are three components of bifurcation: (i) main branch proximal (or) Left Main Stem (LMS) (ii) main branch distal (or) Left Anterior Descending (LAD) and (iii) side branch or Left Circumflex (LCX). Figure 6.3 shows the 7 possible morphologies. (Medina, Suarez de Lezo, & Pan, 2006).

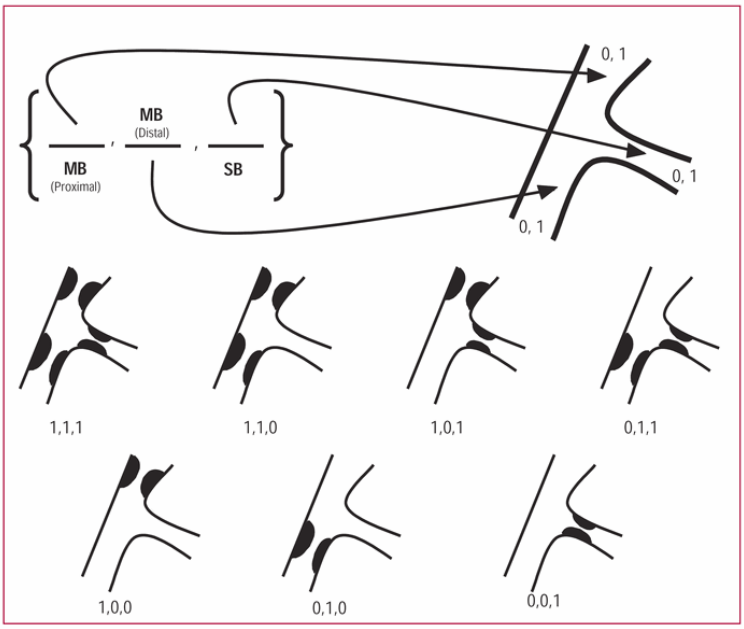

Figure 6.3: Medina classification of bifurcation lesions

Any narrowing with critical stenosis of 50% and above in any segment receives the binary value 1; otherwise, a binary value 0 is assigned starting from the left to right. The three suffixes are separated by commas.

6.2.3. Arterial wall bifurcation angulation and coronary diagnostic parameters

Anatomic severity assessment of bifurcation lesions using angiography is limited due to vessel overlap, angulation and foreshortening (Ziaee et al., 2004). Therefore, a standardized Physiological assessment of bifurcation lesions is required and it can be done with Fractional Flow Reserve (FFR). Previous Studies (Chaichana, et al., 2011; Chaichana, Sun, & Jewkes, 2013a, 2013b; Chiastra et al., 2013) shows that arterial wall angulation in coronary artery bifurcation plays a substantial role on the blood flow behavior. Several experimental, analytical, and computational simulation analyses conducted on the hemodynamic changes in stenotic arteries and computing the severity of stenosis have been reported by many researchers in a simple coronary artery lesion. The influence of artery wall angulation on the diagnostic parameter is unknown.

Among the medina classification of the bifurcation lesions, the (1, 0, 0) type of lesion has been taken into account for the study. Since the LAD and LCX branches immediately after the LMS, their angular variation will give an impact on the blood flow at the downstream of the stenosis of the lesion type (1, 0, 0). In the present study, for a given percent area stenosis (AS) severity (percent AS = 100% × (reference lumen area − minimum lumen area) / reference lumen area), the pressure drop across the stenosis and the FFR, CDP and LFC for various bifurcated coronary artery angulation models are estimated. A possible uncertainty region was identified when the severity of the stenosis assessed by in-vitro, due to bifurcation angulation variation by correlating percent AS and FFR.

6.3. Methodology

6.3.1. Stenosis geometry

For this analysis, 70%, 80%, and 90% AS were used in the bifurcated model with different angulation. The general geometrical form of an ideal model of the bifurcated stenosed rigid artery is shown in Figure 6.4.

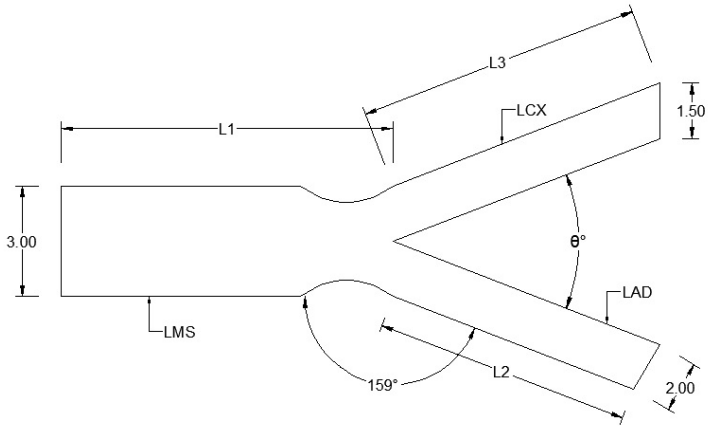

Figure 6.4: The schematic diagram of bifurcated artery with stenosis

The internal diameter of the unobstructed LMS, LAD and LCX are 3, 2 and 1.5 mm, respectively (Chaichana, et al., 2011). As explained in Chapter 5, §5.3 a stenosis has been developed in a concentric manner with a length of L (10 mm) at the lower most part of the LMS where the bifurcated artery LAD and LCX starts immediately as shown in Figure 6.4. The angulation between LAD and LCX is taken as 30°, 60°, and 90° which is falls under realistic bifurcation angulation and keeping the angulation between LMS and LAD as 159° to isolate the effect of single geometric factor (Dong, Sun, Inthavong, & Tu, 2014)

6.3.2. Mathematical formulation

The blood flow through the coronary artery is assumed to be incompressible, unsteady, and governed by the Navier–Stokes equation. The blood is assumed to be non-Newtonian and follows Carreau model. The details are given in the section §3.3 of Chapter 3.

6.3.3. Boundary conditions

A digitized data of transient parabolic velocity u(t) which was described in Chapter 4, § 4.3.5 was applied at the inlet of LMS. There are two outflow boundaries for this problem. The division of flow through LAD and LCX was set according to LAD and LCX diameter which is known as Murray's law at the LAD and stress free boundary condition was set at the outlet of LCX (Taylor, Hughes, & Zarins, 1998). No slip condition was applied at the arterial wall.

The inlet velocity profiles for 70%, 80%, and 90% AS were obtained from the mean hyperemic flow rate $(\tilde{Q})$ of 175, 165, and 115 mL/min as explained in the Chapter 4

and 5. A SST turbulence model was adopted for the simulations. For various angulation models of given percent AS, similar inflow and outflow boundary conditions were applied to analyze the bifurcation angulation effect.

6.3.4. Numerical methodology

The computational domains were initially meshed with hexahedral elements as shown in Figure. 6.5. The mesh elements are generated using ANSYS ICEM CFD version 14.0 (ANSYS, Inc. Canonsburg, PA, USA). The total number of elements varied from 300,000 to 400,000 for 70%, 80%, and 90% AS models.

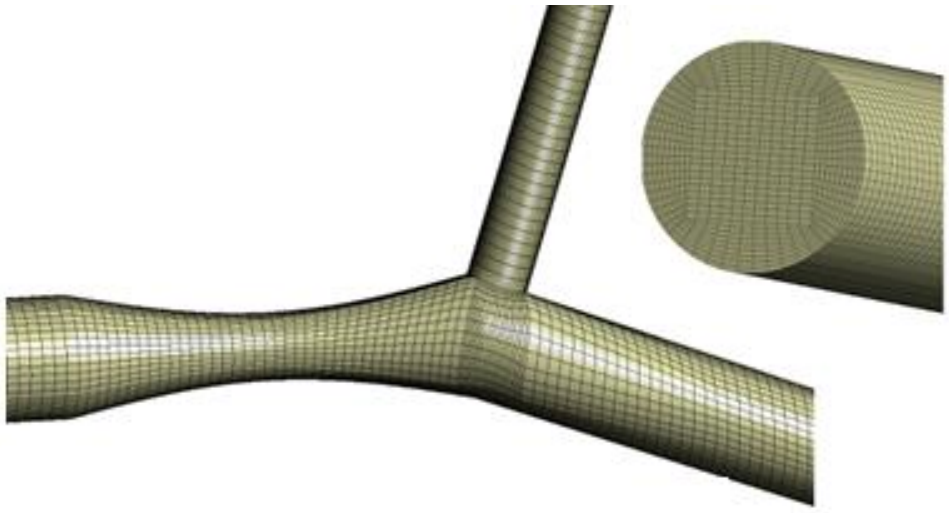

Figure 6.5: Computational mesh used for numerical study in the bifurcated stenotic artery model

Quality of mesh was checked by inspecting various parameters such as skewness, orthogonal quality, element quality etc. as explained in the section §4.5.1 of chapter 4 A finite volume software CFX 14.0 (ANSYS CFX, Canonsburg, PA) was used for the flow simulation. Adaptive time stepping method was used with details having been discussed in Chapter 5, § 5.6.

6.1.1. Parametric studies in numerical models:

A series of parametric study was conducted in 70%, 80% and 90% AS with variable angulation by varying the flow ratio at the outlets to see the influence of outlet boundary conditions and bifurcation angulations on pressure drop across the stenosis.

6.4. Results

For each 30°, 60° and 90° coronary artery angulations model, three cases of AS, 70%, 80% and 90%, a total of 9 models were investigated. Figure 6.6 shows a velocity contour plot in 30° and 90° bifurcation angulation model at t =2s for the lesion type (1,0,0) and it clearly shows that there is changes in the blood flow pattern. From all the bifurcation models, the pressure drop across the stenosis was analyzed first, and then the FFR, CDP and LFC were analyzed from the pressure drop. The FFR- %AS was related for the various coronary angulation models and a region of interest where possible misinterpretation of stenosis severity was found from the correlation by applying the FFR cut off value. The pressure drop and functional diagnostic values obtained in this study were transient time averaged quantities under hyperemic flow conditions.

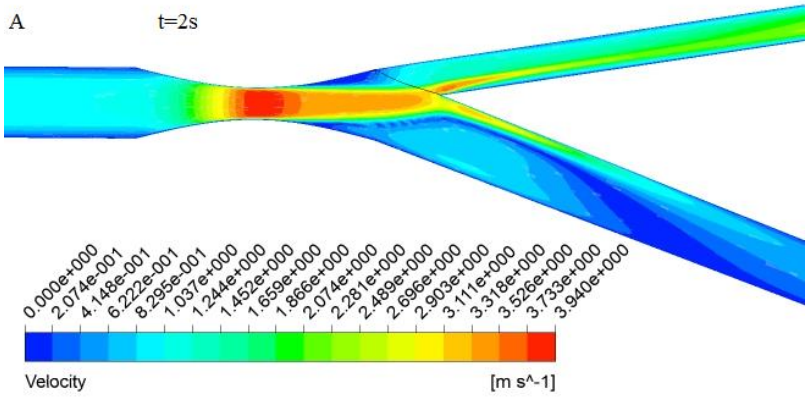

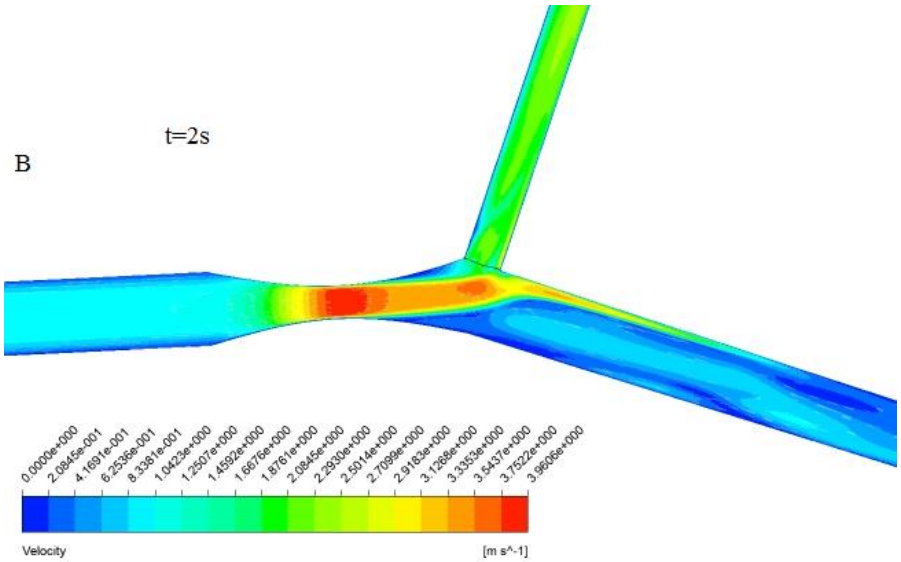

Figure 6.6: Velocity contour in (A) 30° and (B) 90° Bifurcation angulation model.

6.4.1. Pressure drop in bifurcated arteries under transient simulations

In all the bifurcation models, $\tilde{p}_a$ was measured at 3 mm before the stenosis and $\tilde{p}_d$ can be measured at the distal recovery pressure along the axis of the coronary artery either after the origin of LAD or LCX. However, $\tilde{p}_d$ was measured in LAD as it happens to be larger of the two vessels and supplies a larger territory. The overall transient pressure drop $\Delta p = p_a - p_d$ which was taken during the cardiac cycles 3 and 4 and there is no significant difference in the pressure drop found between the cycles 3 and 4 to ensure that the accurate results with numerical data being reported for the third and fourth cycles.

The time averaged pressure drop $\Delta\tilde{p} = \tilde{p}_d - \tilde{p}_a$ under various bifurcation angulation conditions for 70%, 80%, and 90% AS are reported in Table 6.1. The pressure drop increases as the percentage of stenosis severity increases for a given bifurcated

angulation model. However, $\Delta\tilde{p}$ decreases in a non-linear manner as the angle of bifurcation increases in 70% AS. But in the case of intermediate (80% AS) and severe (90% AS) models the pressure drop for the various angulation models are highly unstable.

Table 6.1: Result from computational analysis

Bifurcation Angulation θ°	70% AS		80% AS		90% AS	
	$\tilde{P}_a$ mmHg	$\Delta\tilde{P}$ mmHg	$\tilde{P}_a$ mmHg	$\Delta\tilde{P}$ mmHg	$\tilde{P}_a$ mmHg	$\Delta\tilde{P}$ mmHg
30	97.76	8.8	87.75	16.33	87.63	34.34
60	99.58	8.73	93.48	17.07	92.94	34.97
90	100.85	8.22	95.26	16.54	90.81	30.73

As the angle of bifurcation changes from 30° to 90°, the $\Delta\tilde{p}$ decreases from 8.8 mmHg to 8.22 mmHg (6.81%) in 70% AS. But in the case of 80% AS and 90%AS the $\Delta\tilde{p}$ increases in 60° angulation and then decreases when the angulation between LCX and LAD becomes 90°. It was interesting to note that the proximal pressure $\tilde{P}_a$ increases as the angulation increases for a given percentage AS. Therefore, the major pressure drop is due to the stenosis, which is higher at the region of the minimal area of cross section and the bifurcation angulation of the arterial wall plays a substantial impact on the proximal pressure and pressure drop across the stenosis.

6.4.2. Pressure drop from the parametric study

In all the bifurcation models pressure drop shows decreasing trend as the bifurcation angulation increases from 30 degree to 90 degree. Also the pressure drop shows a significant impact on the flow ratio as shown in Figure 6.7.

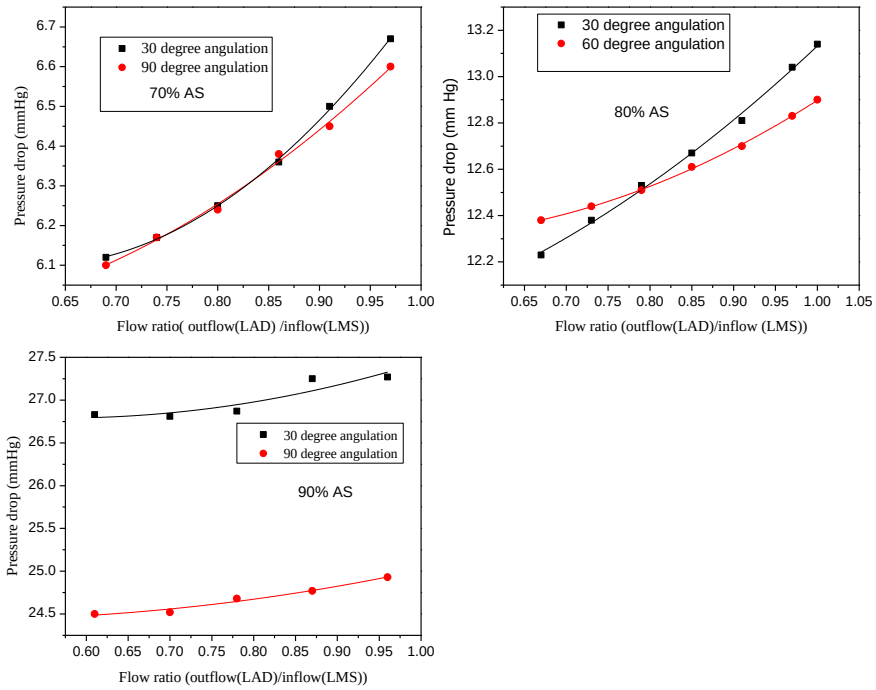

Figure 6.7: pressure drop in 30° and 90° bifurcation angulation numerical models under variable flow ratio

6.5. Effect of coronary bifurcation angulation on the diagnostic parameters

6.5.1. FFR

The FFR value decreases as the percent AS increases. For a given percent AS at the LMS and for the given flow ratio, the FFR value varied considerably when the coronary artery bifurcation angulation increased and are reported in Table1. As the angle of

bifurcation changes from 30° to 90°, the FFR increases from 0.91 to 0.92(1.09%), 0.81 to 0.83 (2.5%), and 0.61 to 0.66 (8.2 %) in 70%, 80%, and 90% AS, respectively. This finding indicates that the presence of wider angulation increases the FFR.

A best fit linear approximation was used to plot the computed values of percent AS and FFR, as shown in Figure 6.8. To estimate a region of uncertainty, a horizontal line representing the cutoff value corresponding to FFR=0.8 and FFR=0.75 was drawn (Konala, et al., 2011; Kristensen, et al., 2010). This horizontal line corresponding to FFR=0.75 intercepted the FFR–percentage AS lines for 0° and 90° bifurcation models at 81.8% and 84.12% AS, respectively. For FFR =0.8 the interceptions were at 78.34% and 80.19% AS for 0° and 90° bifurcation models, respectively. The following discussion and conclusion are based on the cut off value of 0.75 for FFR.

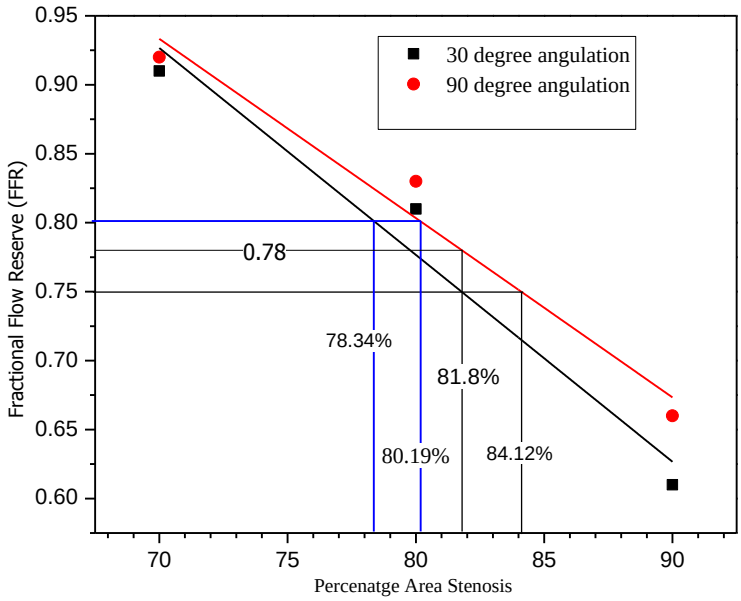

Figure 6.8: Variation of FFR values with the bifurcation angulation. A linear trend line was fitted to FFR data for 0° and 90° bifurcation angulation models. Based on the FFR cut-off value of 0.75 for single vessel stenosis and using the non-linear trend lines, a re region of uncertainty in FFR values was found to be 81.8 %-84.12% AS

6.5.2. CDP and LFC

The values of CDP and LFC are computed using the pressure, flow, and lesion geometry. For a given bifurcation angulation, the CDP and LFC values increased non-linearly with the percent AS. The computed CDP and LFC values are reported in Table 6.2. In 70% AS, the CDP value decreased from 13.1 to 12.24 (6.56%) as the bifurcation angulation varied from 30° to 90°, whereas the LFC increased from 0.65 to 0.67 (3.08%). In 80% AS and in 90% AS the CDP value increases and then decreases as the angulation varied from 30°, 60° and 90°.

Table 6.2: FFR, CDP and LFC values in different angulation models

Angle of curvature θ°	70% AS			80% AS			90% AS		
	FFR	CDP	LFC	FFR mmHg	CDP	LFC	FFR	CDP	LFC
30	0.91	13.1	0.65	0.814	27.41	0.77	0.608	118.74	0.84
60	0.912	13	0.65	0.817	28.65	0.75	0.624	120.92	0.83
90	0.92	12.24	0.67	0.826	27.76	0.76	0.66	106.26	0.89

6.6. Discussion

The vascular geometry is a combination of curved vessels (Wang & Li, 2011), straight vessels (R. K. Banerjee, et al., 2008; Banerjee, et al., 2003) and bifurcated vessel having variable angulation (Chaichana, et al., 2011). It is well known that formation of stenosis normally occur in the region of coronary curvature, bifurcated area and angulation. Chaichana et al. (Chaichana, et al., 2011) showed that there is a direct correlation between the angulation and hemodynamic changes. The primary purpose of the present

study was to reveal the variability in FFR, CDP, and LFC values for a given percentage AS and for the given flow ratio in LCX and LAD due to the angulation of the bifurcated arteries. This variability confirms that when the stenosis severity assessed by in-vitro may lead to misinterpretation of its severity by the clinician to decide upon coronary intervention around the clinically used cutoff value of 0.75(N. H. Pijls, et al., 1996). The present study demonstrates that for the stenosis located at the LMS (Position: 1, 0, 0) and changes in bifurcation angulation give a significant impact on coronary diagnostic parameter when the artery bifurcation angle varied from 30° to 90°.

To study the effect of bifurcation angulation of the artery vessel wall on the flow and pressure field, we compared the pressure drop, and hence, the diagnostic parameters obtained from the models having various bifurcation angulation for the cases of 70%, 80%, and 90% AS stenosis located at LMS. The results showed that a nonlinear increment of pressure drop with an increase in stenosis severity. This was due to the change in the momentum as the flow velocity increased across the stenosis.

For a given percentage AS and for the given inflow and outflow boundary conditions, the proximal pressure (measured at 3 mm before the stenosis) and axial pressure drop $\Delta\tilde{p}$ was varied as the angle of bifurcation changed from 30° to 90° during a cardiac cycle. This is owing to the variation of bifurcation angulation distal to the stenosis. The parametric study (steady state simulations) showed that the pressure drop across the stenosis also depends on the flow ratio and the bifurcation angulation

The FFR, which is derived from pressure drop across the stenosis, decreased as the percentage AS increased, which, in general, is consistent with that reported in a previous in vivo study (Banerjee, et al., 2009). Furthermore, for a fixed percentage AS and flow ratio, the FFR was affected owing to the angulation of the artery. The

computed values of FFR in the bifurcated artery models in this study were in close agreement with the available in vivo results obtained by Koo et al. The impact of bifurcation angulation variations on the FFR was considered separately in order to find misdiagnose region when the stenosis severity assessed by in-vitro.

The FFR value varied around the cutoff value corresponding to 0.75 owing to the angulation of the artery wall and thus a region of uncertainty was found to be 81.8%–84.12% AS. For AS < 81.8%, the FFR values were well above the cutoff value of 0.75, whereas for AS > 84.12%, the FFR values were below the cutoff value of 0.75, irrespective of the given range of bifurcation angulation. It should be noted that in a bifurcated artery, at 81.3% AS, the FFR value for a 30° angulation model is 0.75 whereas for the same severity condition the angulation increased from 30° to 90° the FFR value shown to be 0.78 which is greater than the FFR cutoff value of 0.75. Thus this variability in FFR values due to variation in bifurcation angulation will notably impact on the intermediate stenosis severity which gives a dilemma for the clinician to diagnose the intermediate stenosis severity when it was assessed by in-vitro and may lead to postponement of coronary interventional procedure. Since the FFR is increasing (but, not decreasing) for the wider angulation model, the chance of misdiagnosis (i.e., not being treated) is possible. Our bifurcated stenosed arterial wall models demonstrated that the variation in the angle of bifurcation significantly affects the FFR for a given percentage AS and for the given flow ratio.

Similar to $\Delta\tilde{p}$ and FFR, variations in CDP and LFC were observed in 70%, 80%, and 90% AS in various angulation models and recent meta-analysis study shows that clinical cut-off value of CDP to detect FFR < 0.8 and FFR < 0.75 was at CDP > 27.1

and CDP > 27.9, respectively (K. K. Kolli, et al., 2014). However, the cutoff value for LFC has not yet been decided for clinical evaluation (Peelukhana, et al., 2009).

The collateral vessels downstream to the stenosis supply blood when the main artery fails to supply it to the myocardium whereas in the side branches the main flow diverted through it. In both cases, assessment of stenosis severity might lead to misdiagnose of the stenosis severity. In other words, the angulation of the bifurcated artery can't be ignored during the anatomical assessment of bifurcation lesions severity in addition to the minimum lumen area and diameter.

There are some limitations of the present study. The factors that influence the diagnostic parameters such as arterial wall compliance (Konala, et al., 2011), multiple bend, dynamic curvature variation owing to heart motion (Yang, et al., 2008), wall roughness, and lesion eccentricity were not considered. Furthermore, in future studies, realistic bifurcated coronary artery model needs to be used, which will overcome the limitations to analyze the influence of bifurcation angulation on the coronary diagnostic parameters.

6.7. Conclusion

This computational fluid dynamics simulation study investigated the effects of the bifurcation angulation on the coronary diagnostic parameters in 70%, 80%, and 90% AS coronary artery models under hyperemic flow conditions. In the case of intermediate stenosis severity and from numerical study it is clearly shown that the FFR values varies around the cut-off value of 0.75 owing to the variability in bifurcation angulation, which could lead to misdiagnose of the severity of the stenosis which will be assessed from in-vitro. For a given percent AS and for a fixed flow ratio, the bifurcated artery

angulation of the stenosed arterial wall affected the intraluminal flow, and hence, changes in the diagnostic parameter FFR. From the well-established cutoff value of FFR=0.75 for single vessel CAD, we found a region of misdiagnosis in evaluating functional significance of stenosis severity between 81.8-84.12% AS in a bifurcated stenosed artery by plotting a linear approximate correlation between FFR and percentage AS. We speculated that this difference could possibly be higher owing to more acute and wider angulation, irregular appearance of atherosclerotic plaque and irregular artery, and thus, the computed uncertainty region is likely to be larger and may be clinically relevant. CDP and LFC values for different bifurcation angulation models were found and confirms that bifurcation angulation must be considered when the stenosis severity assessed by in-vitro. Further in vivo studies and validations are required to fix the cutoff value for LFC, similar to FFR.

7. CONCLUSION AND SUGGESTION FOR FUTURE WORK

In this chapter, the findings of the thesis are summarized in § 7.1 and some suggestions on future research are made in § 7.2.

7.1. Conclusion

Computational Fluid dynamic studies were carried out on stenosed coronary model to investigate the pitfall in identifying the functional significance of the stenosis in vitro. The current clinical functional diagnostic parameter FFR and combined functional and anatomic parameters CDP and LFC which are derived from fundamental fluid dynamic principles were investigated in this thesis.

In Chapter 4, the transient pulsatile non- Newtonian blood flow in arterial system having 70%, 80% and 90% AS was numerically investigated by considering the artery wall and the stenosis components were rigid and porous for investigating the effect of porous media on coronary diagnostic parameter. Since the flow through the stenosis take place under hyperemic flow conditions, the flow become turbulent at the site of downstream to the stenosis. To resolve the boundary better, a low Reynolds turbulence SST model was used to get the accuracy in the numerical simulation. In both the models, pressure drop was calculated without guide wire condition. From the analysis of both the models a misdiagnose region was evaluated. The misdiagnose region was found between 81.89% and 83.61% AS from the well-established cut-off value of FFR =0.75 and it could be useful when the intermediate stenosis severity assessed by in-vitro. We speculate that this difference is likely to be higher due to the irregular

appearance of the atherosclerotic plaque and thus the computed area difference is likely to be larger and may be clinically relevant.

In Chapter 5, transient pulsatile non - Newtonian blood flow through curved arterial system having 70%, 80% and 90% AS was numerically investigated by considering various angle of curvature of artery wall models namely 0° (straight artery), 30°, 60°, 90° and 120° for evaluating the influence of curvature on coronary diagnostic parameters. The stenosis was located at the bend of an artery. The location of the stenosis varied such as proximal, central and distal part of the bend. Stenosis located at the bend of an artery significantly influences on the functional evaluation of stenosis severity whereas the position of the stenosis at the bend has negligible impact on the functional evaluation of stenosis severity. Hence, the presented results are based on the stenosis was located centrally at the bend. Since the flow through the curved stenosed artery was under hyperemic flow condition, the flow become turbulent in the low Reynolds number region. The SST turbulence model was used to get the accuracy in the numerical simulation. From the investigation we found that curvature of the artery offer flow resistance in addition to stenosis area restriction. We conclude that when assessing functional significance of stenosis severity using in-vitro assessment such as CCTA images (a fast image capturing technique for the assessment of stenosis severity) underestimate the stenosis severity which does not include the curvature in the assessment. Hence, misdiagnose or postponement of coronary intervention procedure is possible. For the clinical evaluation of functional significance of the stenosis severity, we found a region of uncertainty to be 76.07–79.06% AS and 76.31% -73.66% AS for the clinically cut off value of FFR=0.75 and FFR=0.8, respectively. Similar to FFR, variations in CDP and LFC were observed in 70%, 80%, and 90% AS in various angle of curvature models. We also found that the CDP value increased and the LFC value

decreased as the angle of curvature changed from straight section to curved section for a given percentage AS. However, further in vivo studies and validations are required to fix the cutoff value for CDP and LFC. When interpreting stenosis severity using image technique the clinician must consider both the curvature and area stenosis.

In Chapter 6, transient pulsatile non- Newtonian blood flow through bifurcated arterial system having 70%, 80% and 90% AS was numerically investigated by considering various angulation of the coronary artery wall models namely 30°, 60°, and 90° for evaluating the influence of angle variation of the bifurcated coronary artery on coronary diagnostic parameters. The stenosis was located at the left main stem (LMS) of the bifurcated artery. The LAD and LCX branched immediately the downstream of the stenosis. Since the flow through the bifurcated artery was under hyperemic flow condition, the flow become turbulent in the low Reynolds number region. A SST turbulence model was used to get the accuracy in the numerical simulation. Also inflation algorithm was used to resolve along the boundary in order to resolve the boundary better. Since the diagnostic parameters are derived from the pressure drop across the stenosis, the variation of bifurcation angle influences on the pressure drop and hence the diagnostic parameter. Steady state simulations were conducted by changing the flow ratio in the bifurcation angulation models and found that the flow ratio and the bifurcation angulation plays substantial impact on the pressure drop and hence the coronary diagnostic parameter. From the investigation, the variation in the bifurcation angulation influenced on the proximal pressure too and it was increased when the angulation changed from 30° to 90°. This is due to change in hemodynamics, occurred in the lumen. The FFR value increases when the angulation increases which might lead to misdiagnose of the intermediate stenosis severity to decide upon the coronary intervention procedure. For the clinical evaluation of functional significance

of the stenosis severity, we found a region of uncertainty to be 81.8–84.12% AS and 78.34% -80.19 % AS for the clinically cut off value of FFR=0.75 and FFR=0.8, respectively. Similar to FFR, variations in CDP and LFC were observed in 70%, 80%, and 90% AS in various bifurcation models. When assessing functional significance of the stenosis severity in the bifurcated artery the clinician must consider both the bifurcation angulation and flow ratio around the clinically cutoff value of FFR.

7.2. Future research

In the current work, a computational fluid dynamic study on coronary artery model with various parameter such as porous medium, curvature of an artery and bifurcation of the arterial systems have been considered and found important clinical information. The following proposals are put forward for future research work:

- The stenosis taken in the whole computational fluid dynamic studies are axisymmetric. Models of eccentric and irregular shape such as triangular, elliptical and trapezium could be taken for future research
- We have studied 3D model of coronary artery and arrived clinical relevant information which are clinically useful. Realistic artery model can be obtained from patient coronary artery images by using image processing or image segmentation technique for fluid dynamic analysis which lead to arrive more precise conclusion in the clinical setting.
- We have conducted only fluid interaction with the stenosis and coronary artery by assuming artery wall as rigid but in realistic the artery wall is flexible. So it is desirable to conduct fluid-wall interaction study (FSI) for the better outcome for the clinical evaluation of functional or anatomical significance of the stenosis severity.

REFERENCES

Abdulla, J., Abildstrom, S. Z., Gotzsche, O., Christensen, E., Kober, L., & Torp-Pedersen, C. (2007). 64-multislice detector computed tomography coronary angiography as potential alternative to conventional coronary angiography: a systematic review and meta-analysis. *Eur Heart J, 28*(24), 3042-3050. doi: 10.1093/eurheartj/ehm466

Ai, L., & Vafai, K. (2006). A coupling model for macromolecule transport in a stenosed arterial wall. *International Journal of Heat and Mass Transfer, 49*(9–10), 1568-1591. doi: 10.1016/j.ijheatmasstransfer.2005.10.041

Alfonso, F., Macaya, C., Goicolea, J., Hernandez, R., Segovia, J., Zamorano, J., . . . Zarco, P. (1994). Determinants of coronary compliance in patients with coronary artery disease: an intravascular ultrasound study. *Journal of the American College of Cardiology, 23*(4), 879-884.

ANSYS. (2010). Release 13.0. CFX-Solver modeling guide: Technical report, Ansys.

ANSYS. (2012). ANSYS CFX Introduction.

ANSYS, I. (2009). CFX-Solver Theory Guide: R.

Ashtekar, K. D., Back, L. H., Khoury, S. F., & Banerjee, R. K. (2007). In vitro quantification of guidewire flow-obstruction effect in model coronary stenoses for interventional diagnostic procedure. *Journal of Medical Devices, 1*(3), 185-196.

Ballyk, P. D., Steinman, D. A., & Ethier, C. R. (1994). Simulation of non-Newtonian blood flow in an end-to-side anastomosis. *Biorheology, 31*(5), 565-586.

Banerjee, R., Ashtekar, K., Helmy, T., Effat, M., Back, L., & Khoury, S. (2008). Hemodynamic diagnostics of epicardial coronary stenoses: in-vitro experimental and computational study. *BioMedical Engineering OnLine, 7*(1), 1-22. doi: 10.1186/1475-925x-7-24

Banerjee, R. K., Ashtekar, K. D., Effat, M. A., Helmy, T. A., Kim, E., Schneeberger, E. W., . . . Back, L. H. (2009). Concurrent assessment of epicardial coronary artery stenosis and microvascular dysfunction using diagnostic endpoints derived from fundamental fluid dynamics principles. *J Invasive Cardiol, 21*(10), 511-517.

Banerjee, R. K., Ashtekar, K. D., Helmy, T. A., Effat, M. A., Back, L. H., & Khoury, S. F. (2008). Hemodynamic diagnostics of epicardial coronary stenoses: in-vitro experimental and computational study. *Biomed Eng Online, 7*, 24. doi: 1475-925X-7-24 [pii] 10.1186/1475-925X-7-24

Banerjee, R. K., Back, L. H., Back, M. R., & Cho, Y. I. (2003). Physiological flow analysis in significant human coronary artery stenoses. *Biorheology, 40*(4), 451-476.

Banerjee, R. K., Peelukhana, S. V., & Goswami, I. (2014). Influence of newly designed monorail pressure sensor catheter on coronary diagnostic parameters: An in vitro study. *Journal of Biomechanics, 47*(3), 617-624. doi: http://dx.doi.org/10.1016/j.jbiomech.2013.12.005

Banerjee, R. K., Sinha Roy, A., Back, L. H., Back, M. R., Khoury, S. F., & Millard, R. W. (2007). Characterizing momentum change and viscous loss of a hemodynamic endpoint in assessment of coronary lesions. *Journal of Biomechanics, 40*(3), 652-662. doi: 10.1016/j.jbiomech.2006.01.014

Bear, J., & Bachmat, Y. (1990). *Introduction to modeling of transport phenomena in porous media* (Vol. 4): Springer.

Beavers, G. S., & Joseph, D. D. (1967). Boundary conditions at a naturally permeable wall. *Journal of fluid mechanics, 30*(01), 197-207.

Berger, S. A., & Jou, L.-D. (2000). Flows in Stenotic Vessels. *Annual Review of Fluid Mechanics, 32*(1), 347-382. doi: doi:10.1146/annurev.fluid.32.1.347

Boutsianis, E., Dave, H., Frauenfelder, T., Poulikakos, D., Wildermuth, S., Turina, M., . . . Zund, G. (2004). Computational simulation of intracoronary flow based on real coronary geometry. *European Journal of Cardio-Thoracic Surgery, 26*(2), 248-256. doi: 10.1016/j.ejcts.2004.02.041

Brinkman, H. C. (1949). A calculation of the viscous force exerted by a flowing fluid on a dense swarm of particles. *Applied Scientific Research, 1*(1), 27-34. doi: 10.1007/bf02120313

Brosh, D., Higano, S. T., Lennon, R. J., Holmes Jr, D. R., & Lerman, A. (2005). Effect of lesion length on fractional flow reserve in intermediate coronary lesions. *American Heart Journal, 150*(2), 338-343. doi: http://dx.doi.org/10.1016/j.ahj.2004.09.007

Brown, B. G., Bolson, E. L., & Dodge, H. T. (1984). Dynamic mechanisms in human coronary stenosis. *Circulation, 70*(6), 917-922. doi: 10.1161/01.cir.70.6.917

Chaichana, T., Sun, Z., & Jewkes, J. (2011). Computation of hemodynamics in the left coronary artery with variable angulations. *Journal of Biomechanics, 44*(10), 1869-1878. doi: http://dx.doi.org/10.1016/j.jbiomech.2011.04.033

Chaichana, T., Sun, Z., & Jewkes, J. (2013a). Haemodynamic analysis of the effect of different types of plaques in the left coronary artery. *Computerized Medical Imaging and Graphics, 37*(3), 197-206. doi: http://dx.doi.org/10.1016/j.compmedimag.2013.02.001

Chaichana, T., Sun, Z., & Jewkes, J. (2013b). Hemodynamic impacts of various types of stenosis in the left coronary artery bifurcation: A patient-specific analysis. *Physica Medica, 29*(5), 447-452. doi: http://dx.doi.org/10.1016/j.ejmp.2013.02.001

Chaichana, T., Sun, Z., Wong, K. K., Tu, J., & Hamza, M. (2010). *Plaque Formation at the Left Coronary Artery: Analysis of the Relationship Between Arterial Angulations and Hemodynamics.* Paper presented at the 30th IASTED Conference on Modelling, Identification, and Control.

Chakravarty, S., & Datta, A. (1992). Pulsatile blood flow in a porous stenotic artery. *Mathematical and Computer Modelling, 16*(2), 35-54. doi: http://dx.doi.org/10.1016/0895-7177(92)90005-6

Chakravarty, S., & Sannigrahi, A. K. (1998). An analytical estimate of the flow-field in a porous stenotic artery subject to body acceleration. *International Journal of Engineering Science, 36*(10), 1083-1102. doi: 10.1016/s0020-7225(98)00009-3

Chiastra, C., Morlacchi, S., Gallo, D., Morbiducci, U., Cárdenes, R., Larrabide, I., & Migliavacca, F. (2013). Computational fluid dynamic simulations of image-based stented coronary bifurcation models. *Journal of The Royal Society Interface, 10*(84), 20130193.

Cho, Y. I., Back, L. H., Crawford, D. W., & Cuffel, R. F. (1983). Experimental study of pulsatile and steady flow through a smooth tube and an atherosclerotic coronary artery casting of man. *Journal of Biomechanics, 16*(11), 933-946.

Cho, Y. I., & Kensey, K. R. (1991). Effects of the non-Newtonian viscosity of blood on flows in a diseased arterial vessel. Part 1: Steady flows. *Biorheology, 28*(3-4), 241-262.

Dabagh, M., Jalali, P., Konttinen, Y., & Sarkomaa, P. (2008). Distribution of shear stress over smooth muscle cells in deformable arterial wall. *Medical and Biological Engineering and Computing, 46*(7), 649-657. doi: 10.1007/s11517-008-0338-7

Dash, R. K., Jayaraman, G., & Mehta, K. N. (1999). Flow in a catheterized curved artery with stenosis. *Journal of Biomechanics, 32*(1), 49-61. doi: http://dx.doi.org/10.1016/S0021-9290(98)00142-0

Dash, R. K., Mehta, K. N., & Jayaraman, G. (1996). Casson fluid flow in a pipe filled with a homogeneous porous medium. *International Journal of Engineering Science, 34*(10), 1145-1156. doi: http://dx.doi.org/10.1016/0020-7225(96)00012-2

De Bruyne, B., Pijls, N. H., Heyndrickx, G. R., Hodeige, D., Kirkeeide, R., & Gould, K. L. (2000). Pressure-derived fractional flow reserve to assess serial epicardial stenoses: theoretical basis and animal validation. *Circulation, 101*(15), 1840-1847.

De Bruyne, B., Pijls, N. H. J., Kalesan, B., Barbato, E., Tonino, P. A. L., Piroth, Z., . . . Fearon, W. F. (2012). Fractional Flow Reserve–Guided PCI versus Medical Therapy in Stable Coronary Disease. *New England Journal of Medicine, 367*(11), 991-1001. doi: doi:10.1056/NEJMoa1205361

De Luca, G., Venegoni, L., Iorio, S., Giuliani, L., & Marino, P. (2011). Effects of increasing doses of intracoronary adenosine on the assessment of fractional flow reserve. *JACC: Cardiovascular Interventions, 4*(10), 1079-1084.

Dong, J., Sun, Z., Inthavong, K., & Tu, J. (2014). Fluid–structure interaction analysis of the left coronary artery with variable angulation. *Computer Methods in Biomechanics and Biomedical Engineering*(ahead-of-print), 1-9.

Dupouy, P., Gilard, M., Morelle, J. F., Furber, A., Aptecar, E., Cazaux, P., . . . Dubois Rande, J. L. (2005). Usefulness and clinical impact of a fractional flow reserve and angiographic targeted strategy for coronary artery stenting: FROST III, a multicenter prospective registry. *EuroIntervention, 1*(1), 85-92.

Esses, S. J., Berman, P., Bloom, A. I., & Sosna, J. (2011). Clinical applications of physical 3D models derived from MDCT data and created by rapid prototyping. *AJR Am J Roentgenol, 196*(6), W683-688. doi: 10.2214/ajr.10.5681

Fung, Y. C. (1993). Mechanical Properties of Living Tissues. *Biomechanics*(2nd edition, Springer, Berlin).

Giannoglou, G. D., Antoniadis, A. P., Koskinas, K. C., & Chatzizisis, Y. S. (2010). Flow and atherosclerosis in coronary bifurcations. *EuroIntervention: journal of EuroPCR in collaboration with the Working Group on Interventional Cardiology of the European Society of Cardiology, 6*, J16-23.

Goldsmith, H., & Karino, T. (1995). Flow Patterns and the Localization of Vascular Disease in the Circulation. In R. N. Holtzman, B. Stein & H. Winston (Eds.), *Endovascular Interventional Neuroradiology* (pp. 25-66): Springer New York.

Goubergrits, L., Kertzscher, U., Schöneberg, B., Wellnhofer, E., Petz, C., & Hege, H.-C. (2008). CFD analysis in an anatomically realistic coronary artery model based on non-invasive 3D imaging: comparison of magnetic resonance imaging with computed tomography. *The International Journal of Cardiovascular Imaging, 24*(4), 411-421. doi: 10.1007/s10554-007-9275-z

Gould, K. L. (2006). Physiological severity of coronary artery stenosis. *Am J Physiol Heart Circ Physiol, 291*(6), H2583-2585. doi: 00488.2006 [pii]

0.1152/ajpheart.00488.2006

Gould, K. L., Kirkeeide, R. L., & Buchi, M. (1990). Coronary flow reserve as a physiologic measure of stenosis severity. *J Am Coll Cardiol, 15*(2), 459-474.

Groen, H. C., Simons, L., van den Bouwhuijsen, Q. J., Bosboom, E. M., Gijsen, F. J., van der Giessen, A. G., . . . Wentzel, J. J. (2010). MRI-based quantification of outflow boundary conditions for computational fluid dynamics of stenosed human carotid arteries. *J Biomech, 43*(12), 2332-2338. doi: 10.1016/j.jbiomech.2010.04.039

Han, H.-C. (2012). Twisted blood vessels: symptoms, etiology and biomechanical mechanisms. *Journal of vascular research, 49*(3), 185-197.

Hau, W. (2004). Fractional flow reserve and complex coronary pathologic conditions. *European Heart Journal, 25*(9), 723-727. doi: 10.1016/j.ehj.2004.02.019

Huang, R. F., Yang, T.-F., & Lan, Y.-K. (2010). Pulsatile flows and wall-shear stresses in models simulating normal and stenosed aortic arches. *Experiments in fluids, 48*(3), 497-508.

Johnston, B. M., Johnston, P. R., Corney, S., & Kilpatrick, D. (2004). Non-Newtonian blood flow in human right coronary arteries: steady state simulations. *Journal of Biomechanics, 37*(5), 709-720. doi: 10.1016/j.jbiomech.2003.09.016

Johnston, B. M., Johnston, P. R., Corney, S., & Kilpatrick, D. (2006). Non-Newtonian blood flow in human right coronary arteries: Transient simulations. *Journal of Biomechanics, 39*(6), 1116-1128. doi: 10.1016/j.jbiomech.2005.01.034

Jozwik, K., & Obidowski, D. (2010). Numerical simulations of the blood flow through vertebral arteries. *Journal of Biomechanics, 43*(2), 177-185. doi: http://dx.doi.org/10.1016/j.jbiomech.2009.09.026

Kagadis, G. C., Skouras, E. D., Bourantas, G. C., Paraskeva, C. A., Katsanos, K., Karnabatidis, D., & Nikiforidis, G. C. (2008). Computational representation and hemodynamic characterization of in vivo acquired severe stenotic renal artery geometries using turbulence modeling. *Medical Engineering & Physics, 30*(5), 647-660. doi: http://dx.doi.org/10.1016/j.medengphy.2007.07.005

Kajiya, F., Tsujioka, K., Ogasawara, Y., Wada, Y., Matsuoka, S., Kanazawa, S., . . . Fujiwara, T. (1987). Analysis of flow characteristics in poststenotic regions of the human coronary artery during bypass graft surgery. *Circulation, 76*(5), 1092-1100.

Kaski, J. C., Tousoulis, D., Haider, A. W., Gavrielides, S., Crea, F., & Maseri, A. (1991). Reactivity of eccentric and concentric coronary stenoses in patients with chronic stable angina. *Journal of the American College of Cardiology, 17*(3), 627-633. doi: http://dx.doi.org/10.1016/S0735-1097(10)80175-5

Kaye, E. K., Valencia, A., Baba, N., Spiro, A., 3rd, Dietrich, T., & Garcia, R. I. (2010). Tooth loss and periodontal disease predict poor cognitive function in older men. *J Am Geriatr Soc, 58*(4), 713-718. doi: 10.1111/j.1532-5415.2010.02788.x

JGS2788 [pii]

Kern, M. J., & Samady, H. (2010). Current Concepts of Integrated Coronary Physiology in the Catheterization Laboratory. *Journal of the American College of Cardiology, 55*(3), 173-185. doi: 10.1016/j.jacc.2009.06.062

Khakpour, M., & Vafai, K. (2008). Critical assessment of arterial transport models. *International Journal of Heat and Mass Transfer, 51*(3–4), 807-822. doi: 10.1016/j.ijheatmasstransfer.2007.04.021

Klocke, F. J., Mates, R. E., Canty, J., & Ellis, A. K. (1985). Coronary pressure-flow relationships. Controversial issues and probable implications. *Circulation research, 56*(3), 310-323.

Knight, J., Olgac, U., Saur, S. C., Poulikakos, D., Marshall Jr, W., Cattin, P. C., . . . Kurtcuoglu, V. (2010). Choosing the optimal wall shear parameter for the prediction of plaque location—A patient-specific computational study in human right coronary arteries. *Atherosclerosis, 211*(2), 445-450. doi: 10.1016/j.atherosclerosis.2010.03.001

Koerselman, J., van der Graaf, Y., de Jaegere, P. P., & Grobbee, D. E. (2003). Coronary collaterals: an important and underexposed aspect of coronary artery disease. *Circulation, 107*(19), 2507-2511. doi: 10.1161/01.cir.0000065118.99409.5f

Kolli, K. K., Arif, I., Peelukhana, S. V., Succop, P., Back, L. H., Helmy, T. A., . . . Banerjee, R. K. (2014). Diagnostic performance of pressure drop coefficient in relation to fractional flow reserve and coronary flow reserve. *J INVASIVE CARDIOL, 26*(5), 188-195.

Kolli, K. K., Banerjee, R. K., Peelukhana, S. V., Helmy, T. A., Leesar, M. A., Arif, I., . . . Effat, M. A. (2011). Influence of heart rate on fractional flow reserve, pressure drop coefficient, and lesion flow coefficient for epicardial coronary stenosis in a porcine model. *Am J Physiol Heart Circ Physiol, 300*(1), H382-387. doi: 10.1152/ajpheart.00412.2010

Kolli, K. K., Helmy, T., Effat, M., Imran, A., Leesar, M., Schneeberger, E. W., . . . Banerjee, R. K. (2010). Influence of contractility and heart rate on pressure drop coefficient and fractional flow reserve for epicardial stenosis. *Cardiovascular Revascularization Medicine, 11*(3), 214. doi: http://dx.doi.org/10.1016/j.carrev.2010.03.074

Konala, B. C., Das, A., & Banerjee, R. K. (2011). Influence of arterial wall-stenosis compliance on the coronary diagnostic parameters. *Journal of Biomechanics, 44*(5), 842-847. doi: 10.1016/j.jbiomech.2010.12.011

Koo, B.-K., Erglis, A., Doh, J.-H., Daniels, D. V., Jegere, S., Kim, H.-S., . . . Min, J. K. (2011). Diagnosis of Ischemia-Causing Coronary Stenoses by Noninvasive Fractional Flow Reserve Computed From Coronary Computed Tomographic Angiograms: Results From the Prospective Multicenter DISCOVER-FLOW (Diagnosis of Ischemia-Causing Stenoses Obtained Via Noninvasive Fractional Flow Reserve) Study. *Journal of the American College of Cardiology, 58*(19), 1989-1997. doi: 10.1016/j.jacc.2011.06.066

Koo, B.-K., Kang, H.-J., Youn, T.-J., Chae, I.-H., Choi, D.-J., Kim, H.-S., . . . Tahk, S.-J. (2005). Physiologic Assessment of Jailed Side Branch Lesions Using Fractional Flow Reserve. *Journal of the American College of Cardiology, 46*(4), 633-637. doi: 10.1016/j.jacc.2005.04.054

Kristensen, T. S., Engstrøm, T., Kelbæk, H., von der Recke, P., Nielsen, M. B., & Kofoed, K. F. (2010). Correlation between coronary computed tomographic angiography and fractional flow reserve. *International Journal of Cardiology, 144*(2), 200-205. doi: 10.1016/j.ijcard.2009.04.024

Ku, D. N. (1997). Blood flow in arteries. *Annual Review of Fluid Mechanics, 29*(1), 399-434. doi: doi:10.1146/annurev.fluid.29.1.399

Latib, A., & Colombo, A. (2008). Bifurcation Disease: What Do We Know, What Should We Do? *JACC: Cardiovascular Interventions, 1*(3), 218-226. doi: http://dx.doi.org/10.1016/j.jcin.2007.12.008

Lefèvre, T., Louvard, Y., Morice, M. C., Dumas, P., Loubeyre, C., Benslimane, A., . . . Piéchaud, J. F. (2000). Stenting of bifurcation lesions: classification, treatments, and results. *Catheterization and cardiovascular interventions, 49*(3), 274-283.

Libby, P., Ridker, P. M., & Maseri, A. (2002). Inflammation and atherosclerosis. *Circulation, 105*(9), 1135-1143.

Libby, P., & Theroux, P. (2005). Pathophysiology of coronary artery disease. *Circulation, 111*(25), 3481-3488.

Lim, M. J., & Kern, M. J. (2006). Coronary Pathophysiology in the Cardiac Catheterization Laboratory. *Current Problems in Cardiology, 31*(8), 493-550. doi: 10.1016/j.cpcardiol.2006.04.002

Liu, B. (2007). The influences of stenosis on the downstream flow pattern in curved arteries. *Medical Engineering & Physics, 29*(8), 868-876. doi: 10.1016/j.medengphy.2006.09.009

Liu, X., Fan, Y. B., & Deng, X. Y. (2010). Effect of the Endothelial Glycocalyx Layer on the Transport of LDLs in the Artery. In C. T. Lim & J. C. H. Goh (Eds.), *6th World Congress of Biomechanics (WCB 2010). August 1-6, 2010 Singapore* (Vol. 31, pp. 406-409): Springer Berlin Heidelberg.

López-Palop, R., Carrillo, P., Frutos, A., Cordero, A., Agudo, P., Mashlab, S., & Bertomeu-Martínez, V. (2013). Comparison of effectiveness of high-dose intracoronary adenosine versus intravenous administration on the assessment of fractional flow reserve in patients with coronary heart disease. *The American journal of cardiology, 111*(9), 1277-1283.

MacCarthy, P., Berger, A., Manoharan, G., Bartunek, J., Barbato, E., Wijns, W., . . . De Bruyne, B. (2005). Pressure-derived measurement of coronary flow reserve. *Journal of the American College of Cardiology, 45*(2), 216-220. doi: 10.1016/j.jacc.2004.09.063

Mallinger, F., & Drikakis, D. (2002). Instability in three-dimensional, unsteady, stenotic flows. *International Journal of Heat and Fluid Flow, 23*(5), 657-663. doi: 10.1016/s0142-727x(02)00161-3

Medina, A., Suarez de Lezo, J., & Pan, M. (2006). A new classification of coronary bifurcation lesions. *Rev Esp Cardiol, 59*(2), 183.

Meijboom, W. B., Van Mieghem, C. A. G., van Pelt, N., Weustink, A., Pugliese, F., Mollet, N. R., . . . de Feyter, P. J. (2008). Comprehensive Assessment of Coronary Artery Stenoses: Computed Tomography Coronary Angiography Versus Conventional Coronary Angiography and Correlation With Fractional Flow Reserve in Patients With Stable Angina. *Journal of the American College of Cardiology, 52*(8), 636-643. doi: http://dx.doi.org/10.1016/j.jacc.2008.05.024

Melikian, N., De Bondt, P., Tonino, P., De Winter, O., Wyffels, E., Bartunek, J., . . . De Bruyne, B. (2010). Fractional Flow Reserve and Myocardial Perfusion Imaging in Patients With Angiographic Multivessel Coronary Artery Disease. *JACC: Cardiovascular Interventions, 3*(3), 307-314. doi: 10.1016/j.jcin.2009.12.010

Menter, F., Kuntz, M., & Langtry, R. (2003). *Ten years of Industrial experience with the {SST} model.* Paper presented at the Turbulence, Heat and Mass Transfer 4.

Menter, F. R. (2009). Review of the shear-stress transport turbulence model experience from an industrial perspective. *International Journal of Computational Fluid Dynamics, 23*(4), 305-316. doi: 10.1080/10618560902773387

Naghavi, M., Libby, P., Falk, E., Casscells, S. W., Litovsky, S., Rumberger, J., . . . Willerson, J. T. (2003). From vulnerable plaque to vulnerable patient: a call for new definitions and risk assessment strategies: Part II. *Circulation, 108*(15), 1772-1778. doi: 10.1161/01.cir.0000087481.55887.c9

Nissen, S. E., & Gurley, J. C. (1991). Application of intravascular ultrasound for detection and quantitation of coronary atherosclerosis. *Int J Card Imaging, 6*(3-4), 165-177.

Nissen, S. E., & Yock, P. (2001). Intravascular ultrasound: novel pathophysiological insights and current clinical applications. *Circulation, 103*(4), 604-616.

Nosovitsky, V. A., Ilegbusi, O. J., Jiang, J., Stone, P. H., & Feldman, C. L. (1997). Effects of Curvature and Stenosis-Like Narrowing on Wall Shear Stress in a Coronary Artery Model with Phasic Flow. *Computers and Biomedical Research, 30*(1), 61-82. doi: http://dx.doi.org/10.1006/cbmr.1997.1434

Ochoa-Tapia, J. A., & Whitaker, S. (1995). Momentum transfer at the boundary between a porous medium and a homogeneous fluid—II. Comparison with experiment. *International Journal of Heat and Mass Transfer, 38*(14), 2647-2655. doi: http://dx.doi.org/10.1016/0017-9310(94)00347-X

Park, S.-J., Kang, S.-J., Ahn, J.-M., Shim, E. B., Kim, Y.-T., Yun, S.-C., . . . Park, S.-W. (2012). Visual-Functional Mismatch Between Coronary Angiography and Fractional Flow Reserve. *JACC: Cardiovascular Interventions, 5*(10), 1029-1036. doi: 10.1016/j.jcin.2012.07.007

Park, S. H., & Koo, B. K. (2012). Clinical applications of fractional flow reserve in bifurcation lesions. *J Geriatr Cardiol, 9*(3), 278-284. doi: 10.3724/sp.j.1263.2012.05091

Peelukhana, S. V., Back, L. H., & Banerjee, R. K. (2009). Influence of coronary collateral flow on coronary diagnostic parameters: An in vitro study. *Journal of Biomechanics, 42*(16), 2753-2759. doi: 10.1016/j.jbiomech.2009.08.013

Perktold, K., Hofer, M., Rappitsch, G., Loew, M., Kuban, B. D., & Friedman, M. H. (1997). Validated computation of physiologic flow in a realistic coronary artery branch. *Journal of Biomechanics, 31*(3), 217-228. doi: 10.1016/s0021-9290(97)00118-8

Pijls, N. H. (2006). Assessment of the collateral circulation of the heart. *European heart journal, 27*(2), 123-124.

Pijls, N. H., Bech, G. J., De Bruyne, B., & van Straten, A. (1997). Clinical assessment of functional stenosis severity: use of coronary pressure measurements for the decision to bypass a lesion. *Ann Thorac Surg, 63*(6 Suppl), S6-11.

Pijls, N. H., De Bruyne, B., Bech, G. J., Liistro, F., Heyndrickx, G. R., Bonnier, H. J., & Koolen, J. J. (2000). Coronary pressure measurement to assess the hemodynamic significance of serial stenoses within one coronary artery: validation in humans. *Circulation, 102*(19), 2371-2377.

Pijls, N. H., De Bruyne, B., Peels, K., Van Der Voort, P. H., Bonnier, H. J., Bartunek, J. K. J. J., & Koolen, J. J. (1996). Measurement of fractional flow reserve to assess the functional severity of coronary-artery stenoses. *N Engl J Med, 334*(26), 1703-1708. doi: 10.1056/NEJM199606273342604

Pijls, N. H., Kern, M. J., Yock, P. G., & De Bruyne, B. (2000). Practice and potential pitfalls of coronary pressure measurement. *Catheter Cardiovasc Interv, 49*(1), 1-16.

Pijls, N. H., Van Gelder, B., Van der Voort, P., Peels, K., Bracke, F. A., Bonnier, H. J., & el Gamal, M. I. (1995). Fractional flow reserve. A useful index to evaluate the influence of an epicardial coronary stenosis on myocardial blood flow. *Circulation, 92*(11), 3183-3193.

Pijls, N. H. J., & Sels, J.-W. E. M. (2012). Functional Measurement of Coronary Stenosis. *Journal of the American College of Cardiology, 59*(12), 1045-1057. doi: http://dx.doi.org/10.1016/j.jacc.2011.09.077

Prosi M Fau - Perktold, K., Perktold K Fau - Ding, Z., Ding Z Fau - Friedman, M. H., & Friedman, M. H. Influence of curvature dynamics on pulsatile coronary artery flow in a realistic bifurcation model. (0021-9290 (Print)).

Prosi, M., Zunino, P., Perktold, K., & Quarteroni, A. (2005). Mathematical and numerical models for transfer of low-density lipoproteins through the arterial walls: a new methodology for the model set up with applications to the study of disturbed lumenal flow. *Journal of Biomechanics, 38*(4), 903-917. doi: 10.1016/j.jbiomech.2004.04.024

Rajabi-Jaghargh, E., Kolli, K. K., Back, L. H., & Banerjee, R. K. (2011). Effect of guidewire on contribution of loss due to momentum change and viscous loss to the translesional pressure drop across coronary artery stenosis: An analytical approach. *BioMedical Engineering OnLine, 10*(1), 51. doi: 10.1186/1475-925x-10-51

Ramanathan, T., & Skinner, H. (2005). Coronary blood flow. *Continuing Education in Anaesthesia, Critical Care & Pain, 5*(2), 61-64. doi: 10.1093/bjaceaccp/mki012

Roy, A. S., Back, L. H., & Banerjee, R. K. (2008). Evaluation of compliance of arterial vessel using coupled fluid structure interaction analysis. *MCB Molecular and Cellular Biomechanics, 5*, 229-246.

Roy, A. S., Banerjee, R. K., Back, L. H., Back, M. R., Khoury, S., & Millard, R. W. (2005). Delineating the guide-wire flow obstruction effect in assessment of fractional flow reserve and coronary flow reserve measurements. *Am J Physiol Heart Circ Physiol, 289*(1), H392-397. doi: 00798.2004 [pii] 10.1152/ajpheart.00798.2004

Santamarina, A., Weydahl, E., Siegel, J. M., Jr., & Moore, J. E., Jr. (1998). Computational analysis of flow in a curved tube model of the coronary arteries: effects of time-varying curvature. *Ann Biomed Eng, 26*(6), 944-954.

Schilt, S., Moore Jr, J. E., Delfino, A., & Meister, J.-J. (1996). The effects of time-varying curvature on velocity profiles in a model of the coronary arteries. *Journal of Biomechanics, 29*(4), 469-474. doi: http://dx.doi.org/10.1016/0021-9290(95)00082-8

Seiler, C. (2003). The human coronary collateral circulation. *Heart, 89*(11), 1352-1357.

Seiler, C., Stoller, M., Pitt, B., & Meier, P. (2013). The human coronary collateral circulation: development and clinical importance. *Eur Heart J, 34*(34), 2674-2682. doi: 10.1093/eurheartj/eht195

Serruys, P. W., di Mario, C., Piek, J., Schroeder, E., Vrints, C., Probst, P., . . . Boersma, E. (1997). Prognostic value of intracoronary flow velocity and diameter stenosis in assessing the short- and long-term outcomes of coronary balloon angioplasty: the DEBATE Study (Doppler Endpoints Balloon Angioplasty Trial Europe). *Circulation, 96*(10), 3369-3377.

Shalman, E., Rosenfeld, M., Dgany, E., & Einav, S. (2002). Numerical modeling of the flow in stenosed coronary artery. The relationship between main hemodynamic parameters. *Computers in biology and medicine, 32*(5), 329-344.

Shanmugavelayudam, S. K., Rubenstein, D. A., & Yin, W. (2010). Effect of Geometrical Assumptions on Numerical Modeling of Coronary Blood Flow Under Normal and Disease Conditions. *Journal of Biomechanical Engineering, 132*(6), 061004-061004. doi: 10.1115/1.4001033

Siebes, M., Chamuleau, S. A. J., Meuwissen, M., Piek, J. J., & Spaan, J. A. E. (2002). Influence of hemodynamic conditions on fractional flow reserve: parametric analysis of underlying model. *American Journal of Physiology - Heart and Circulatory Physiology, 283*(4), H1462-H1470. doi: 10.1152/ajpheart.00165.2002

Siebes, M., Verhoeff, B. J., Meuwissen, M., de Winter, R. J., Spaan, J. A., & Piek, J. J. (2004). Single-wire pressure and flow velocity measurement to quantify coronary stenosis hemodynamics and effects of percutaneous interventions. *Circulation, 109*(6), 756-762. doi: 10.1161/01.cir.0000112571.06979.b2

Sinha Roy, A., Back, L. H., & Banerjee, R. K. (2006). Guidewire flow obstruction effect on pressure drop-flow relationship in moderate coronary artery stenosis. *Journal of Biomechanics, 39*(5), 853-864. doi: 10.1016/j.jbiomech.2005.01.020

Sinharoy, A., Back, M., Khoury, S., Schneeberger, E., Back, L., Velury, V., . . . Banerjee, R. (2008). Functional and Anatomical Diagnosis of Coronary Artery Stenoses. *Journal of Surgical Research, 150*(1), 24-33. doi: 10.1016/j.jss.2007.10.018

Stein, P. D., & Sabbah, H. N. (1976). Turbulent blood flow in the ascending aorta of humans with normal and diseased aortic valves. *Circ Res, 39*(1), 58-65.

Sun, Z., & Cao, Y. (2011). Multislice CT angiography assessment of left coronary artery: Correlation between bifurcation angle and dimensions and development of coronary artery disease. *European Journal of Radiology, 79*(2), e90-e95. doi: http://dx.doi.org/10.1016/j.ejrad.2011.04.015

Takeshita, A., Koiwaya, Y., Nakamura, M., Yamamoto, K., & Torii, S. (1982). Immediate appearance of coronary collaterals during ergonovine-induced arterial spasm. *Chest, 82*(3), 319-322.

Tang, D., Yang, C., Kobayashi, S., Zheng, J., Woodard, P. K., Teng, Z., . . . Ku, D. N. (2009). 3D MRI-Based Anisotropic FSI Models With Cyclic Bending for Human Coronary Atherosclerotic Plaque Mechanical Analysis. *Journal of Biomechanical Engineering, 131*(6), 061010. doi: 10.1115/1.3127253

Taylor, C. A., Hughes, T. J. R., & Zarins, C. K. (1998). Finite element modeling of blood flow in arteries. *Computer Methods in Applied Mechanics and Engineering, 158*(1–2), 155-196. doi: http://dx.doi.org/10.1016/S0045-7825(98)80008-X

Thakker, A., & Hourigan, F. (2005). A comparison of two meshing schemes for CFD analysis of the impulse turbine for wave energy applications. *Renewable Energy, 30*(9), 1401-1410. doi: http://dx.doi.org/10.1016/j.renene.2004.10.006

Tobis, J., Azarbal, B., & Slavin, L. (2007). Assessment of Intermediate Severity Coronary Lesions in the Catheterization Laboratory. *Journal of the American College of Cardiology, 49*(8), 839-848. doi: 10.1016/j.jacc.2006.10.055

Tonino, P. A. L., De Bruyne, B., Pijls, N. H. J., Siebert, U., Ikeno, F., van `t Veer, M., . . . Fearon, W. F. (2009). Fractional Flow Reserve versus Angiography for Guiding Percutaneous Coronary Intervention. *New England Journal of Medicine, 360*(3), 213-224. doi: doi:10.1056/NEJMoa0807611

Tripathi, D. (2013). Study of transient peristaltic heat flow through a finite porous channel. *Mathematical and Computer Modelling, 57*(5–6), 1270-1283. doi: http://dx.doi.org/10.1016/j.mcm.2012.10.030

Tu, C., & Deville, M. (1996). Pulsatile flow of non-Newtonian fluids through arterial stenoses. *Journal of Biomechanics, 29*(7), 899-908. doi: http://dx.doi.org/10.1016/0021-9290(95)00151-4

Vafai, K., & Tien, C. L. (1981). Boundary and inertia effects on flow and heat transfer in porous media. *International Journal of Heat and Mass Transfer, 24*(2), 195-203. doi: http://dx.doi.org/10.1016/0017-9310(81)90027-2

van Werkhoven, J. M., Schuijf, J. D., Jukema, J. W., Pundziute, G., de Roos, A., Schalij, M. J., . . . Bax, J. J. (2009). Comparison of Non-Invasive Multi-Slice Computed Tomography Coronary Angiography Versus Invasive Coronary Angiography and Fractional Flow Reserve for the Evaluation of Men With Known Coronary Artery Disease. *The American Journal of Cardiology, 104*(5), 653-656. doi: 10.1016/j.amjcard.2009.04.045

Varghese, S. S., & Frankel, S. H. (2003). Numerical modeling of pulsatile turbulent flow in stenotic vessels. *J Biomech Eng, 125*(4), 445-460.

Versteeg, H. K., & Malalasekera, W. (2007). *An introduction to computational fluid dynamics: the finite volume method*: Pearson Education.

Vicini, P., & Bassingthwaighte, J. B. (2014). 17 - Blood–Tissue Exchange Modelling. In E. Carson & C. Cobelli (Eds.), *Modelling Methodology for Physiology and Medicine (Second Edition)* (pp. 381-415). Oxford: Elsevier.

Vlodaver, Z., & Lesser, J. (2012). Anatomy of Coronary Vessels. In Z. Vlodaver, R. F. Wilson & D. J. Garry (Eds.), *Coronary Heart Disease* (pp. 1-18): Springer US.

Walburn, F. J., & Schneck, D. J. (1976). A constitutive equation for whole human blood. *Biorheology, 13*(3), 201-210.

Wang, X., & Li, X. (2011). Biomechanical behaviors of curved artery with flexible wall: A numerical study using fluid–structure interaction method. *Computers in biology and medicine, 41*(11), 1014-1021.

Wellnhofer, E., Osman, J., Kertzscher, U., Affeld, K., Fleck, E., & Goubergrits, L. (2010). Flow simulation studies in coronary arteries—Impact of side-branches. *Atherosclerosis, 213*(2), 475-481. doi: 10.1016/j.atherosclerosis.2010.09.007

Wijpkema, J., Dorgelo, J., Willems, T., Tio, R., Jessurun, G., Oudkerk, M., & Zijlstra, F. (2007). Discordance between anatomical and functional coronary stenosis severity. *Netherlands Heart Journal, 15*(1), 5.

Wilcox, D. A. (1994). Simulation of Transition with a Two-Equation Turbulence Model. *AIAA Journal, 32*(2), 247-255. doi: 10.2514/3.59994

Wilson, R. F., Johnson, M. R., Marcus, M. L., Aylward, P. E., Skorton, D. J., Collins, S., & White, C. W. (1988). The effect of coronary angioplasty on coronary flow reserve. *Circulation, 77*(4), 873-885.

Wiwatanapataphee, B., Wu, Y. H., Siriapisith, T., & Nuntadilok, B. (2012). Effect of branchings on blood flow in the system of human coronary arteries. *Mathematical biosciences and engineering: MBE, 9*(1), 199-214.

Yamashita, T., Nishida, T., Adamian, M. G., Briguori, C., Vaghetti, M., Corvaja, N., . . . Tobis, J. M. (2000). Bifurcation lesions: two stents versus one stent—immediate and follow-up results. *Journal of the American College of Cardiology, 35*(5), 1145-1151.

Yang, C., Tang, D., Kobayashi, S., Zheng, J., Woodard, P. K., Teng, Z., . . . Ku, D. N. (2008). Cyclic Bending Contributes to High Stress in a Human Coronary Atherosclerotic Plaque and Rupture Risk: In Vitro Experimental Modeling and Ex Vivo MRI-Based Computational Modeling Approach. *Mol Cell Biomech, 5*(4), 259-274.

Yao, H., Ang, K. C., Yeo, J. H., & Sim, E. K. (2000). Computational modelling of blood flow through curved stenosed arteries. *J Med Eng Technol, 24*(4), 163-168.

Zegers, E. S., Meursing, B. T., Zegers, E. B., & Oude Ophuis, A. J. (2007). Coronary tortuosity: a long and winding road. *Neth Heart J, 15*(5), 191-195.

Ziaee, A., Parham, W. A., Herrmann, S. C., Stewart, R. E., Lim, M. J., & Kern, M. J. (2004). Lack of relation between imaging and physiology in ostial coronary artery narrowings. *Am J Cardiol, 93*(11), 1404-1407, A1409. doi: 10.1016/j.amjcard.2004.02.041

PUBLICATIONS

Govindaraju, K., Badruddin, I. A., Viswanathan, G. N., Ramesh, S. V., & Badarudin, A. (2013). Evaluation of functional severity of coronary artery disease and fluid dynamics' influence on hemodynamic parameters: A review. *Physica Medica*, *29*(3), 225-232. doi: http://dx.doi.org/10.1016/j.ejmp.2012.03.008

Govindaraju, K., Kamangar, S., Badruddin, I. A., Viswanathan, G. N., Badarudin, A., & Salman Ahmed, N. J. (2014). Effect of porous media of the stenosed artery wall to the coronary physiological diagnostic parameter: A computational fluid dynamic analysis. *Atherosclerosis*, *233*(2), 630-635. doi: http://dx.doi.org/10.1016/j.atherosclerosis.2014.01.043

ARTICLES UNDER REVIEW

Govindaraju, K., Badruddin, I. A., Viswanathan, G. N., Kamangar, S., & Badarudin, A. (2015). The influence of artery wall curvature on the anatomical assessment of stenosis severity derived from fractional flow reserve: A computational fluid dynamics study. Computer Methods in Biomechanics and Biomedical Engineering.

Govindaraju, K., Badruddin, I. A., Viswanathan, G. N., Kamangar, S., & Badarudin, A. (2015). A parametric study of the effect of arterial wall curvature on non-invasive assessment of stenosis severity: Computational fluid dynamic study. Current science online.

Govindaraju, K., Badruddin, I. A., Viswanathan, G. N., Kamangar, S., & Badarudin, A. (2015). The influence of variable bifurcation angulation and outflow boundary condition in 3D finite element modelling of left coronary artery on coronary diagnostic parameter. Current science online.